EFFECT OF PORE-WATER SURFACE TENSION ON TENSILE STRENGTH OF UNSATURATED SAND

PRATEEK JINDAL

A THESIS SUBMITTED TO

THE FACULTY OF GRADUATE STUDIES

IN PARTIAL FULFILLMENT OF THE REQUIREMENTS

FOR THE DEGREE OF

MASTER OF SCIENCE

GRADUATE PROGRAM IN

EARTH AND SPACE SCIENCE

YORK UNIVERSITY

TORONTO, ONTARIO

January 2016

© PRATEEK JINDAL, 2016

ABSTRACT

Tensile behaviour of unsaturated sand was investigated both experimentally and theoretically. A custom-built direct tension apparatus was employed to perform direct tension tests on unsaturated silica sand specimens at different saturations levels and packing dry densities. Attempt was made to understand the effect of surface tension of pore-liquid and tensile loading rate on the tensile strength. It was found that the tensile strength decreases, as the surface tension of the pore-liquid decreases and rate of loading increases. However, tensile strength does not decrease as a simple multiple of ratio of surface tension of pore-liquid. The experimental results were also compared with the predicted results from two theoretical tensile strength models, namely, micro-mechanical and the macro-mechanical models. Results predicted using the micro-mechanical model agreed well with the experimental results, but only for specimens containing distilled water in the pendular saturation regime. On the other hand, the macro-mechanical model followed the experimental trend across pendular and funicular saturation regimes for specimens containing distilled water reasonably well. However, at reduced surface tension of pore-liquid, both models significantly under-predicted the experimental tensile strength results.

ACKNOWLEDGEMENTS

Foremost, I would like to express the deepest appreciation to my thesis supervisor and mentor, Dr. Jitendrapal Sharma, who has the attitude and the substance of a genius. Without his guidance and relentless encouragement, my thesis would not have been possible. I would also like to thank him for his financial support throughout the course of the researchwork. Thanks for everything, Dr. Sharma.

In addition, a big thank you to my co-supervisor Dr. Rashid Bashir, whose expertise in unsaturated soil mechanics helped me to structure my research and thesis. He has shared valuable insights in the relevance of the study and made this research successful. I would also like to thank my thesis committee members, Dr. Dan Palermo and Dr. Ryley Beddoe, for their kindness, encouragement and insightful comments.

I would also like to express my appreciation to Dr. Dieter Stolle and Mr. Peter Koudys from McMaster University, for their contribution to the development of the direct tension apparatus. My special thanks to Adam Hammerlindl from University of Saskatchewan for his tremendous assistance in setting up the direct tension apparatus and LabVIEW system.

I would also like to thank my friends and colleagues at University of Saskatchewan and York University – Mohit, Azza, Sunil, Zeeshan, Arafat, Ramtin, Jacob and Eros for their endless support and motivation.

I would also take this opportunity to thanks Mitacs Globalink Graduate Fellowship program for providing financial assistance, which went a long way in making this research possible.

Last, but not least, I would like to thank my mom, dad, and Nikita for their unconditional love and support during the course of my Masters studies and throughout my life.

This one is for you, Ma.

TABLE OF CONTENTS

LIST OF TABLES

LIST OF FIGURES

LIST OF SYMBOLS

GREEK SYMBOLS

Symbol	Description	Unit
α	*Contact angle*	*degrees*
α'	*Inverse of air-entry value*	*$(N/m^2)^{-1}$*
α_0	*Contact angle of reference fluid*	*degrees*
θ	*Filling angle*	*degrees*
ρ_l	*Density of the liquid*	*g/cm^3*
ρ_s	*Density of the solid*	*g/cm^3*
σ	*Normal stress*	*N/m^2*
σ'	*Effective stress*	*N/m^2*
σ^s	*Suction stress*	*N/m^2*
σ_{tc}	*Tensile strength in capillary state*	*N/m^2*
σ_{tf}	*Tensile strength in pendular state*	*N/m^2*
σ_{ti}	*Isotropic tensile strength*	*N/m^2*
σ_{tp}	*Tensile strength in pendular state*	*N/m^2*
σ_{tu}	*Uniaxial tensile strength*	*N/m^2*
τ	*Shear stress*	*N/m^2*
ϕ	*Internal friction angle*	*degrees*
ϕ'	*Effective internal friction angle associated with net normal stress*	*degrees*
ϕ^b	*Internal friction angle associated with matric suction*	*degrees*
χ	*Bishop's effective stress parameter*	-
Ψ	*Pressure head*	*m*
ψ_t	*Total suction*	*N/m^2*
ψ_m	*Matric suction*	*N/m^2*
ψ_o	*Osmotic suction*	*N/m^2*

ROMAN SYMBOLS

Symbol	Description	Unit
a/d	*Particle separation distance ratio*	-
a'	*Schubert's model parameter*	-
C	*Apparent cohesion*	N/m^2
c	*Concentration of surfactant in solution*	-
c_0	*Concentration of reference solution*	-
c'	*Cohesion at zero matric suction and zero normal stress*	N/m^2
d	*Diameter of idealized sand particle (Rumpf's model)*	*mm*
d_{50}	*Average particle size*	*mm*
d_{10}	*Effective particle size*	*mm*
e	*Void ratio*	-
F_c	*Force component due to pressure difference across liquid bridge*	*N*
F_s	*Force component due to surface tension*	*N*
F_t	*Total bonding force due to surface tension and pressure difference across liquid bridge*	*N*
G_s	*Specific gravity*	-
g	*Acceleration due to gravity*	m/s^2
k	*Co-ordination number*	-
m_s	*Mass of the solid*	*kg*
m_l	*Mass of the liquid*	*kg*
n	*Pore-size distribution factor*	-
n_p	*Porosity*	-
P_c	*Capillary pressure*	N/m^2
r, h	*Radii of the curvature describing the liquid bridge (Rumpf's model)*	*mm*
r^*, h^*	*Dimensionless radii of the curvature describing the water bridge*	-
R	*Radius of idealized spherical particle*	*mm*
R_1, R_2	*Principal radii of curvature of air-water interface in double curvature model*	*mm*
S	*Degree of saturation*	-
S_c	*Capillary saturation*	-
S_e	*Effective or normalized saturation*	-
S_f	*Degree of saturation between funicular and pendular state*	-
S_r	*Residual saturation*	-
T_s	*Surface tension*	*mN/m*
T_{s0}	*Surface tension of reference fluid*	*mN/m*
T_{ss}	*Surface tension mobilized*	*mN/m*

Symbol	Description	Unit
u_a	*Pore-air pressure*	N/m^2
u_w	*Pore-water pressure*	N/m^2
V_{bridge}	*Volume of the liquid bridge*	mm^3
V_l	*Volume of the liquid*	mm^3
V_s	*Volume of the solid*	mm^3
w	*Water content*	-
z_c	*Height of capillary rise*	*m*

1 INTRODUCTION

Soil, in general, involves a three-phase system wherein the soil mass comprises of solid particles that contain void spaces filled with gaseous phase and/or liquid phase. On this basis, soil could be either completely saturated, unsaturated or completely dry. **Figure 1.1** illustrates a typical soil profile showing the saturated and unsaturated zones. Classical soil mechanics focus mainly on completely saturated and dry soils. However, unsaturated soils do not adhere to classical soil mechanics. The difference between unsaturated and saturated soils becomes significant when considering the constitutive soil properties and the resulting physical behaviour. For instance, unsaturated soil is subjected to negative pore-water pressure relative to pore-air pressure and shows different engineering behaviour over the entire range of degree of saturation.

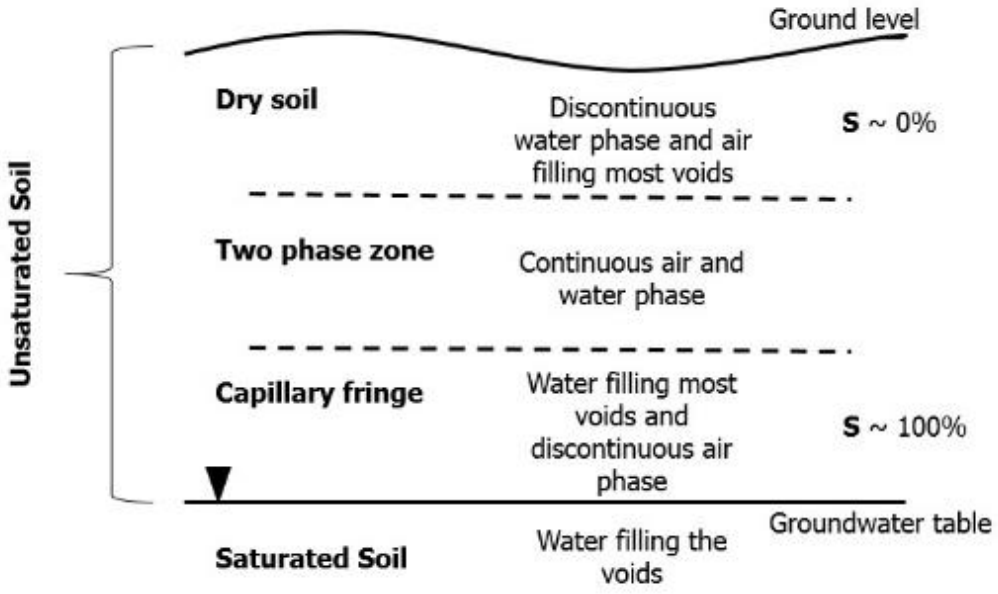

Figure 1.1 Saturated and unsaturated soil profile (modified from Fredlund 2000)

Fredlund (1998) pointed out several limitations associated with classical saturated soil mechanics. He noted that the theories and formulations for saturated soils do not directly apply for unsaturated soils. Also, the moisture flux boundary condition that plays a significant role during the interaction between soil and atmosphere has been ignored in the classical theory.

Difficulty in the measurement of negative pore-water pressure and other unsaturated soil properties prevents us from having a true representation of the unsaturated soil behaviour. The measurement of negative pore-water pressure is a crucial parameter comparable to the measurement of positive pore-water pressure for saturated soils. Similarly, several theoretical and practical challenges associated with unsaturated soils have limited their application in current engineering practice. Further research is required to develop and formulate a more generalized approach towards soil mechanics, which is able to encompass the theoretical and practical implications of both saturated and unsaturated soil behaviour.

Although unsaturated soil mechanics did not emerge simultaneously with classical saturated soil mechanics, a number of important theoretical and experimental developments in other inter-related disciplines led to the gradual emergence of unsaturated soil mechanics. Numerous contributions have been noted in the fields related to agriculture, such as soil sciences and agronomy, powder technology and interface physics. The importance of tensile strength of unsaturated soils in the field of agronomy has long been recognized (Snyder and Miller 1985). Tensile strength is important in determining the degree of soil breakup produced by tillage (Farrell et al. 1967; Vomocil et al. 1967). Evidence suggests that granular aggregates subjected to compressive loads may fail in tension as a result of tensile stresses developed on the planes perpendicular to the line of action of the compressive loads (Rogowski et al. 1968; Rogowski and Kirkham 1976; Braunack et al. 1979). Griffith (1921) observed that solids subjected to shear stresses could fail in tension due to tensile stresses developed at the apexes. Many researchers in the field of geotechnical engineering have used these concepts to study the mechanics of unsaturated soils, both quantitatively and qualitatively (Farrell et al. 1967; Bishop and Garga 1969; Rogowski and Kirkham 1976). It is also a common practice to use tri-axial cells and oedometers for geotechnical testing, wherein, total stresses are applied to the soil mass. On the other hand, researchers in the field of soil-sciences and agronomy used pressure plate techniques to apply stresses to the liquid phase. It was eventually realized that the pressure plate techniques could prove to be useful in understanding unsaturated soil behaviour in the context of geotechnical engineering (Fredlund et al. 2012). Currently, pressure plate techniques (e.g. Tempe cells) are extensively used to determine the relation between soil suction and degree of saturation in unsaturated soils, also known as soil-moisture characteristic curve (SMCC) or soil-moisture retention curve.

Similarly, considerable amount of research has been done to study the properties and behaviour of granular materials, such as powders and glass beads. Capillary forces, generated in granular materials by adding small amounts of liquid, play a crucial role in agglomeration, flow behaviour, moisture retention and strength properties (Schubert et al. 1984). Among other physical properties, tensile strength is considered to be an important parameter in powder characterization (Pierrat and Caram 1997) and has important industrial applications (Ashton et al. 1965; Cheng 1968). Theories proposed by Rumpf (1961) and Schubert (1975*a*, 1984) to predict tensile strength of powders have found its application in the field of unsaturated granular soils. Likewise, many experimental methods developed to measure tensile strength of glass beads and powders have been used to determine tensile strength of unsaturated sands (Schubert 1975b, Pierrat and Caram 1997; Perkins 1991).

1.1 UNSATURATED SOIL MECHANICS IN GEOTECHNICAL ENGINEERING

According to classical saturated soil mechanics, the strength of granular soils (e.g. sands) is governed by Mohr-Coulomb failure criterion. It assumes that dry or completely saturated granular soils have no cohesion except due to interlocking in very dense states. As a result, granular soils are considered to have only shear strength and no or insignificant tensile strength. However, this is not applicable in the case of unsaturated sands. In unsaturated soil, coexistence of solid, liquid and gaseous phases give rise to various capillary mechanisms, which can generate significant amount of cohesion and tensile strength.

The existence of tensile behaviour of unsaturated sands can be understood by a simple example – by considering stability of slopes in fine, uniform sand. If the slope is completely dry, the slope surface will readily undergo translational failure or adjust to its natural angle of repose. Similarly, if this dry slope becomes completely saturated, due to infiltration or precipitation, it will also result in failure of the slope. This is due to the fact that negative pore-water pressure and capillarity clearly does not exist in saturated conditions. However, under unsaturated conditions (e.g. above ground water table), a slope surface can be sustained due to negative pore-water pressure and capillary forces in the soil medium. Such slopes remain stable due to the apparent cohesion provided by the negative pore-water pressure and capillary forces acting in the medium. This apparent cohesion takes the form of tensile strength in the unsaturated sand. However, the slopes will fail with the loss of the apparent cohesion under

condition of saturation of the soil by infiltrating water or desaturation due to evapo-transpiration. Similar behaviour is also observed in case of sandcastles. They stand by themselves at steep angles without any support because capillary forces act to support the soil, in the form of apparent cohesion and tensile strength. Hence, it can be argued that tensile strength of unsaturated sands should not be neglected completely (**Figure 1.2**).

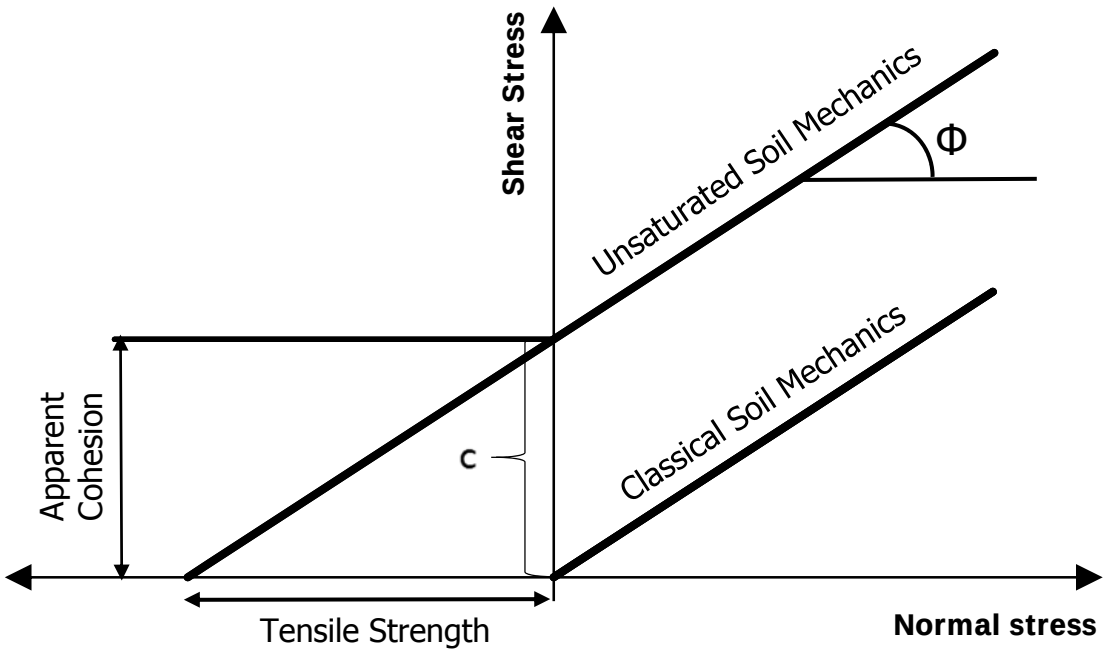

Figure 1.2 Mohr-Coulomb failure envelope for classical soil mechanics vs unsaturated soil mechanics. (modified after Kim 2001)

There are situations where the tensile strength of unsaturated soil becomes important, e.g. shallow slope stability, rainfall-induced landslides, lateral earth pressure, excavations, and shallow footing design. Many researchers have tried to consider the effect of apparent cohesion and tensile strength of unsaturated sands in geotechnical practice. For example, Kim (2001) showed the importance of apparent cohesion and tensile strength in sand by considering the examples of bearing capacity, excavation and laterally loaded piles. Drained analysis was performed on a rigid circular footing of radius 0.1 m on a sand layer (4 m deep and φ = 31˚), using PLAXIS© and Mohr-Coulomb failure criterion was adopted. Significant increase in the bearing capacity of the foundation was observed when apparent cohesion and tensile strength of unsaturated sands were considered. Similarly, the influence of tensile strength on excavation

in sands was demonstrated by performing plain-strain analysis using PLAXIS ©. It was reported that the displacement of the excavated surface was significantly smaller when tensile strength of unsaturated sands was considered. The above examples demonstrate that the tensile strength of unsaturated sands can be of great significance in geotechnical applications and cannot be ignored completely.

1.2 PROBLEM STATEMENT

There is a vast scope in proper quantification of the tensile strength of unsaturated granular soils which takes into account the properties of the soil medium (e.g. SMCC, packing density, degree of saturation, etc.) and properties of the pore-liquid (e.g. surface tension, contact angle, viscosity) as well as field conditions (e.g. evapo-transpiration, surface run-off, etc.). Most of the previous work related to tensile strength of the unsaturated soils has been limited to fine-grained soils, such as clay or clayey silt, or cemented fine-grained soils (Bishop and Garga 1969; Bofinger 1970; Al-Hussaini and Townsend 1973 and others). Only in the past few decades, advances have been made on the qualitative and quantitative understanding of the capillary attraction mechanism in unsaturated granular materials (Rumpf 1961; Schubert et al. 1975*a*, 1975*b*; Orr et al. 1975; Dobbs and Yeomans 1992; Pierrat and Caram 1997; Kim 2001; Karube and Kawai 2001; Kim and Hwang 2003; Kim and Sture 2004; Molenkamp and Nazemi 2003; Lu et al., 2007).

As mentioned earlier, negative pore-water pressure and capillary forces due surface tension within granular materials are responsible for generating tensile strength in unsaturated sands. The magnitude of capillary mechanisms is a function of surface tension of the pore-liquid (Aitchison 1960; Bear 1972). It is known that most of the surface-active organic compounds or surfactants significantly alter the surface tension of distilled water in relation to their aqueous concentrations (Bikerman 1970; Smith 1999; Henry et al. 1999, 2001). Hence, any reduction in the surface tension caused by a surfactant can directly affect the negative pore-water pressure and capillary forces in unsaturated soils. This will in turn affect the tensile strength of unsaturated sand. The effect of concentration-dependent surface tension on tensile strength of unsaturated sands is not understood properly. Such a study is warranted as many surface-active compounds might occur naturally or through anthropogenic activities such as application of surfactants for infiltration enhancement or sub-surface remediation. Presence of

these surface-active compounds can then significantly alter the strength behaviour of the soil. Hence, the motivation of this research is to develop a reliable technique for tensile strength measurements and to study the effect of concentration-dependent surface tension of pore water on the tensile strength of unsaturated sands.

1.3 OBJECTIVES

The first objective of this research work is to understand the effect of surface tension of pore-liquid on the tensile strength of unsaturated sands. A modified, custom-built direct tension apparatus is used to experimentally measure the tensile strength of unsaturated sands. Using load cell and linear-variable differential transformer, the apparatus is capable of determining the exact time of tensile failure and tensile strength at failure with good accuracy.

The second objective is to compare the experiment results with the predicted results calculated using two theoretical models – micro-mechanical and macro-mechanical. The main purpose of the comparison is to check the efficacy of the theoretical model to predict the tensile strength of the unsaturated sands at reduced surface tension of the pore-liquid.

1.4 THESIS ORGANIZATION

The proposed thesis will be divided into six chapters followed by two appendices. Chapter 1 constitutes the introduction chapter. It describes the importance of tensile strength of unsaturated sands in geotechnical engineering, motivation towards this research, the problem statement and objectives of the research program. Chapter 2 contains background knowledge and literature review and it will be divided in to four major sections. First, an overview of soil suction, soil-moisture characteristic curve (SMCC), capillary phenomenon, and influence of surface tension on SMCC is presented. Second, a theoretical basis of predicting tensile strength will be presented, wherein two tensile strength theoretical models is described in details. Third section of Chapter 2 covers the literature review where the tensile strength experimental data is presented from previous studies. The final section includes a comprehensive review of tensile strength measuring techniques developed by researchers previously. Chapter 3 explains the materials and methods used to develop this research. This chapter includes the properties of soil specimen and pore-liquid used as well as the modified direct tension apparatus and details of the experimental program. The details of the results from

all the experimental programs are presented in Chapter 4. In Chapter 5, the discussions and in-depth analysis of the results are presented. Predictions from tensile strength theoretical models are compared with the experimental results. Chapter 6 provides conclusions derived from this research and some recommendations for future studies. References cited and appendices, including calibration of the LVDT and load cell and calculation of friction in the direct tension apparatus, follow.

2 BACKGROUND KNOWLEDGE AND LITERATURE REVIEW

This chapter presents an overview on the background knowledge and a detailed literature review regarding tensile strength of unsaturated granular soils. Important concepts of soil suction, soil-moisture characteristic curves, and capillarity are discussed to understand the origins of tensile strength in unsaturated soils. A particular emphasis has been given to theoretically understand the effect of reduced surface tension of pore-water on capillary mechanisms, soil suction and tensile strength. Micro-mechanical and macro-mechanical theoretical models which are used to predict tensile strength in unsaturated granular soils are described herein. Tensile strength experiments performed on moist granular materials, for example, glass beads, powders, silts and sands have been reviewed. Experimental techniques (e.g. direct tension apparatus) developed previously to determine the tensile strength are also described.

2.1 UNSATURATED SOIL MECHANICS

2.1.1 Soil suction

Total soil suction is defined conceptually as the ability of unsaturated soil to attract or retain water (or any liquid) and is expressed in terms of pressure (e.g. kPa) or head (e.g. m). Thermodynamically, soil suction quantifies the potential of soil pore water relative to reference potential of free water. Free water can be defined as water with no dissolved solutes, having no external forces except gravitational force and having no physical and physicochemical interactions with other phases (solid, liquid or gas). If gravity, temperature, and inertial effects are neglected, mechanisms responsible for soil suction are capillarity, short-range adsorption mechanisms, and osmotic effects. While the latter two mechanisms may occur under saturated or unsaturated conditions, the capillarity mechanism is unique to unsaturated soil.

Short-range adsorptive effects arise primarily from electrical and van der Waals forces within the vicinity of solid-liquid interface, i.e. the soil-pore water interface. Hydration mechanism is a function of both the surface area and charge properties of the solid, and thus

are particularly important for fine-grained soils, such as clays. Osmotic effects are related to dissolved solutes in the pore-water, which may be present as externally introduced solutes or naturally occurring solutes adsorbed by the soil surfaces. Again, these effects are also more pronounced in clay and other fine-grained soils. The capillarity phenomenon is exclusively observed in unsaturated soils and forms the dominant suction mechanism in unsaturated coarse-grained soils. Capillarity includes capillary forces due to surface tension and negative pore-water pressure.

Total suction, quantitatively, is considered to be the algebraic sum of a matric and osmotic suction components:

$$\psi_t = \psi_m + \psi_o \quad \textbf{(2-1)}$$

where: ψ_t is the total suction; ψ_o is the osmotic suction; and ψ_m is the matric suction. Matric suction is expressed as the difference between the pore-air and pore-water pressures:

$$\psi_m = (u_a - u_w) \quad \textbf{(2-2)}$$

where: u_a *is* the pore-air pressure, and u_w is the pore-water pressure. The effects of capillarity and short-range adsorption mechanisms are combined to form the matric suction, while the presence of dissolved solutes forms the osmotic suction. Thus, matric suction and osmotic suction originate from physical interaction effects and chemical interaction effects, respectively. The capillary mechanism can be directly applied to unsaturated coarse-grained soils, in which pore-water is present as free water and soil pores are analogous to capillary tubes (**Figure 2.1**).

2.1.2 Capillarity and surface tension

A very convenient model to visualize the capillary phenomenon in unsaturated granular soils is water in a capillary tube. In a capillary tube inside a water container, the water rises up the tube until capillary forces and gravitational forces are in equilibrium. This results in a formation of curved air-water interface. The capillary rise is proportional to the surface tension

of the water, cosine of the contact angle and inverse of the radius of the capillary tube. The pressure difference just below the air-water interface (**Figure 2.2**) is given by (Bear 1972):

$$P_c = u_a - u_w = \frac{2T_s \cos \alpha}{R} \quad \textbf{(2-3)}$$

where: P_c is the capillary pressure; T_s is the surface tension of water; α is the contact angle; and R is the radius of curvature of the capillary meniscus formed at the air-water interface. When $R \to \infty$, $u_a = u_w$ which means that there is zero pressure difference across the air-water interface and the interface is flat. If atmospheric condition is considered, $u_a = 0$ and capillary pressure becomes equal to the negative pore-water pressure, i.e. $P_c = -u_w$.

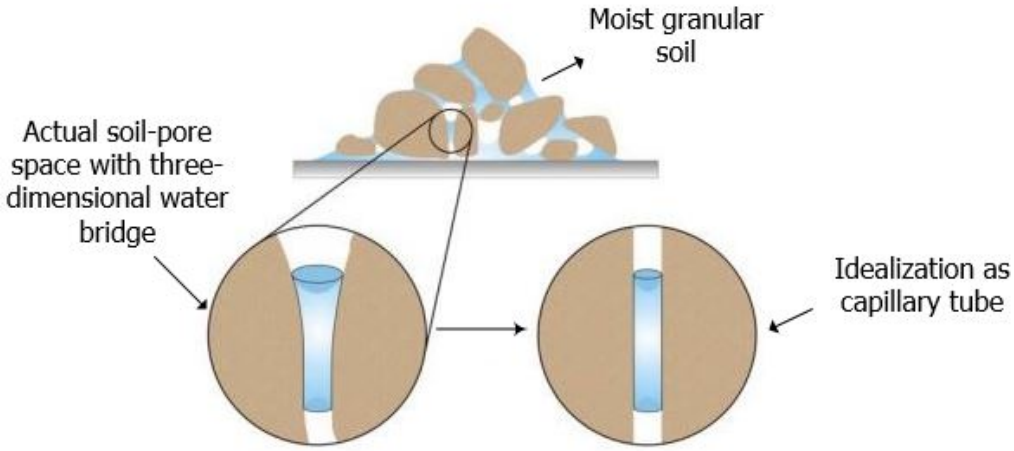

Figure 2.1 Idealization of soil pore space as simple capillary tubes (taken from Or and Tuller 2005)

Equation (2-3) can be considered as a special case of Young-Laplace equation (1805), which is given by **Equation (2-4)**:

$$u_a - u_w = T_s \cos \alpha \left(\frac{1}{R_1} + \frac{1}{R_2}\right) \quad \textbf{(2-4)}$$

where: R_1 and R_2 are two principal radii of curvature of any double curvature interface. The quantity in parentheses on the right hand side of the **Equation (2-4)** can be considered as twice of the mean curvature of the surface, R, such that:

$$\frac{1}{R} = \frac{1}{2}\left(\frac{1}{R_1} + \frac{1}{R_2}\right) \quad \textbf{(2-5)}$$

In three-phase unsaturated soil system, mechanical equilibrium of air-water interface is maintained by pore-air pressure, pore-water pressure and the surface tension of the water phase. Surface tension of air phase can be practically ignored. A curved air-water interface is an indication of pressure difference between the two phases. Usually, the phase with smaller-pressure tends to expand resulting in a concave interface towards the higher-pressure side. This change in interface geometry induces the surface tension, which ultimately maintains the equilibrium. Under most practical circumstances, for unsaturated soil, concave side is associated with the air phase as the pore water pressure is lower than the pore air pressure.

The capillary tube model provides a useful conceptualization of capillary pressure in unsaturated granular soils. However, the above model and equations may not be directly applied to real soil, because of the complex geometry of pores and its distribution.

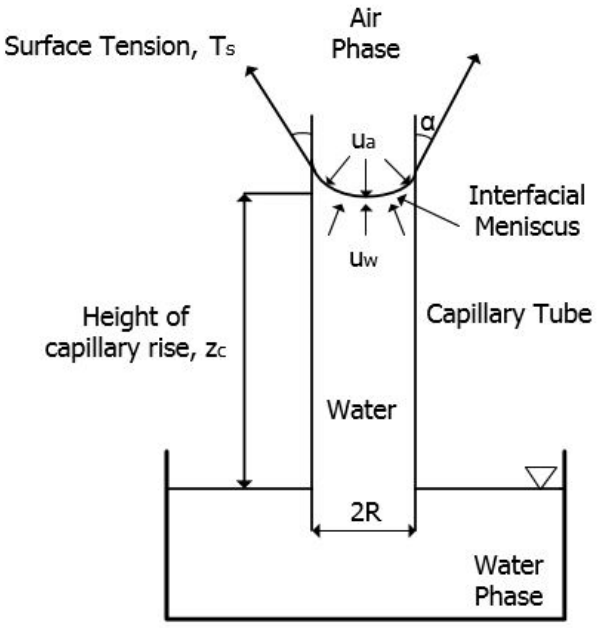

Figure 2.2 Free-body diagram of capillary meniscus formed at air-water interface in a capillary tube.

2.1.3 Soil-moisture characteristic curve

One of the most important and fundamental constitutive relationship in unsaturated soil mechanics is the relation between matric suction and degree of saturation (or volumetric moisture content). This relationship is called soil-moisture characteristic curve (SMCC) or soil-moisture retention curve. The schematic representation the SMCC is shown in **Figure 2.3**.

Consider a completely saturated soil media undergoing a drying cycle (evaporation or drainage). As the drainage begins, the soil media is said to be in the capillary state, when the liquid pressure becomes lower than the air pressure and matric suction becomes positive. Beyond the capillary state, matric suction increases rapidly as the liquid menisci at the boundaries are pulled inward due to evaporation or drainage. At a particular value of suction, the air phase breaks into the soil media and it is described as the air-entry value (AEV) or bubbling pressure. AEV is inversely proportional to the pore size, thus, finer the particles, higher is the AEV. AEV generally occurs at saturation levels of 90% to 100% (Cho and Santamarina 2001). As air phase starts to enter the soil media, a state of unsaturation is established but pore liquid stills forms a continuous phase. This is the funicular state. As the liquid content decreases, the suction pressure increases gradually, following a quasi-linear trend. At a point, when most of the voids are filled with air, and the rest of the liquid forms a thin film around the contact points between adjacent soil particles, the system is said to reach the pendular state. In the pendular state, a small change of the liquid content results in a relatively large change in matric suction. Even at very high values of matric suction, some amount of liquid is present in the form of very thin films around soil particles or adsorbed on surface of the soil particles. This is described as residual saturation. **Figure 2.4** shows a schematic representation of the three saturation states in unsaturated soils.

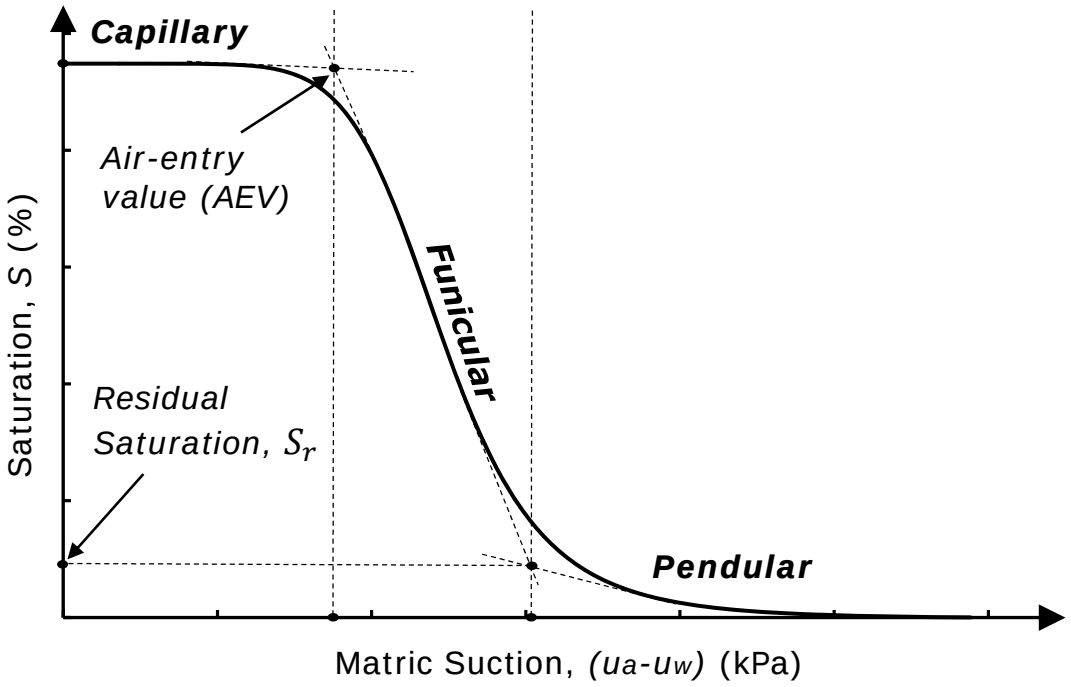

Figure 2.3 Typical SMCC with three saturation states

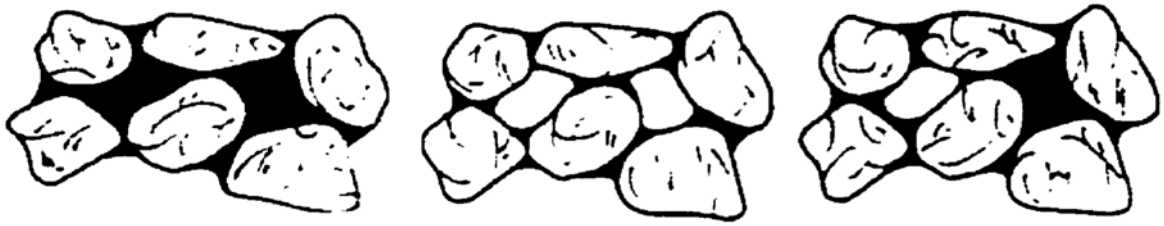

(a) **(b)** **(c)**

Figure 2.4 States of saturation in unsaturated soils. (a) Pendular state (b) Funicular state (c) Capillary state. (Schubert et al. 1975)

SMCC is hysteretic in nature and there is a pronounced difference between the wetting and drying curves. For the same level of saturation, soil in the drying cycle has higher suction compared to the soil in the wetting cycle. This effect is shown in **Figure 2.5**. As discussed earlier, the drying cycle starts from the completely saturated state until the residual saturation state. All the three saturation states can be clearly defined by AEV and residual saturation. In

the wetting cycle, SMCC begins from dry state and the soil is wetted until full saturation. At higher saturation states, the air phase becomes discontinuous and many occluded air bubbles can be found between the continuous liquid phases. As a result, the determination of upper saturation limit of the funicular state becomes difficult and relationship between matric suction and degree of saturation cannot be defined for complete range of saturation (Fredlund and Rahardjo 1993).

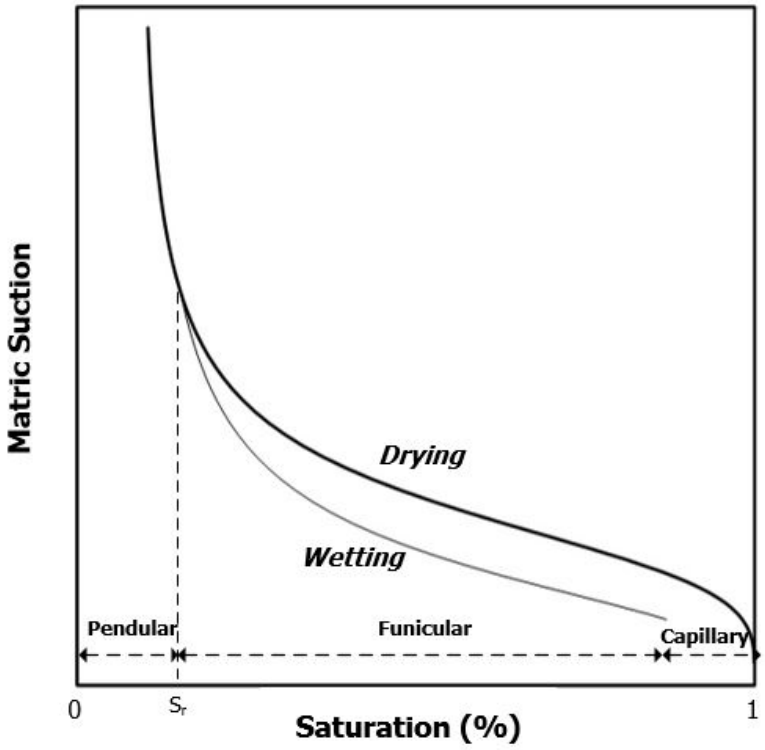

Figure 2.5 Hysteresis in SMCC

2.2 TENSILE STRENGTH THEORETICAL MODELS

As mentioned earlier, the primary sources of suction in unsaturated soils include capillarity, osmotic suction and short-range adsorption mechanism. For unsaturated granular soils, in particular, capillarity stands out as the most dominant mechanism and contributes to its tensile strength. To calculate tensile strength, the first step is to quantitatively study the capillary mechanisms in the pendular, funicular and capillary states. In the following section, two theoretical models are described, namely, micro-mechanical and macro-mechanical models, which are used to predict tensile strength in unsaturated sands.

2.2.1 Micro-mechanical Model of Tensile Strength

Consider two sand particles in the form of two mono-sized spheres of diameter, d, as shown in **Figure 2.6**. As in case of pendular state, a liquid bridge exists between the two particles such that they are separated by a distance, a. The two components of the capillary forces in the pendular state are (1) surface tension force acting along the pore water-particle contact line, F_s, and (2) force due to pressure difference between outside and inside of the liquid bridge, F_c. Both of the force components are given in a dimensionless form as:

$$\frac{F_s}{T_s d} = \pi sin\theta \sin(\theta + \alpha) \tag{2-6}$$

$$\frac{F_c}{T_s d} = \pi \left(\frac{1}{r^*} - \frac{1}{h^*}\right)\left(\frac{sin\theta}{2}\right)^2 \tag{2-7}$$

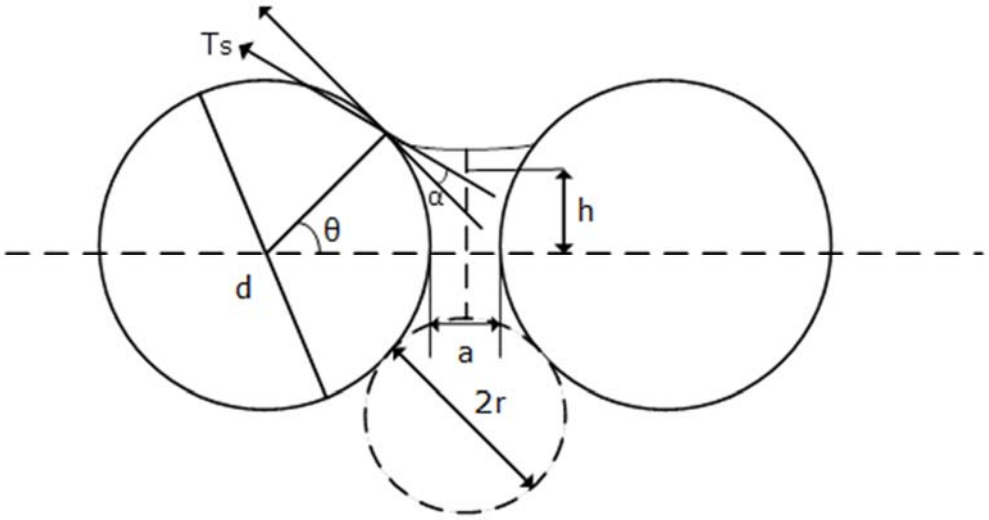

Figure 2.6 Meniscus geometry between two idealized mono-sized sand particles with non-zero contact angle

where: θ is the filling angle; and, r^* and h^* are the two dimensionless radii of curvature of the liquid bridge when taken as arcs of a circle (**Equations (2-8)** and **(2-9)**). The total bonding force, F_t, is the sum of the two force components as shown in **Equation (2-10)**. **Figure 2.7**

shows one-dimensional free-body diagram illustrating the two components of the bonding forces and the total bonding force.

$$h^* = \frac{h}{d} = \frac{\sin\theta}{2} + \frac{r}{d}[\sin(\theta + \alpha) - 1] \quad \textbf{(2-8)}$$

$$r^* = \frac{r}{d} = \frac{(1 - \cos\theta) + \frac{a}{d}}{2\cos(\theta + \alpha)} \quad \textbf{(2-9)}$$

$$\frac{F_t}{T_s d} = \pi \sin\theta \left[\sin(\theta + \alpha) + \frac{\sin\theta}{4}\left(\frac{1}{r^*} - \frac{1}{h^*}\right)\right] \quad \textbf{(2-10)}$$

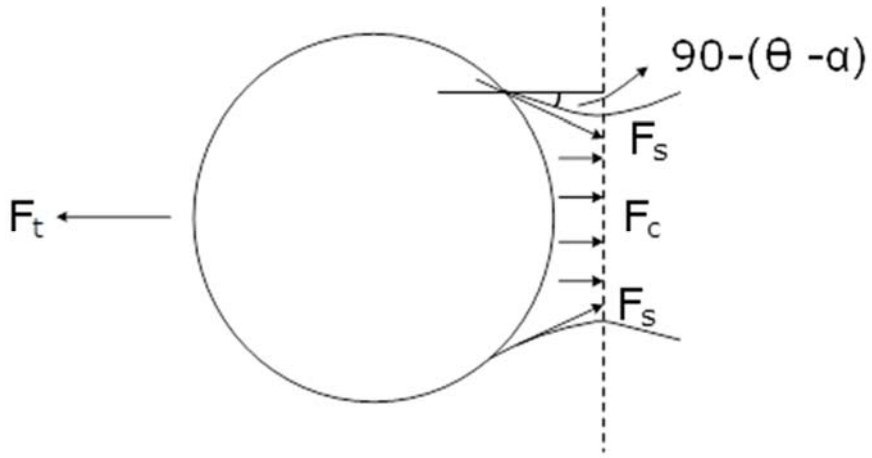

Figure 2.7 One-dimensional free-body diagram of inter-particle bonding forces. (from Kim 2001)

Equation (2-10) uses five parameters, namely, filling angle (θ), contact angle (α), surface tension of the pore-liquid (T_s), diameter of soil particle (d) and a/d ratio. For any given unsaturated soil medium, the average diameter of the sand particles and surface tension of the pore-liquid is generally known or can be determined using known procedures. Contact angle (α) is usually assumed to be zero for very fine sand. But this assumption is debatable and the contact angles may vary from 0˚ (drying front) to as high as 60 to 80˚ (wetting front) (Letey et al. 1962; Malik et al. 1979; Kumar and Malik 1990). The a/d ratio is the ratio of the average distance between the particles to the average diameter of the particles. For perfectly

smooth solids, a/d = 0. But in real soils, a/d = 0 is not possible, as sand particles are not smooth. Generally, values of a/d ratio in the range of 0.005 - 0.05 are considered to be more appropriate for granular materials, depending on the particle size and pore size distributions (Pierrat and Caram 1997; Kim 2001).

Filling angle (θ) is a function of the gravimetric moisture content of the soil. Gravimetric moisture content of the soil is defined as the ratio between the mass of liquid to the mass of the dry soil and is given by the following relation:

$$w = \frac{m_l}{m_s} = \frac{V_l \rho_l}{V_s \rho_s} = \frac{k\left({}^{V_{bridge}}/_{2}\right)\rho_l}{({}^{\pi d^3}/_{6})\rho_s} = \frac{6k}{G_s}.\frac{V_{bridge}}{2\pi d^3} \quad \textbf{(2-11)}$$

where: m_l and m_s are the masses of the liquid and soil particle, respectively; V_l and V_s are the volumes of liquid and soil particle, respectively; k is the mean coordination number, V_{bridge} is the volume of the liquid bridge; G_s is the specific gravity of soil solids; and ρ_l and ρ_s are the water and particle densities, respectively. Several researchers have attempted to calculate the volume of the liquid bridge. Equations derived by Dallavale (1948), Pietsch and Rumpf (1967), Cho and Santamarina (2001) and Lu and Likos (2004) have been used in previous studies. If the moisture content is known, **Equation (2-11)** along with any equation among **Equations (2-12)** to **(2-15)** can be used to calculate filling angle for the corresponding moisture content, assuming α and a/d are constant.

Dallavale (1948)

$$V_{bridge} = \frac{\pi d^3 sin^4 \frac{\theta}{2}}{cos^2 \frac{\theta}{2}}\left[1 - \tan\theta\left(\frac{\pi}{2} - \theta\right)\right] \quad \textbf{(2-12)}$$

Pietsch and Rumpf (1967)

$$V_{bridge} = 2\pi d^3 \left\{ [r^{*2} + (r^* + h^*)^2] r^* \cos(\theta + \alpha) - \frac{r^{*3}\cos(\theta+\alpha)^3}{3} - r^{*2}(r^* + h^*)\left[\cos(\theta+\alpha)\sin(\theta+\alpha)\left(\frac{\pi}{2} - \theta - \alpha\right)\right] - \frac{1}{24}(2+\cos\theta)(1-\cos\theta)^2 \right\} \quad \textbf{(2-13)}$$

Cho and Santamarina (2001)

$$V_{bridge} = \frac{3\pi d^3}{8k}\left(\frac{\mu^4}{1-\mu^4}\right)\left[1 - \frac{\mu(2-\mu)}{2(1-\mu)}\sin^{-1}\left\{\frac{2(1-\mu)}{\mu^2 + 2(1-\mu)}\right\}\right], where\ \mu = \frac{2h}{d} \quad \textbf{(2-14)}$$

Lu and Likos (2004)

$$V_{bridge} = \frac{\pi d^3 sin^2\theta}{4} - \frac{\pi d^3 sin^2\theta\ cos\theta}{4} - \frac{\pi d^3(1-cos\theta)^2(2+cos\theta)}{12} - V_r \quad \textbf{(2-15)}$$

$$where: V_r = \pi\left[h + r - \frac{2}{3}\frac{rcos^3(\theta+\alpha)}{\frac{\pi}{2} - (\theta+\alpha) - sin(\theta+\alpha)\ cos(\theta+\alpha)}\right] r^2[\pi - 2 - sin2(\theta+\alpha)]$$

The contribution of the two dimensionless force components and the total dimensionless force as a function of filling angle is shown in **Figure 2.8** using **Equation (2-13)**, where dimensionless separation distance (a/d) and contact angle (α) are assumed to be 0.025 and 0˚, respectively. As the filling angle increases, liquid bridge grows in size and the length of the contact line between the liquid bridge and soil particle increases. This results in an increase in the magnitude of the force component due to surface tension (F_s), which is the product of the length of the contact line and surface tension of the pore-liquid. However, the force component due to pressure difference (F_c) shows a different trend. Its magnitude increases initially, reaches a maximum value, and eventually starts to decrease. This is because when the filling angle approaches close to 53˚, adjacent liquid bridges start to overlap and the attractive component due to F_c is lost. The dimensionless total force (F_t), however, remains

positive for the entire range of filling angle and the overall effect of the forces due to liquid bridge is attractive in nature.

Figure 2.9 shows the effect of separation distance (a/d) on dimensionless total force (F_t). With the increase in a/d ratio, the magnitude of F_t decreases. The highest magnitude of dimensionless force is observed for perfectly contacting, smooth particles, e.g. glass beads ($a/d = 0$). The inter-particle bonding weakens as the particles move away from each other. **Figure 2.10** shows dimensionless total force (F_t) as a function of contact angle (α). As the contact angle increases, total dimensionless force decreases. With the increasing contact angle, the air-water interface becomes flatter and the pressure difference between air and water phase decreases. Hence, the matric suction as well as the magnitude of total dimensionless force decreases.

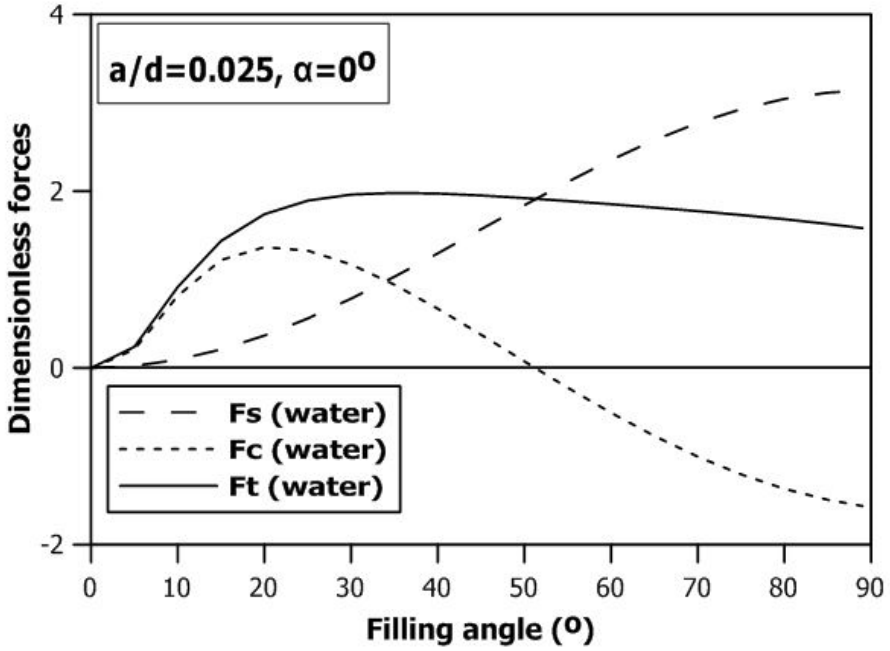

Figure 2.8 Dimensionless force components due to liquid bridge as a function of filling angle

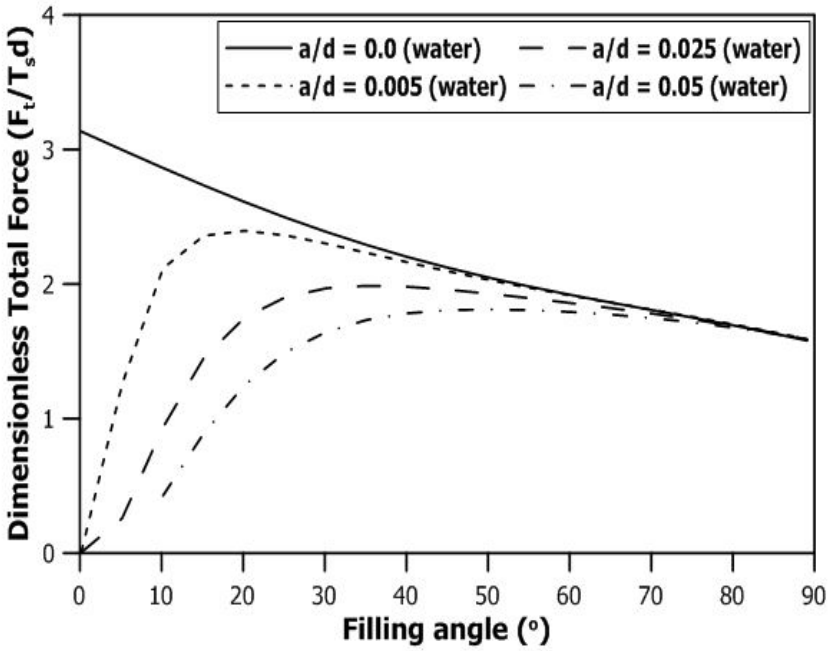

Figure 2.9 Dimensionless total force due to liquid bridge as a function of particle separation distance

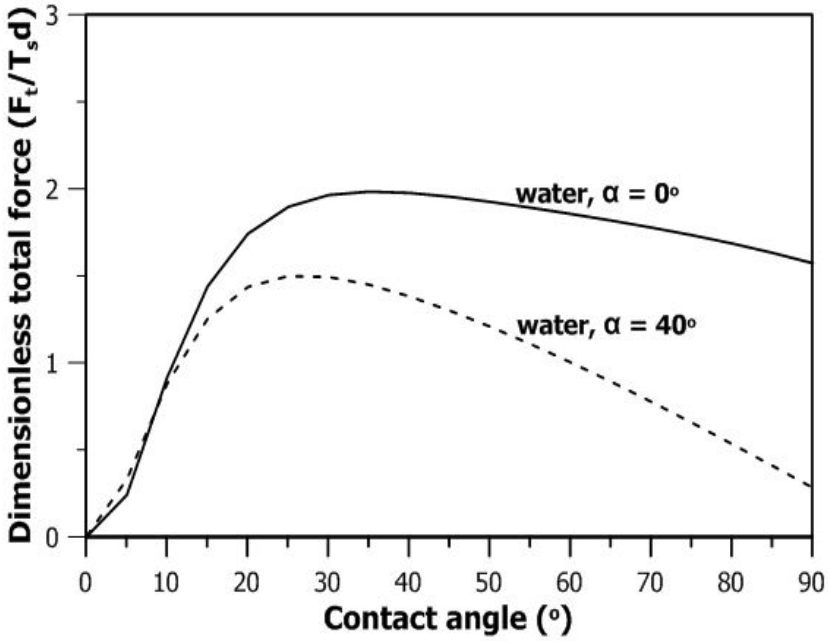

Figure 2.10 Dimensionless total force due to liquid bridge as a function of contact angle

Rumpf (1961) proposed an equation to calculate the tensile strength for granular materials in pendular state based on the two capillary force components as discussed above. The equation was formed on two main assumptions. Primary assumption was that all the particles are idealized as smooth, mono-sized spheres and they are arranged in a uniform packing arrangement. It was also assumed that the liquid bridges are statistically distributed across the surface and over various spatial directions within the soil skeleton. Using **Equation (2-16)**, the tensile strength in pendular state can be given as:

$$\sigma_{tp} = \frac{(1-n_p)}{n_p}.\frac{F_t}{d^2} = \frac{(1-n_p)}{n_p}.\frac{\pi T_s}{d}.\sin\theta\left[\sin(\theta+\alpha) + \frac{\sin\theta}{4}\left(\frac{1}{r^*} - \frac{1}{h^*}\right)\right] \quad \textbf{(2-16)}$$

where: n_p is the porosity of the soil medium. The validity of the above expression is constrained by degrees of saturation within the pendular state. The capillary forces in the liquid bridges gradually diminish with the increase in saturation levels. At higher moisture level, all the liquid bridges increase in volume and merge together to form a continuous liquid phase. In the capillary state, capillary forces exist in the form of negative capillary pressure and interfacial forces at the surface of the unsaturated soil medium (F_s). Funicular state is a transitional saturation state between capillary and pendular states. In this state, either pore spaces fill up completely to form continuous liquid phase or form liquid bridges between soil particles. Therefore, the capillary forces from both surface tension and negative pore water pressure contribute to the total tensile force. Hence, **Equation (2-16)** cannot be directly used to calculate the tensile strength in capillary and funicular states. The capillary forces in the capillary and funicular regimes have to be modeled correctly to account for the tensile strength generated.

Schubert (1984) proposed a model for tensile strength in the capillary regime (σ_{tc}) which is given by the following equation:

$$\sigma_{tc} = SP_c \quad \textbf{(2-17)}$$

where: S is the degree of saturation; and P_c is the capillary pressure (or matric suction). Their values can be determined directly from SMCC or can be estimated using (Schubert 1984):

$$P_c = a'.\frac{1-n_p}{n_p}.\frac{T_s}{d} \quad \textbf{(2-18)}$$

where: a' is a constant that changes with particle size. For particles with a narrow size range, a' = 6~8 and for particles with a wider particle size range, a' = 1.9~14.5.

Schubert (1984) also proposed a model for predicting tensile strength (σ_{tf}) in the funicular state by combining the expressions for the tensile strength in the pendular and capillary state as follows:

$$\sigma_{tf} = \sigma_{tp}.\frac{S_c - S}{S_c - S_f} + \sigma_{tc}.\frac{S - S_f}{S_c - S_f} \quad \textbf{(2-19)}$$

where: σ_{tp} and σ_{tc} are the tensile strength for the pendular and capillary states, respectively. Each term is normalized by establishing saturation boundaries between the three saturation states such that S_c and S_f are the upper saturation limits for the funicular and pendular states, respectively. These saturation limits can be inferred from the general shape of the SMCC for degrees of saturation near the AEV and residual saturation.

Kim (2001) also proposed an equation for calculating the tensile strength beyond the pendular state. The equation predicts that the tensile strength in the funicular and capillary states is a product of degree of saturation and matric suction, both of which can be obtained directly from SMCC. Based on experimental results from Kim (2001), the proposed equation was able to predict the general trend of tensile strength within the funicular and capillary states but further experimental validation of the proposed equation is required.

$$\sigma_{tc\ or\ tf} = S(u_a - u_w) \quad \textbf{(2-20)}$$

2.2.2 Macro-mechanical Model of Tensile Strength

Unlike the micro-mechanical model where soil medium is considered as an agglomerate of discrete, spherical particles, macro-mechanical model uses the concept of suction stress (Lu and Likos 2006) to predict tensile strength of unsaturated granular soils. As

described later in this section, suction stress has also been used to define effective stress in unsaturated coarse-grained soil.

Classical effective stress (σ') equation, developed by Terzaghi (1943), is the difference between total stress (σ) and pore-water pressure (u_w) and is a special case for saturated soils,

$$\sigma' = \sigma - u_w \tag{2-21}$$

Ever since Terzaghi proposed the classical effective stress equation for saturated soils, numerous attempts have been made to formulate a generalized expression which would be applicable to both saturated and unsaturated soils. For unsaturated granular soils, the capillary forces are complex functions of soil particles, pore size and distribution, degree of saturation, matric suction and properties of pore liquid, for example surface tension and contact angle. The true effective stress equation, hence, needs to be more general including both the macroscopic stresses (total stress, pore-air pressure and pore-water pressure) and microscopic interparticle stresses (physicochemical and capillary forces).

When soil is fully saturated, pore-water pressure is compressive in nature and, consequently, the effective stress reduces. On the other hand, when the soil mass is relatively dry, pore water can sustain negative pore-water pressure and pull the soils grains together. This causes an increase in effective stress. Many researchers have attempted to describe the behaviour of soil in the range between the two extremes by extending Terzaghi's classic effective stress equation (Bishop and Blight 1963; Lambe and Whitman 1969; Mitchell 1976; Fredlund and Morgenstern 1977; Kohgo et al. 1993*a*, 1993*b*; Khalili et al. 2004; Lu and Likos 2004, 2006; Lu et al. 2009).

A modified effective stress model was developed by Bishop (1959). In this model, Terzaghi's classic effective stress equation is written as:

$$\sigma' = (\sigma - u_a) + \chi(u_a - u_w) \tag{2-22}$$

where: χ is referred to as effective stress parameter. The quantities $(\sigma - u_a)$ and $(u_a - u_w)$ are known as net normal stress and matric suction, respectively. The component of net normal

stress is applicable to the bulk soil, while the product $\chi(u_a - u_w)$ represents the interparticle stress due to suction. The effective stress parameter varies between zero and unity as a function of the degree of saturation. For $\chi = 0$ (completely dry condition) and $\chi = 1$ (completely saturated condition), equation reduces to Terzaghi's effective stress equation for saturated soils. For χ values between 0 and 1, $\chi(u_a - u_w)$ quantifies the contribution of matric suction to the effective stress. Similar expressions were given by Aitchison and Donald (1956) and Jennings (1961). Bishop (1959) also suggested that the effective stress parameter is equal to the normalized (or equivalent) degree of saturation, S_e.

$$\chi = S_e = \frac{S - S_r}{1 - S_r} \tag{2-23}$$

where: S is the saturation at a given water content; and S_r is the residual saturation.

There are several drawbacks associated with this model. First, it is difficult to measure the value of χ for different soils at different degrees of saturation, both, analytically and experimentally (Lu and Likos 2006). Second, it is believed that combining macroscopic and microscopic stresses into a single equation is incorrect (Burland 1965). Finally, it was shown that on wetting (i.e., reducing suction), unsaturated soil samples collapsed during consolidation tests (Jennings and Burland 1962). Based on **Equation (2-22)**, the effective stress should decrease on reducing the suction and unsaturated soil samples should have expanded. This discrepancy also questions the validity of Bishop's effective stress principle.

Fredlund and Morgenstern (1977) developed an independent stress state variable model to describe the macroscopic behaviour of unsaturated soil in effective stress framework. Net normal stress and matric suction are treated independently in this model. Within this framework, Fredlund et al. (1978) described the shear strength relationship for unsaturated soils as:

$$\tau = c' + (\sigma - u_a)\tan\phi' + (u_a - u_w)\tan\phi^b \tag{2-24}$$

where: c' is the cohesion at zero matric suction and zero net normal stress; ϕ' is the internal friction angle variable associated with the net normal stress variable; and ϕ^b is the internal

friction angle associated with matric suction that describes the rate of increase in shear strength relative to matric suction. The first two terms of the equation comprise the classical Mohr-Coulomb criterion and the third term captures the contribution of matric suction to shear strength. **Figure 2.11** describes the extended Mohr-Coulomb criterion for unsaturated soils.

This approach, similar to Bishop's effective stress approach, has experimental and conceptual limitations related to ϕ^b and its uniqueness over wide range of saturation (Fredlund et al. 1987; Gan et al. 1988). Another drawback of this approach is that it cannot be reconciled with classical soil mechanics, wherein, effective stress (single stress variable) can be used for both shear strength and deformation or volume change analyses (Lu et al. 2010).

Lu et al. (2009) developed a theory based on the concept of suction stress characteristic curve. Suction stress (σ^s) is defined as the isotropic interparticle stress generated through capillary mechanisms in unsaturated soils. Suction stress differs from Terzaghi's classical effective stress in the sense that the forces contributing to the suction stress are in equilibrium at interparticle level and, hence, do not pass from one particle to another. It also differs from Bishop's effective stress concept as it eliminates the need to define the effective stress parameter and only depends on soil suction. The effective stress principle under the framework of suction stress can be expressed as:

$$\sigma' = \sigma - u_a - \sigma^s \qquad \textbf{(2-25)}$$

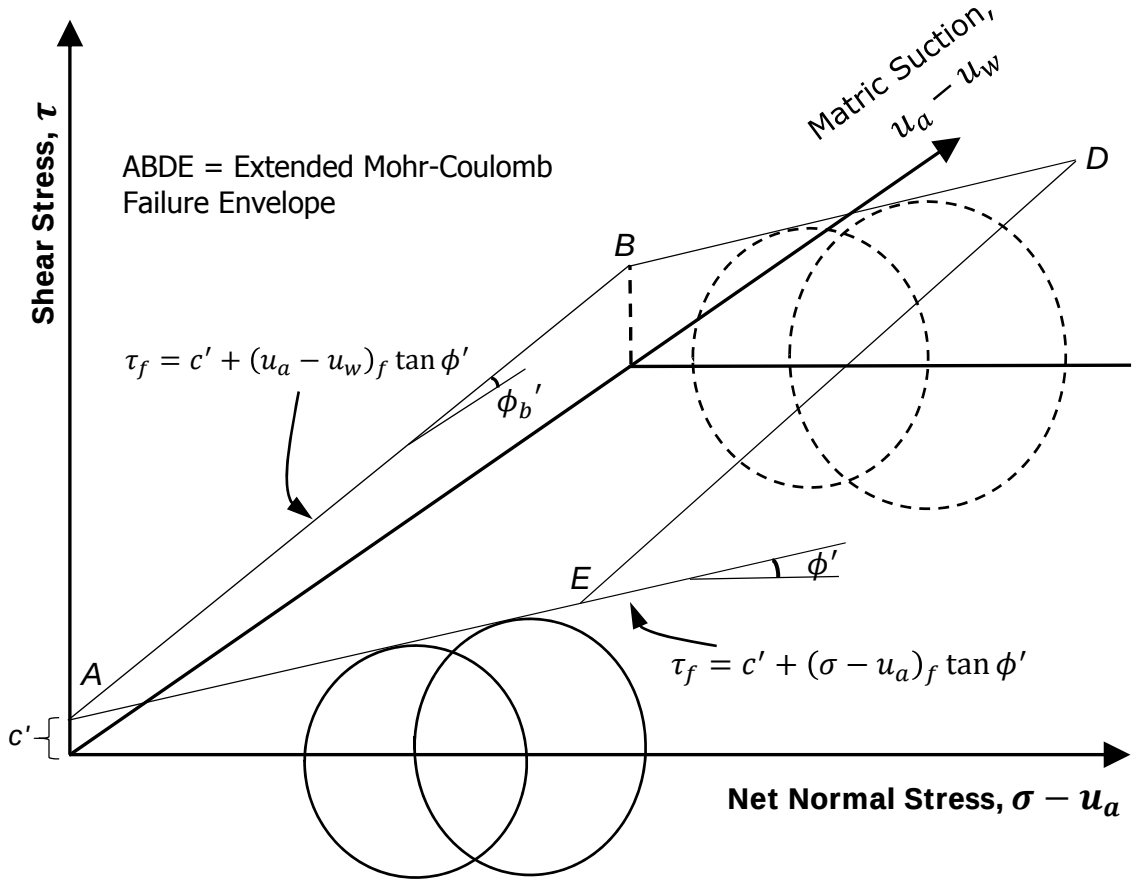

Figure 2.11 Extended Mohr-Coulomb failure envelope for unsaturated soil as suggested by Fredlund and Morgenstern (1977)

Suction stress is a function of soil matric suction and, thus, it depends on degree of saturation as well. A general functional form of σ^s can be given as:

$$\sigma^s = f(u_a - u_w) = f(S) \qquad \textbf{(2-26)}$$

Comparing Equation **(2-26)** to Bishop's effective stress equation **(2-22)**, suction stress can be expressed as:

$$\sigma^s = -(u_a - u_w).S_e \qquad \textbf{(2-27)}$$

The relationship between the soil suction and normalized degree of saturation is given by the model proposed by van Genuchten (1980) as:

$$S_e = \left\{\frac{1}{1 + [\alpha'(u_a - u_w)]^n}\right\}^{1-1/n} \quad \textbf{(2-28)}$$

where: α' and n are the fitting parameters, with α' being the inverse of AEV (kPa^{-1}) and n being the pore size distribution parameter. Closed form expressions of suction stress can be formulated at by substituting **Equation (2-28)** into **Equation (2-27)**; by eliminating matric suction, $(u_a - u_w)$ or normalized degree of saturation (S_e).

$$\sigma^s = -\frac{(u_a - u_w)}{(1 + [\alpha'(u_a - u_w)]^n)^{(n-1)/n}} \quad \textbf{(2-29)}$$

$$\sigma^s = -\frac{S_e}{\alpha'}\left(S_e^{\frac{n}{(1-n)}} - 1\right)^{\frac{1}{n}} \quad \textbf{(2-30)}$$

This definition of suction stress can be used to calculate the tensile strength in unsaturated granular soils. In previous chapter, the concept of tensile strength was introduced by extending the classical Mohr-Coulomb failure envelope beyond the cohesive intercept (C) on the shear stress axis till it touches the negative normal stress axis. This point, shown in **Figure 2.12** on the far left of negative normal stress axis, represents isotropic tensile strength (σ_{ti}). Isotropic tensile strength is defined as the interparticle bonding stress developed in unsaturated granular soil by surface tension and negative pore water pressure (Lu et al. 2009). No shear stress develops when soil fails under isotropic tensile stress and this stress exists with or without the presence of any external stress. Many direct tension tests, developed previously, measures uniaxial tensile strength of unsaturated granular soils. This is represented by σ_{tu} in the **Figure 2.12**. It is defined as the strength mobilized by unsaturated soil under tensile stress applied normal to one principal plane while no stress (compressive or tensile) is applied to the corresponding orthogonal planes. From the **Figure 2.12**, it can be derived that,

$$\frac{C}{\sigma_{ti}} = -\tan\phi \quad \textbf{(2-31)}$$

$$\frac{C}{\sigma_{tu}} = -\frac{1}{2\tan\left(\frac{\pi}{4}-\frac{\phi}{2}\right)} \quad \textbf{(2-32)}$$

Hence, by combining the equations, we get:

$$\frac{\sigma_{tu}}{\sigma_{ti}} = 2\tan\phi\tan\left(\frac{\pi}{4}-\frac{\phi}{2}\right) \quad \textbf{(2-33)}$$

Since suction stress is defined as the isotropic tensile stress, **Equations (2-29)** and **(2-30)** can be combined into **Equation (2-33)** to calculate the uniaxial tensile strength. If the internal angle of friction (ϕ) and van Genuchten SMCC parameters (n and α') are known, **Equations (2-34)** and **(2-35)** can be used to predict uniaxial tensile strength as a function of matric suction or normalized degree of saturation.

$$\sigma_{tu} = 2\tan\phi\tan\left(\frac{\pi}{4}-\frac{\phi}{2}\right)\frac{(u_a-u_w)}{(1+[\alpha'(u_a-u_w)]^n)^{(n-1)/n}} \quad \textbf{(2-34)}$$

$$\sigma_{tu} = 2\tan\phi\tan\left(\frac{\pi}{4}-\frac{\phi}{2}\right)\frac{S_e}{\alpha'}\left(S_e^{\frac{n}{(1-n)}}-1\right)^{\frac{1}{n}} \quad \textbf{(2-35)}$$

From **Equation (2-34)**, it can be seen that macro-mechanical model involves only three parameters, i.e. ϕ, n and α' and these parameters can be determined by common and established experimental methods. There are several established techniques to measure SMCC and van Genuchten parameters (n and α') can be obtained by fitting model SMCC curve with experimental suction values. Direct shear test can be used to calculate the internal angle of friction (ϕ). Several techniques are available in literature which describes direct shear tests on unsaturated sand over wide range of normal stresses (Sture et al. 1998; Khalili and Khabbaz 1998; Kim 2001; Khalili et al. 2004). Compared to nine-parameter micro-mechanical framework, macro-mechanical model uses only four parameters, but the effectiveness and reliability of one model over the other is yet to be verified.

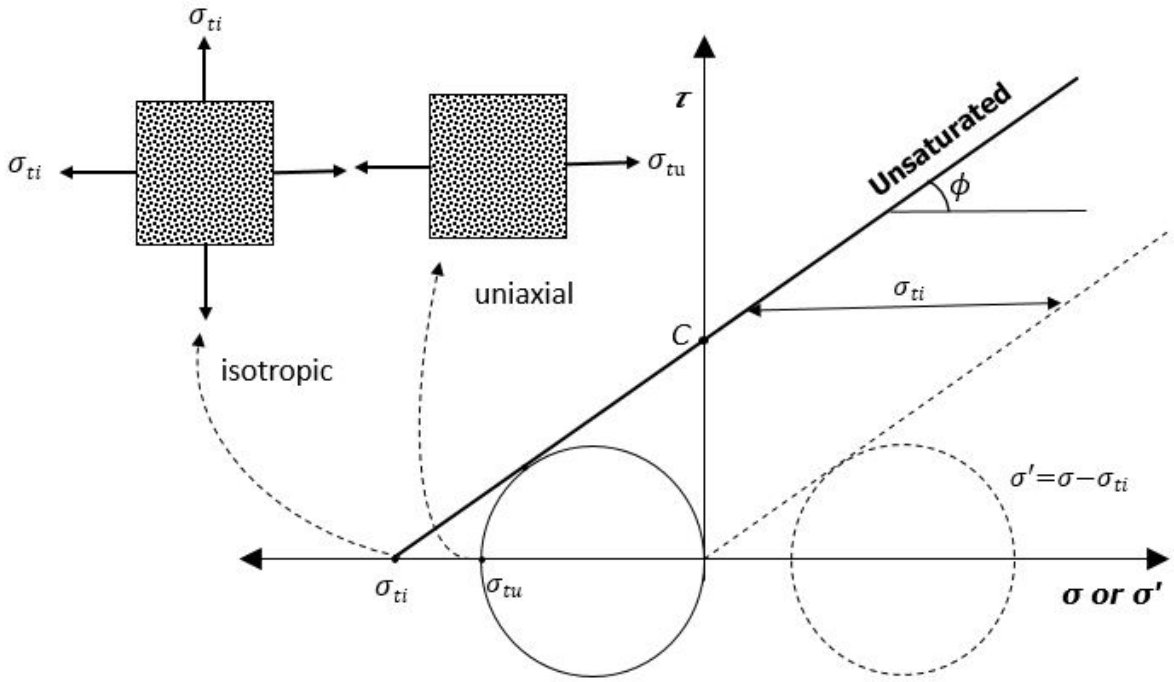

Figure 2.12 Illustration of isotropic tensile strength, uniaxial tensile strength, and apparent cohesion for extended Mohr-Coulomb criterion

2.3 EFFECT OF REDUCED SURFACE TENSION ON MATRIC SUCTION AND TENSILE STRENGTH

Surface tension of pure water can be manipulated by introducing surface-active agents (or surfactants). Reduction in surface tension of the pore-liquid can have a direct impact on the properties of solid-liquid and liquid-gas interfaces. In real-world scenario, various organic compounds are found in the unsaturated zone from either naturally occurring processes (humic substances) or as a result of anthropogenic activities (sub-surface remediation processes). Many scientists have reported that the presence of such compounds might alter the soil-moisture characteristics, hydraulic conductivity and induce unsaturated flow as a result of capillary pressure gradients (Smith 1995; Dury et al. 1998; Smith and Gillham 1999; Bashir 2007; Bashir et al. 2007). In addition, it has been also reported that changes in the 'salt content' of the soil changes would result in a change in the overall volume and strength of the soil (Fredlund and Rahardjo 1993). Hence, these observations need to be taken into account while understanding the role of surface tension of pore-liquid in tensile behaviour of the unsaturated granular soils.

Surface tension of the pore water plays a major role in capillarity. The effect of surface tension on capillary pressure (P_c) and matric suction ($u_a - u_w$) is reflected through **Equation (2-3)**. In terms of negative pressure head, **Equation (2-3)** can be re-written as **Equation (2-36)** (Bear 1972).

$$\Psi = \frac{2T_s \cos \alpha}{\rho_l g R} \quad \textbf{(2-36)}$$

where: Ψ is the soil-water pressure head, ρ_l is the density of the liquid and g is the acceleration due to gravity. It reveals that a decrease in surface tension results in a proportional decrease in capillary pressure.

Surfactants, such as 1-butanol, renex, zonyl, etc., decrease the surface tension of pure water. As surface tension gets reduced, the soil-moisture characteristic curve (SMCC) shifts along the matric suction or negative capillary pressure head axis. According to **Equation (2-3)** and **(2-36)**, this shift is proportional to the change in the surface tension of the corresponding solution to that of distilled water. It also means that at the same saturation levels, two different values of matric suction can be achieved for a soil by altering the surface tension of the pore water. Using this relationship, matric suction in any unsaturated soil system wetted with surfactant is scaled by the ratio of the surface tension of the solution to the surface tension of the water (or any reference liquid). Karagunduz et al. (2001) reported that in addition to surface tension, the presence of surfactant might also alter the contact angle of the liquid-gas interface. Hence, the scaling of SMCC along the suction becomes proportional to the product of surface tension and cosine of contact angle ($T_s \cos \alpha$). These two scaling relationships are described in **Equations (2-37)** and **(2-38)** in terms of pressure head. There are other scaling relationships reported in the literature based on the works of Demond and Roberts (1991), Desai et al. (1992) and Demond et al. (1994).

$$\Psi(w, c) = \frac{T_s}{T_{s0}} \psi(w, c_0) \quad \textbf{(2-37)}$$

$$\Psi(w,c) = \frac{T_s \cos\alpha}{T_{s0} \cos\alpha_0} \psi(w,c_0) \quad \textbf{(2-38)}$$

where: ψ is the pressure head measured at moisture content w and reference concentration c_0; and Ψ is the scaled pressure head at the same moisture content and surfactant concentration c. The scaling relationship represented by **Equation (2-37)** has been used in previous research work to calculate the SMCCs for silica sand wetted with 7% w/w 1-butanol solution (Smith 1995; Dury et al. 1998; Smith and Gillham 1999). **Figure 2.13** shows the SMCCs for silica sand wetted with water and 7% w/w 1-butanol solution (data from Smith and Gillham 1999). The experimental data is fitted using van Genuchten SMCC equation. It can be observed that the ratio of surface tension of 7% w/w 1-butanol solution and distilled water is approximately equal to the ratio of their corresponding matric suction across the entire range of saturation. Further, as the SMCC curve for 7% w/w 1-butanol solution shifts along the suction axis, the water holding capacity (or wettability) of the silica sand decreases significantly.

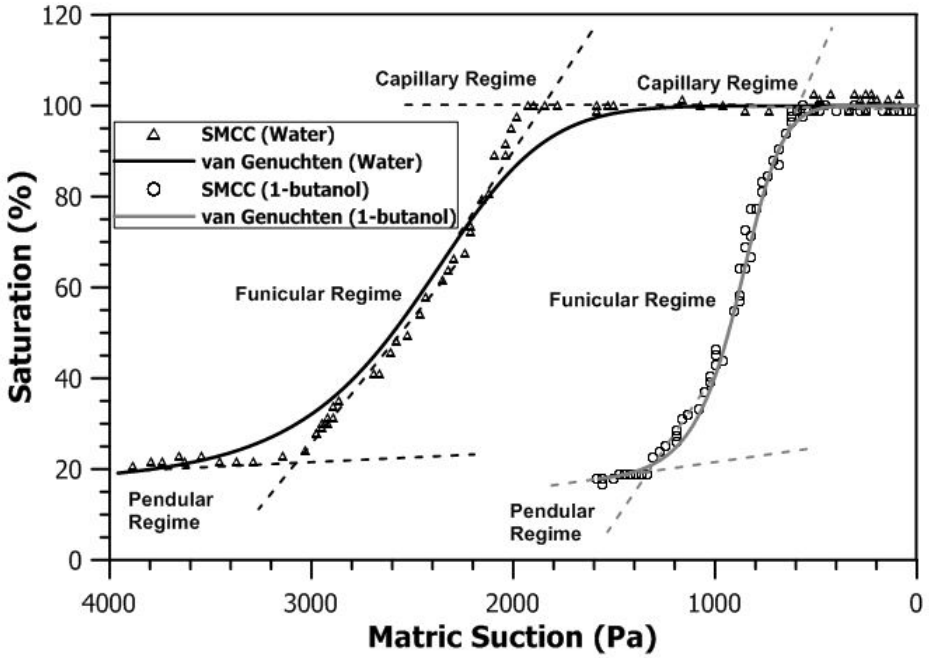

Figure 2.13 SMCCs for silica sand wetted with water and 7% w/w 1-butanol solution (data from Smith and Gillham 1999)

It has been already explained that the matric suction in the unsaturated granular soils contributes to the tensile strength. As the suction is related to the concentration-dependent

surface tension of the pore-liquid, tensile strength of unsaturated sands can also be expected to follow a similar trend. In micro-mechanical model, force components (F_c and F_s) and negative pore-water pressure contribute to the tensile strength. The magnitude of these force components are directly linked to the surface tension of the pore-liquid (see **Equations (2-6), (2-7)** and **(2-10)**). **Figure 2.14** to **Figure 2.16** compare the dimensionless force components as functions of filling angle, contact angle and separation distance for sample wetted with water and 7% w/w 1-butanol solution, respectively. From these figures, it is clear that when surface tension is reduced, the dimensionless force components gets scaled in the ratio of the surface tension of water to 7% w/w 1-butanol solution. **Figure 2.17** compares predicted tensile strength of unsaturated sands wetted with water and 7% w/w 1-butanol solution using the micro-mechanical model. Once again, it can be concluded that the tensile strength decreases significantly when the pore-liquid is changed from distilled water to 7% w/w 1-butanol.

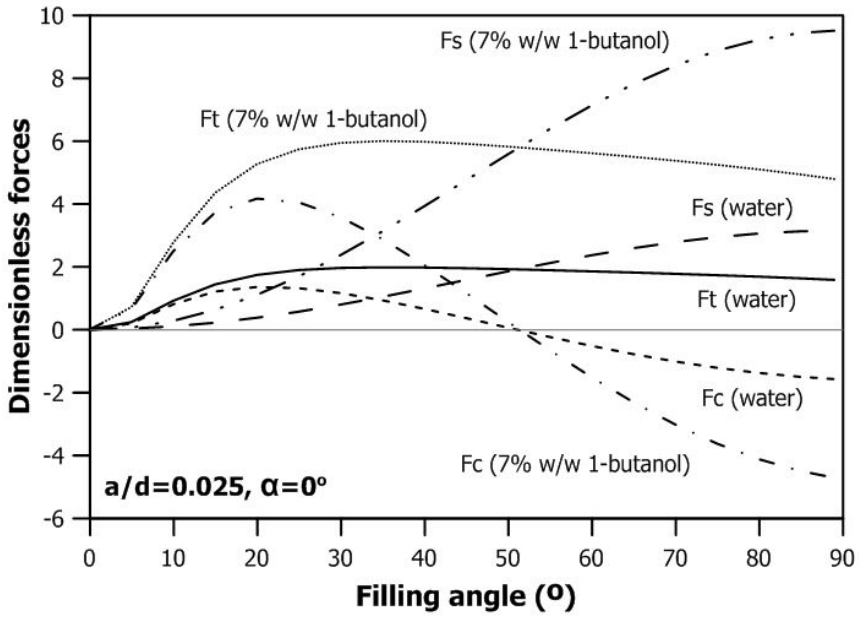

Figure 2.14 Effect of filling angle on dimensionless forces with water and 7% w/w 1-butanol

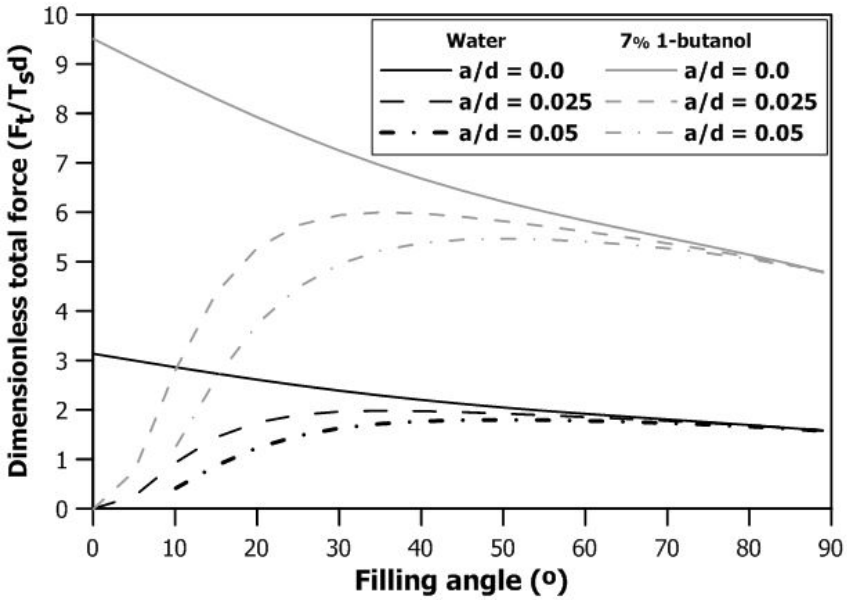

Figure 2.15 Effect of separation distance on dimensionless total force with water and 7% w/w 1-butanol solution (*α=0°*)

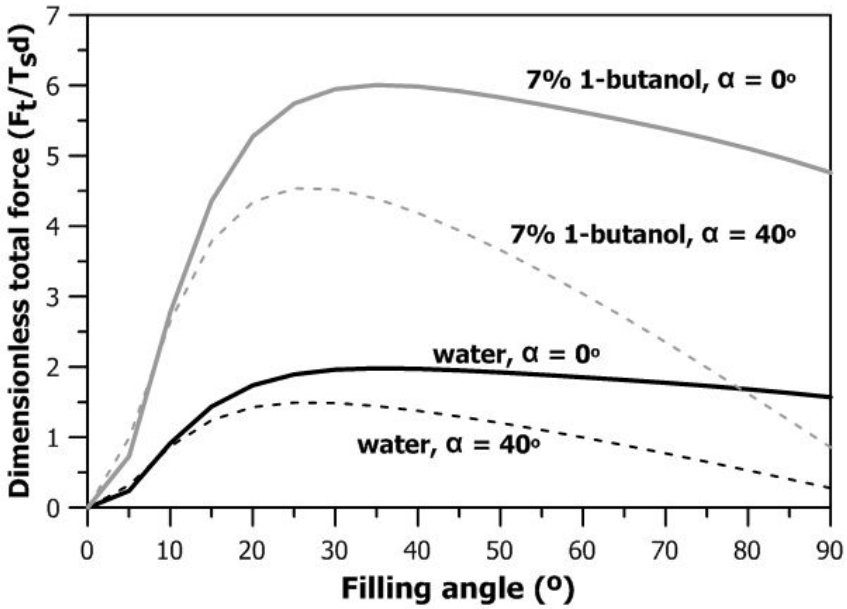

Figure 2.16 Effect of contact angle on dimensionless total force for water and 7% w/w 1-butanol solution (*a/d=0.025*)

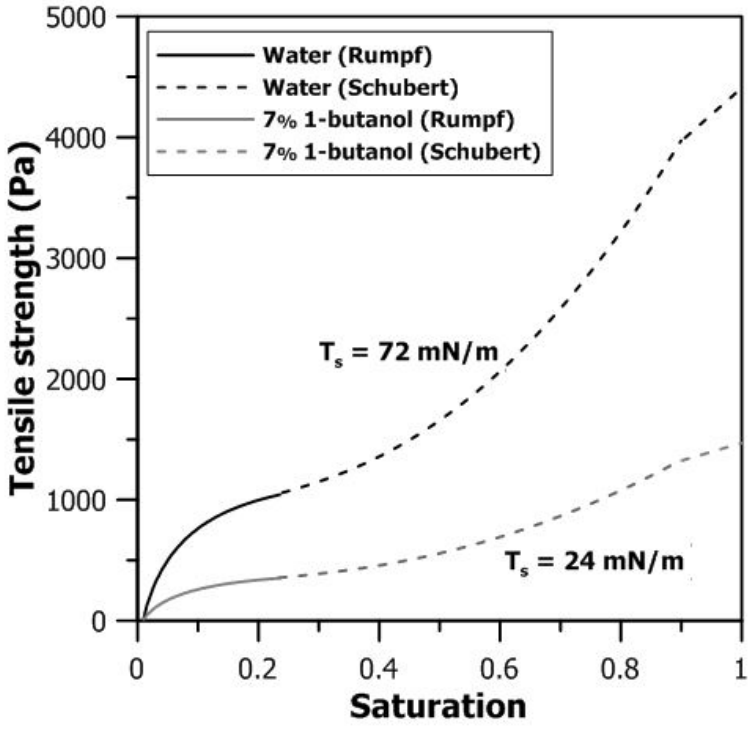

Figure 2.17 Predicted tensile strength of unsaturated sands for water and 7% w/w butanol solution using micro-mechanical model

According to the macro-mechanical model, the uniaxial tensile strength of unsaturated sands, given by **Equations (2-37)** and **(2-38),** is based on matric suction at a given saturation, internal friction angle and van Genuchten SMCC fitting parameters (n and α'). **Figure 2.18** shows a comparison of tensile strength model curves and SMCCs for water and 7% w/w 1-butanol solution cases using macro-mechanical model. As the SMCC shifts on the suction axis due to reduced surface tension of 7% w/w 1-butanol, the α' parameter also gets reduced by a factor equal to the ratio of surface tension of 7% w/w 1-butanol to pure water. As a result, the tensile strength decreases significantly in case of 7% w/w 1-butanol.

The effect of surface tension on matric suction and tensile strength can be qualitatively understood through both micro-mechanical and macro-mechanical models. However, both these models are based on many assumptions and idealizations and may not be truly representative of real soils. Hence, it is important to carry out experimental studies to comprehend the effect of concentration-dependent surface tension on tensile strength behaviour of unsaturated granular soils. Theoretical models must be validated against the experimental results and their efficacies and drawbacks must be analyzed.

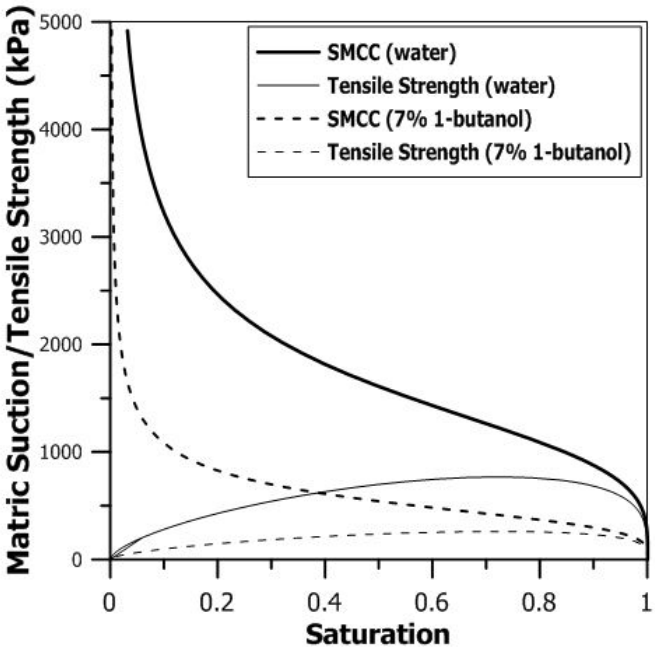

Figure 2.18 Tensile strength characteristic curve for water and 7% w/w 1-butanol solution using macro-mechanical model

2.4 REVIEW OF TENSILE STRENGTH EXPERIMENTS ON UNSATURATED GRANULAR MATERIALS

2.4.1 Pietsch and Rumpf 1967 & Pietsch 1968

Pietsch (1968) performed experiments on eight different limestone fractions with average particle size in the range of 0.004 mm to 0.22 mm. The tensile testing equipment was custom-built to load cylindrical pellets made out of limestone fractions at various moisture content levels. Water was used to prepare unsaturated specimens and the degree of saturation was in the range of 2% to 80%. Pietsch reported certain limitations for preparing samples below 2% or higher than 80%. Some of the results have been highlighted in **Figure 2.19**. The tensile strength increased sharply and reached a plateau value in the pendular state. In the funicular state, the tensile strength increased due to the attractive forces of liquid bridges and saturated voids that contribute to the bonding of the granular agglomerates. Tensile tests beyond the funicular state were not performed due to experimental limitations. The experimental results have also been compared with theoretical equations proposed by Pietsch (1968) and Pietsch and Rumpf (1967). The predicted curves were able to capture the general trend in tensile

strength in pendular and funicular states. It is expected that the tensile strength decreases in the capillary state and would ultimately become zero at full saturation. However, the predicted curve does not reflect this expected trend.

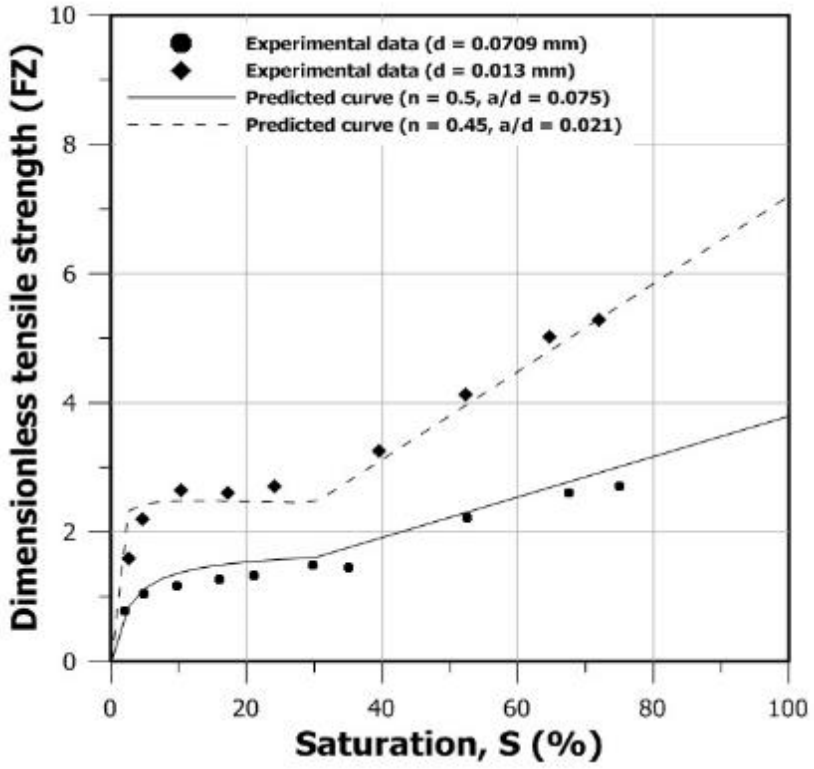

Figure 2.19 Tensile strength of limestone agglomerates. (Pietsch et al. 1968)

2.4.2 Schubert 1984

In 1984, Schubert studied the tensile strength behaviour in moist glass beads due to capillary forces. Following the micro-mechanical model, two mono-sized, smooth spherical particles were considered with moisture present in the agglomerate in the form of liquid bridge between the particles. Tensile strength in the pendular state can be calculated using Rumpf's model with good accuracy. It was proposed that the tensile strength of the moist granular media in the capillary zone was a linear function of the capillary pressure (p_c) and was equal to the product of degree of saturation and capillary pressure corresponding to the saturation level. In the funicular state, tensile mechanisms from both the pendular and capillary states contributed to the overall strength. The contribution of each mechanism was considered to be a function of

normalized saturation (**Equation (2-19)**). This new model was significantly different from the Pietsch and Rumpf model as it could predict tensile strength in capillary state more accurately.

Schubert (1979) measured the tensile strength of limestone agglomerates using a split-table direct tension apparatus, which is described in details in **Section 2.5**. The experimental data was compared with Schubert's (1984) model. The comparison is shown in **Figure 2.20**. The tensile strength increased with saturation in the pendular and funicular state. In the capillary state, the tensile strength decreased to zero very steeply. When compared to experimental results, Schubert's model followed the trend in the capillary state almost perfectly. But the model over-predicted the tensile strength in the funicular state. A possible reason could be the over-simplification of the tensile mechanisms in the funicular state (Kim 2001).

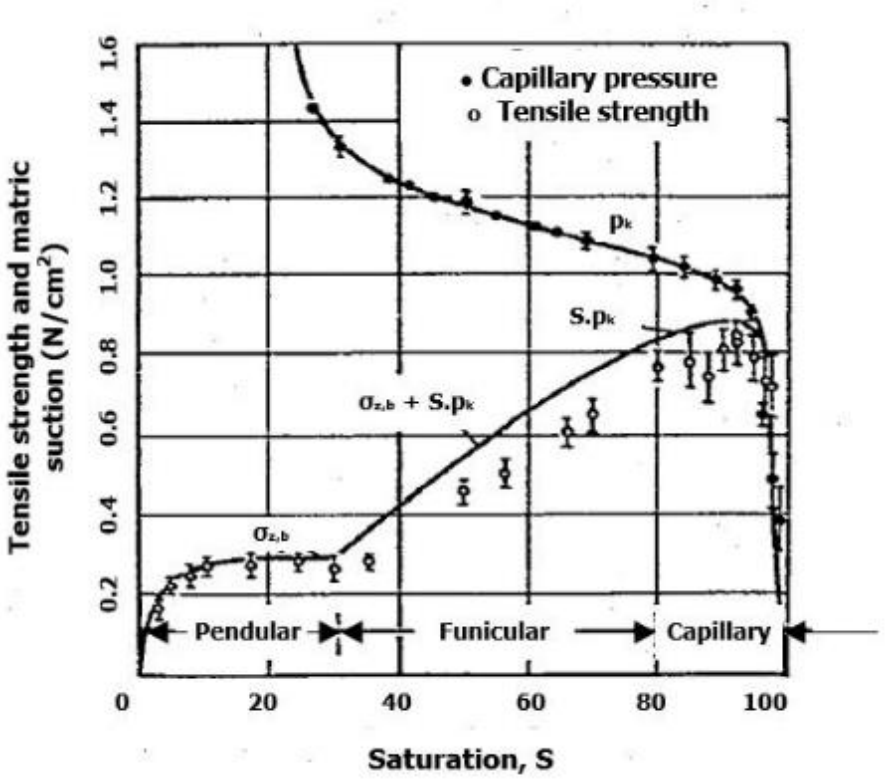

Figure 2.20 Measured and predicted tensile strength values and measure capillary pressure of moist agglomerates (data from Schubert 1979; figure from Schubert 1984)

2.4.3 Mikulitsch and Gudehus 1995

Mikulitsch and Gudehus (1995) performed direct tension experiments on disturbed specimens of sand and silts at different void ratios and degrees of saturation. The experimental results for four different soil samples have been summarized in **Figure 2.21**. It was observed that the tensile strength depends on both the void ratio and degree of saturation. With the increase in saturation, the tensile strength initially increased up to a peak strength. After reaching this maximum value, the tensile strength started to show a decreasing trend with increase in saturation. Samples with lower void ratio showed higher tensile strength and vice versa. However, this effect was less prominent at very low and very high saturation states. The peak tensile strength also decreased with increasing void ratio of the specimen. Besides, the saturation level at which the peak strength was observed shifted towards higher saturation levels with increase in void ratio.

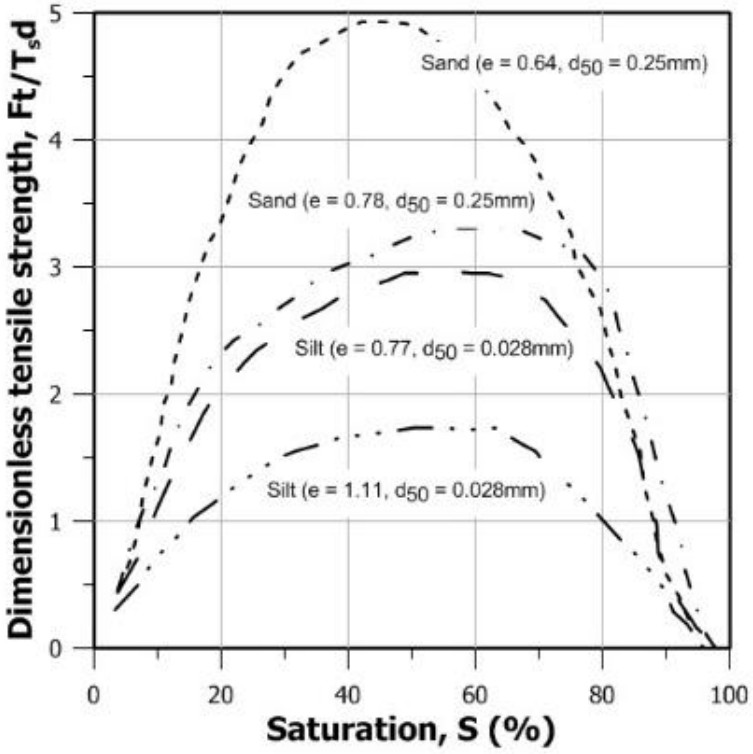

Figure 2.21 Tensile strength of sands and silts. (Data from Mikulitsch and Gudehus 1995)

2.4.4 Pierrat and Caram 1997

In 1997, Pierrat and Caram performed tensile tests on glass beads using split cell tester developed by Hartley and Parfitt (1984). Experiments were performed on glass beads of average diameter 0.093 mm with packing density of 2.46 g/cm^3. The samples were tested at low saturation levels only (i.e. within the pendular state). This was done to study the effects of moisture on the tensile strength of the glass beads particularly at very low moisture contents and to check the efficacy of Rumpf's model to predict tensile strength in pendular state. Five different solutions with different surface tensions were used to study the effect of surface tension on the tensile strength.

Figure 2.22 shows tensile strength of glass beads as a function of saturation when wetted with water up to a saturation level of 30%. The experimental results were compared with predicted values using the Rumpf's model. The predicted values were calculated using a void ratio of 0.45 and dimensionless separation distances of 0.035 and 0.09. The model clearly over-predicted the experimental results for a/d = 0.035. However, the model curve followed the expected trend with a sharp increase in tensile strength at lower saturation and plateau value for higher saturation levels within the pendular state. For a/d = 0.09, the model values were relatively closer to the experimental results but did not follow the trend perfectly.

Table 2.1 compares the ratio of the tensile strength and surface tension of distilled water to other solutions. It was observed that the ratio of decrease in tensile strength of glass beads was almost equal to the ratio of the surface tension of distilled water to other solutions. This result is in complete agreement with the micro-mechanical model and the scaling relationship defined by **Equation (2-37)**. However, the validity of the micro-mechanical model and scaling relationship to study the effect of surface tension on tensile strength of granular soils is yet to be verified.

Table 2.1 Ratio of tensile strength and surface tension (Pierrat and Caram 1997)

Solution used	Water	Zonyl	Renex	Aquashed	SLS
Tensile Strength (Pa)	1007.6	229.4	467.4	496	531.2
Ratio of Tensile Strength	1	0.228	0.464	0.492	0.527
Ratio of Surface Tension	1	0.278	0.444	0.482	0.533

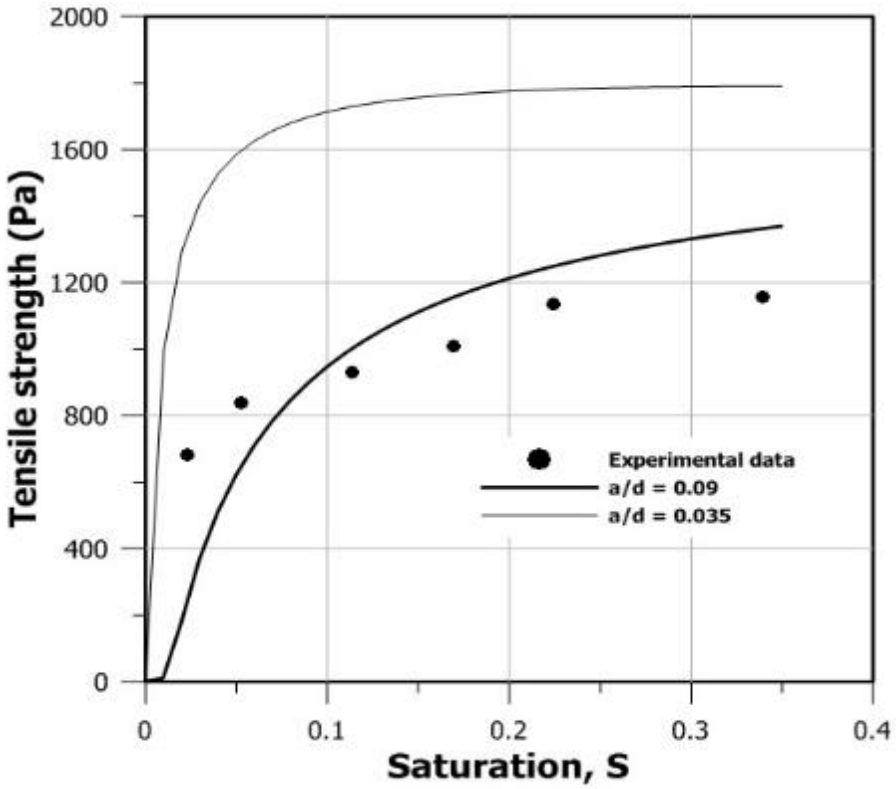

Figure 2.22 Tensile strength of glass beads from Peirrat and Caram (1997) and comparison with Rumpf's model (d = 0.093 mm; e = 0.45)

2.4.5 Kim 2001

A series of direct tension tests were carried out by Kim (2001) on two different gradations of F-75 Ottawa sand - with no fines (particles smaller than 0.075 mm) and with 2% fines. The direct tension apparatus used was a modified version of the equipment described by Perkins (1991) and is described in **Section 2.5** of the thesis. Three different relative densities were used (D_r = 30%, 50% and 70%) and ten different water contents in the range of 0.3% to 18% were adopted. The results of the two F-75 variety of sand with no fines and with 2% fines are shown in **Figure 2.23**. The experimental results obtained from the F-75 Ottawa sand (with no fines and D_r = 50%) were compared with the theoretical prediction micro-mechanical model (**Figure 2.24**). In pendular state, the experimental data fitted well with the theoretical model. However, at higher saturation levels, the model deviated from the experimental results. The experimental tensile strength shows a decreasing trend after reaching water content of 15%. But Schubert's model continued to show an increasing trend in the funicular and capillary states. As mentioned earlier, this discrepancy is possibly due to the oversimplification of the tensile mechanisms in funicular and capillary state in Schubert's model (Kim 2001; Kim and Sture 2008). A modified model was proposed in which capillary pressure from experimentally calculated drying and wetting curves of SMCC for F-75 Ottawa sand was used to calculate the tensile strength instead of the equations proposed by Schubert's model (**Equation (2-20)**). The modified model using the drying curve of SMCC predicted the experimental results with more accuracy and followed the general trend. However, the model using the wetting curve under predicted the tensile strength and prediction of the tensile strength beyond the saturation level of 55% was not possible.

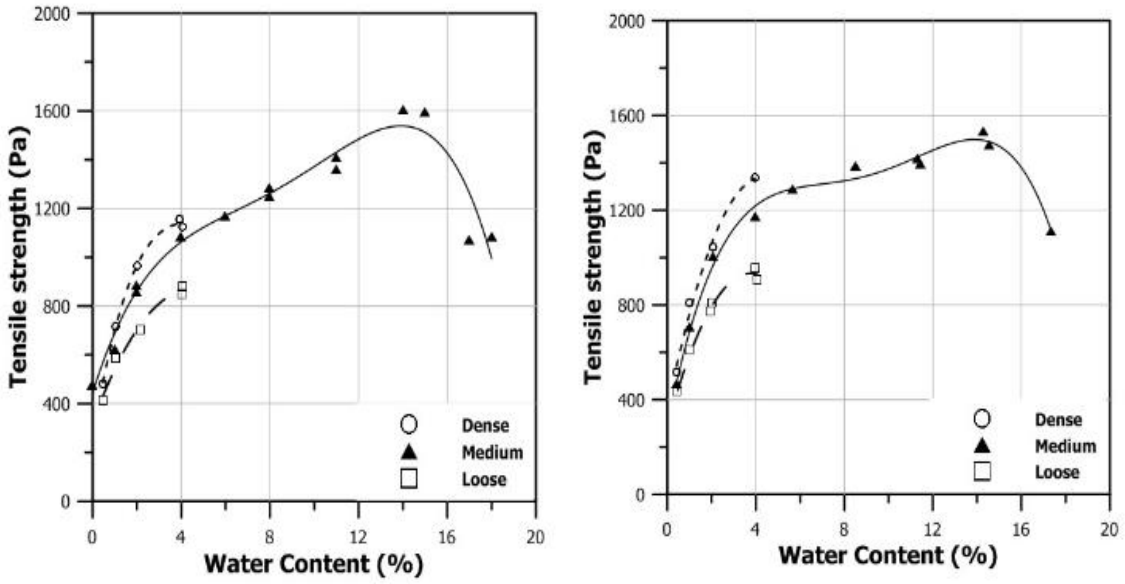

Figure 2.23 Tensile strength of F-75 Ottawa sand, (a) with no fines; (b) with 2% fines (Kim 2001)

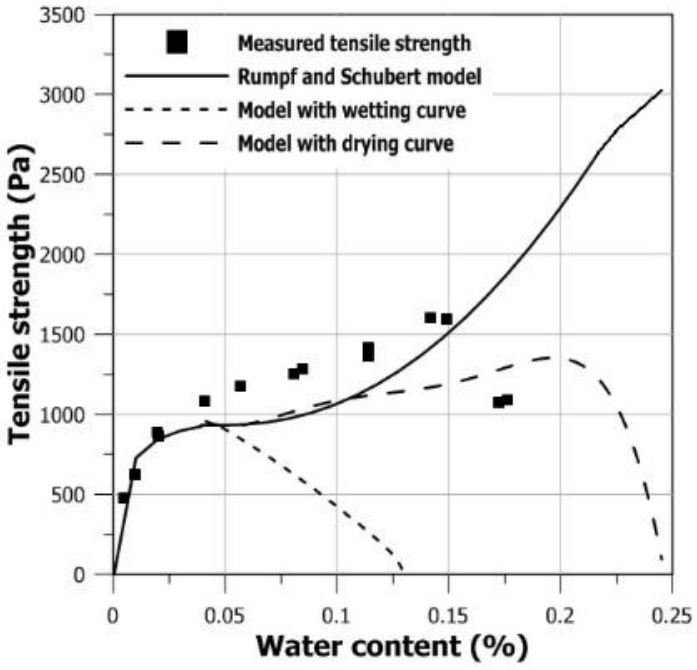

Figure 2.24 Comparison of experimental tensile strength data with theoretical prediction for F-75 Ottawa sand with no fines (Kim 2001)

2.4.6 Lu et al. 2007

Lu et al. (2005, 2007) investigated the magnitude and characteristics of the tensile strength in granular soils. Tensile strength measurements were performed over the full range of saturation. Samples were prepared using silica sand with a wide range of particles sizes – from silty sand (d_{mean} = 0.105 mm) to fine (d_{mean} =0.167 mm) and medium sand (d_{mean} =0.451 mm). Distilled water was used to prepare unsaturated specimens. The direct tensile testing equipment used for the measurements has been explained in details in **Section 2.5**. While the tests on silty sands were done at a porosity of 0.45, tension tests were performed at two different porosities for fine sand (n = 0.45 and 0.37) and medium sand (n = 0.4 and 0.47). The results from the direct tension tests have been summarized in the **Figure 2.25**. It was observed that in case of silty sand, the tensile strength increases steeply up to a saturation of 20% and then decreases. For fine sand, the tensile strength showed two peak values at saturation of 20% and 90%. In case of medium sands, the tensile strength increased almost linearly until capillary saturation. The experimental measurements of tensile strength were compared with the predicted values using micro-mechanical model (**Figure 2.26**). It can be seen that the comparisons were made within the pendular state only. The model curve over-predicted the experimental results at a contact angle of 0˚. No comparisons were made between the theoretical predictions and experimental values in the funicular and capillary states. It is interesting to note that the three different sands used for direct tension tests show different tensile behaviour beyond the pendular state.

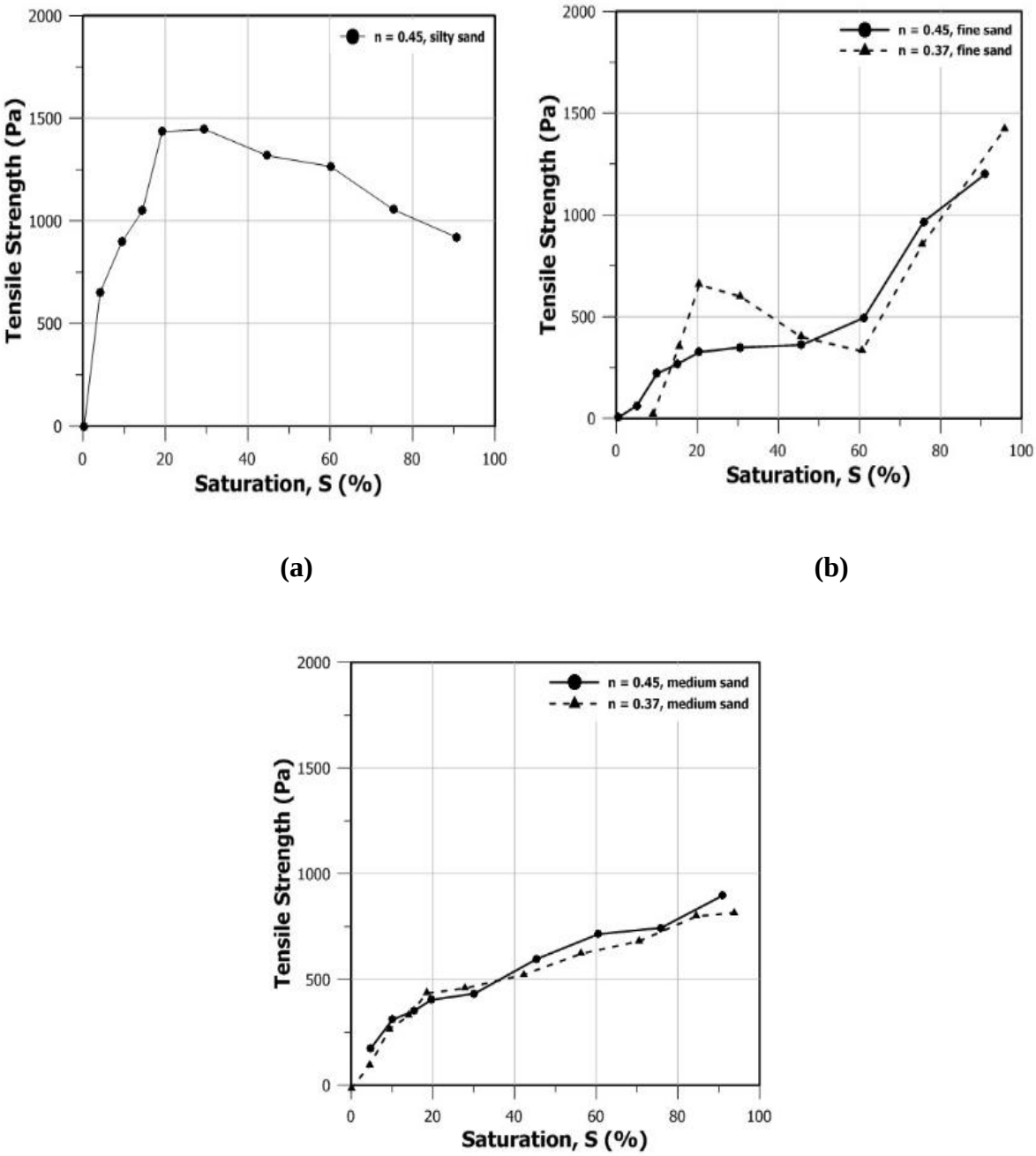

(a) **(b)**

(c)

Figure 2.25 Measured tensile strength of (a) silty, (b) fine and (c) medium sands (Lu et al. 2007)

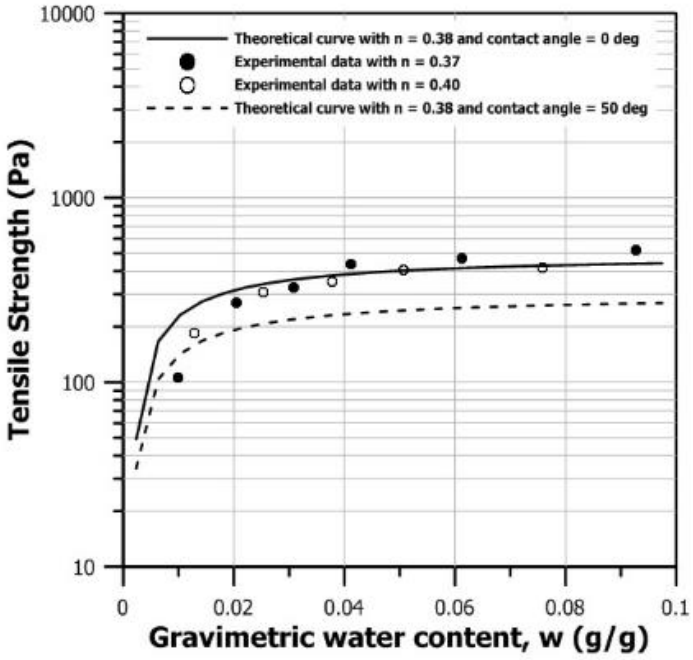

Figure 2.26 Comparison of tensile strength between measured and theoretical values for medium sand: d = 0.452 mm and a/d = 0.05 (Lu et al. 2007)

2.4.7 Lu et al. 2009

Lu et al. (2009) developed the tensile strength model for unsaturated sand by considering suction stress concept proposed by Lu and Likos (2006). Experimental results from Lu et al. (2007) and Kim and Sture (2008) were compared with the theoretical curves predicted by new model (macro-mechanical model). Tensile tests were also performed on Esperance sand using the direct tension apparatus described by Lu et al. (2005, 2007) and compared with theoretical predictions. The results are plotted in the **Figure 2.27 to Figure 2.29**. It was observed that the theoretical prediction accords well with the experimental values obtained for the three different sands over entire range of saturation. However, the model fit the experimental data at higher values of internal friction angles (~50˚ to 70˚). Although the internal friction angle can be expected to increase significantly for most soils under small normal stresses (Sture et al. 1998; Likos et al. 2007; Lu et al. 2009), further investigations are needed to confirm the high internal friction angle in unsaturated soils at small normal stress and non-linear yield behaviour of unsaturated sands at small normal stress. Since only distilled water was used, the efficacy of model to predict the tensile strength of unsaturated sands when surface tension of the pore-liquid is manipulated is yet to be established.

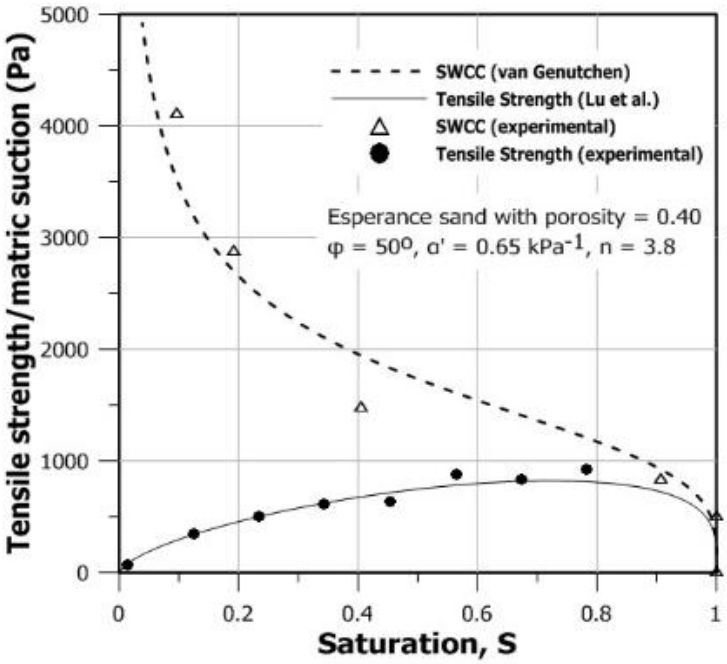

(a)

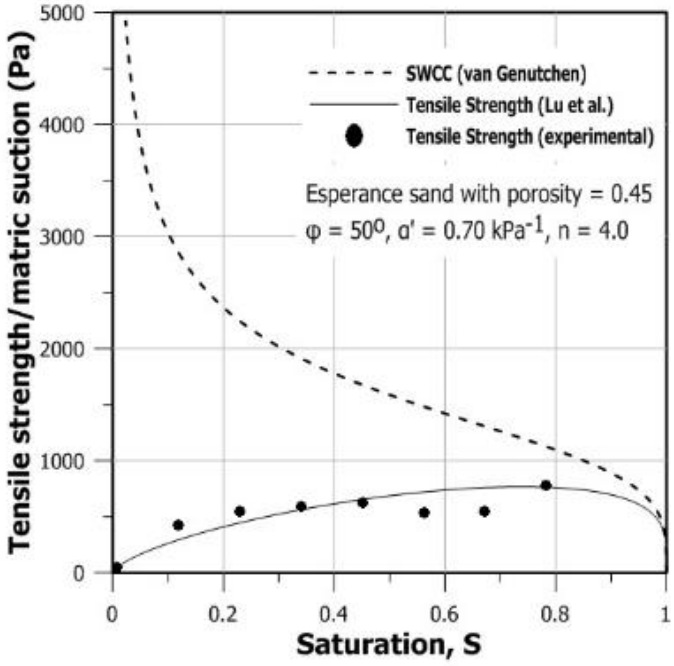

(b)

Figure 2.27 Tensile strength and SMCC of Esperance sand and it comparison with predicted values: (a) *n* = 0.4; (b) *n* = 0.45 (Lu et al. 2009)

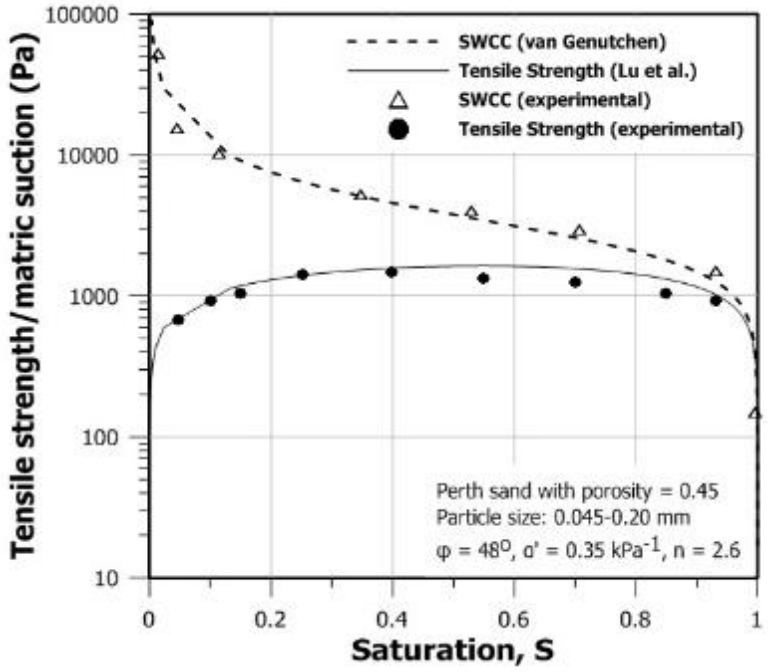

(a)

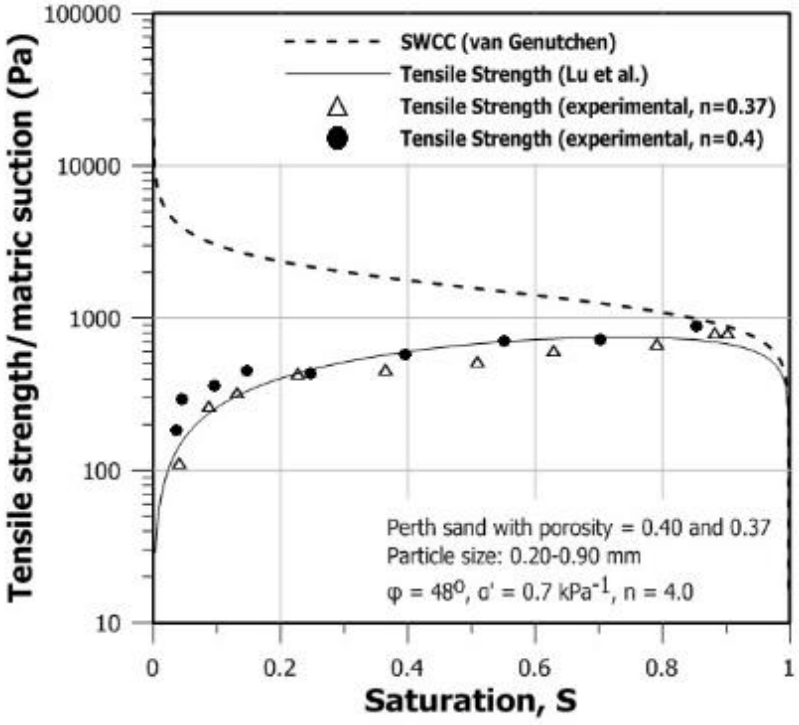

(b)

Figure 2.28 Tensile strength and SWCC of Perth sand and it comparison with predicted values: (a) *n* = 0.45; (b) *n* = 0.40 and 0.37 (Lu et al. 2009)

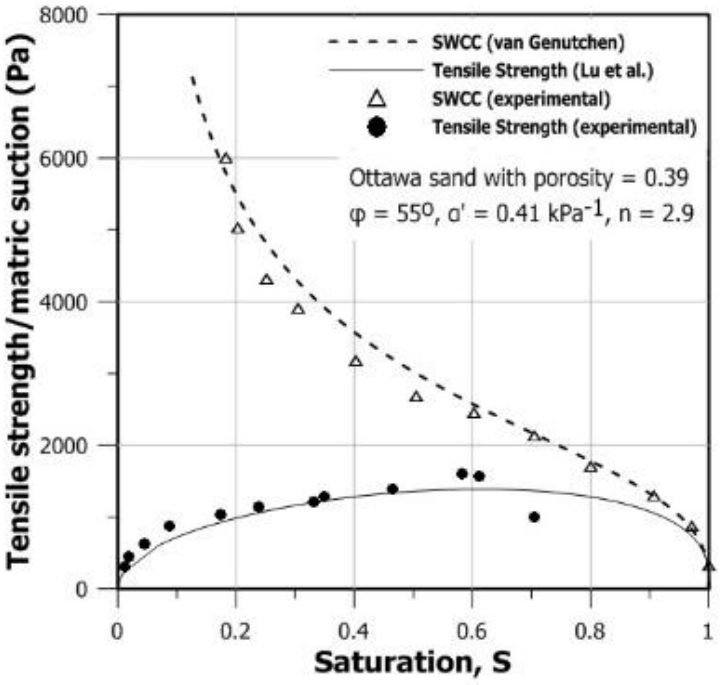

(a)

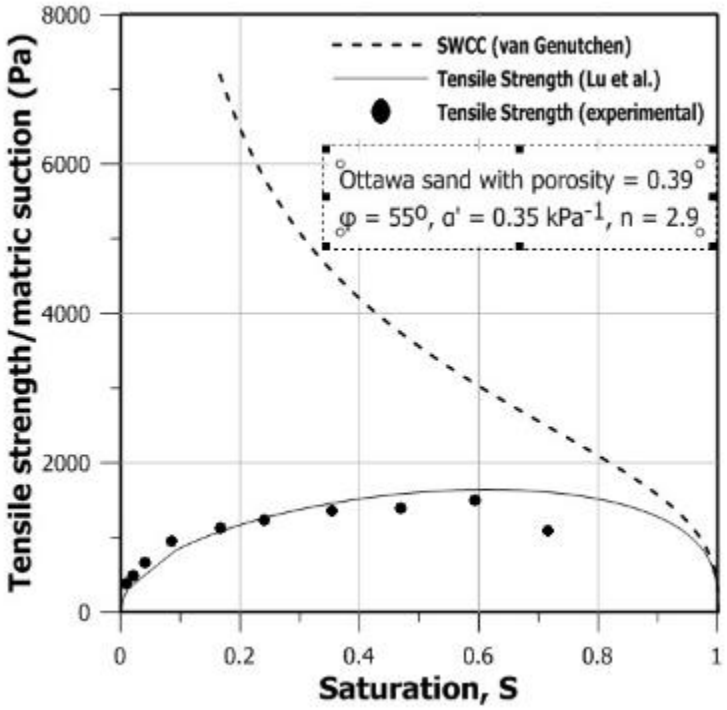

(b)

Figure 2.29 Tensile strength and SWCC of Ottawa sand and it comparison with predicted values: (a) with no fines; (b) with 2% fines (Lu et al. 2009)

2.5 REVIEW OF TENSILE STRENGTH MEASUREMENT TECHNIQUES

To estimate the tensile strength of soils, several apparatus have been designed and constructed. Based on the literature, the available test methods for tensile testing of soils can be grouped into direct tension, indirect tension and other tests. Other tests includes hollow cylinder test, double punch test and tri-axial extension test. In this section, main focus has been given to review direct tension tests. Direct tension tests measure the uniaxial tensile strength of unsaturated sands. This means that during a direct tension test, specimen is subjected to tensile stresses on principal plane and zero stress in other orthogonal planes. Further these stresses should be uniform throughout the specimen such that no bending or flexure, or stress concentration occur. The tensile force is directly applied to the specimen along its longitudinal axis until failure occurs. The tensile strength can be calculated from the failure load and the cross sectional area upon which the load acts. The direct tension apparatus used in this research is also based on the principle of direct uniaxial tension.

There are very limited number of tensile testing apparatuses available for unsaturated sands. Most of them have been derived from the techniques originally developed for fine-grained and cemented soils. As a result, some tensile tests related to clays and clayey silts are also discussed herein.

Tschebotarioff et al. (1953) conducted tensile strength testing of four different clays to study the effect of clay mineralogy on the stress-strain behaviour. Clay soils were compacted into a briquette-shaped mould that had a length of 132 cm with a reduced rectangular central section of 15.2 cm x 7.6 cm x 40.7 cm as shown in **Figure 2.30(a)**. The pulling load was applied horizontally through the movable end of the metal supports that encased the edges as shown in **Figure 2.30(b)**. Strain measurements were made using extensometers which were attached to the central necked portion of the specimen. The specimen was supported by ball-bearing rollers to prevent sagging of the specimen. However, sagging at the central portion of the specimen and bending under self-weight were still a concern due to the large specimen size. The oversized bell-shape of the specimen might have also contributed to the non-uniform stress distribution across the specimen.

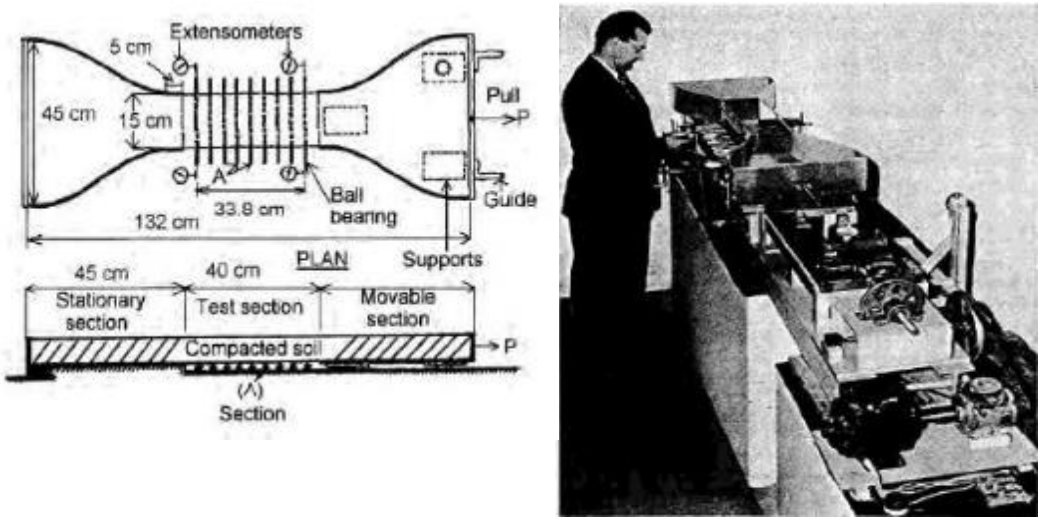

(a) **(b)**

Figure 2.30 Direct tension test for clays (a) Shape of the tensile specimen, (b) tensile test apparatus. (Tschebotarioff et al. 1953)

Conlon (1966) conducted unconfined tension experiments on a soft clayey silt, having liquid limit of 22 and plasticity index of 4. The specimen was similar to that used in the conventional tri-axial apparatus with the exception of the central portion of the specimen. It was necked down to induce tensile failure in this constricted zone and to reduce the necking effects (**Figure 2.31**). Each end of the specimen was held by split rings clamped at the ends of the specimen and the loading head. The inside of the split rings was lined with a fine emery paper to promote interlocking of the specimen with the cylindrical clamp. A ball and socket arrangements were used at both ends of the specimen to avoid bending or flexure. The maximum tensile strength of about 16.6 kPa was reported at an axial deformation of 0.0254 cm. This apparatus had many disadvantages. The split rings caused stress concentrations at end of the specimen and thus, uniform stress distribution across the specimen was questionable. It was also difficult to determine the effective length of the specimen, which rendered the strain measurements unreliable.

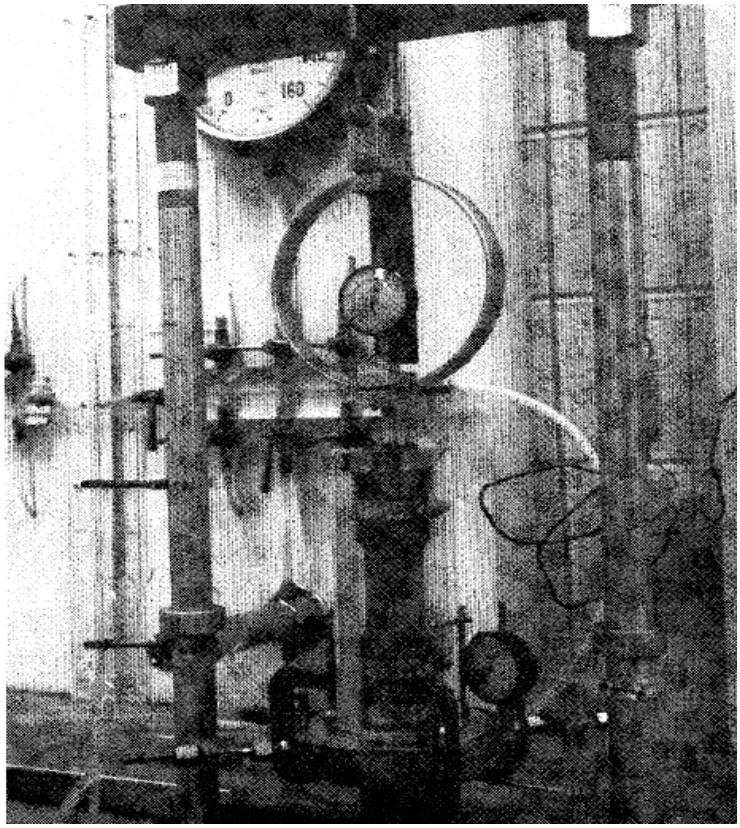

Figure 2.31 Set-up for direct tension test developed by Conlon (1966)

Bishop and Garga (1969) used similar tri-axial extension tests on soil specimens with reduced cross-section at the center. Confining pressure was used to produce tensile stresses instead of pulling the ends of the specimen. The main idea behind this approach was to develop tensile vertical stress at the central reduced cross-section of the specimen while the stresses at the end of the specimen were compressive. The tests were conducted tests on undisturbed London Clay having liquid limit of 75 and plasticity index of 46. The tensile strength was found to be in the range of 26.6 kPa to 33.2 kPa with axial extension strains at failure ranging between 2.2% to 16.7%. The tri-axial apparatus used in this study is shown in **Figure 2.32** and was used to test a soil specimen of 2.54 cm in diameter at the ends and 14.24 cm high. The central part of the specimen was necked down to 1.9 cm in diameter. One of the major drawbacks of the setup was that it could not make accurate strain measurements, since only the necked part of the specimen was in tension and the rest of the specimen was in compression.

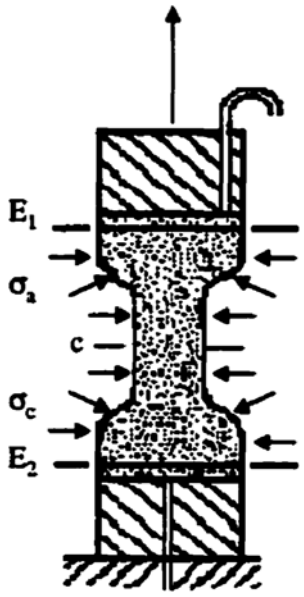

Figure 2.32 Bishop and Garga's tensile testing apparatus

The techniques described so-far are mainly suited for clay, clayey silts or cemented soils which can be tested in tri-axial apparatus. There are many other tensile testing techniques available in literature for fine-grained soils (Haefeli 1951; Uchida and Matsumoto 1961; Hasegawa and Ikeuti 1964; Ajaz and Parry 1976; Krishnayya et al. 1974; Snyder and Miller 1985; Leavell and Peters 1987; Heibrock et al. 2005). The techniques discussed above are not suitable for coarse-grained soils such as sand, because of the difficulty in preparation of the specimen for tri-axial testing. The tensile strength of granular soil could be measured by these techniques, but only up to a certain level of accuracy and quality of the results would be questionable. Some of the techniques developed for measuring tensile strength of granular materials, such as glass beads, are described below. These techniques have been further modified to accommodate direct tension testing of unsaturated sands.

Schubert (1975b) used split table method for measuring the tensile strength of powders (granular agglomerates). A schematic representation of the split plate apparatus is shown in **Figure 2.33**. The set-up consisted of a fixed base plate and two movable plates, each of them supported by three spheres and carrying the bulk material under test. The tensile force was applied by filling the container, which was suspended from a thin thread. In this apparatus, the capillary pressure of the specimens could be simultaneously measured with a U-tube

manometer. A suitable filter was installed which prevented the material from penetrating into the manometer. Since the equilibrium capillary pressure took some time to establish, the apparatus was covered from the top to prevent loss of moisture due to evaporation. Although this technique had many limitations and drawbacks, it provided the basis for many tensile testing apparatuses for granular soils.

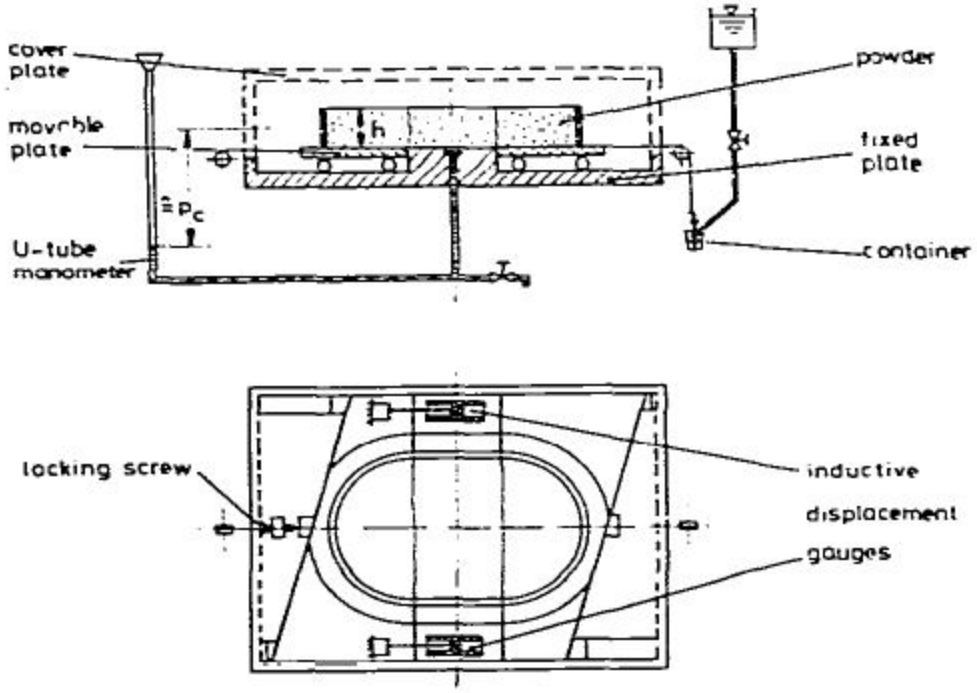

Figure 2.33 Diagrammatic setup of the split plate apparatus; side view (top) and plan view (bottom). (Schubert 1975)

In 1991, Perkins developed a direct tension apparatus to measure the tensile strength of MLS-l (Minnesota Lunar Simulant), which is a granular material. This testing device was designed to accommodate a 17.8 cm cubical specimen in a box split into two equal halves as shown in **Figure 2.34**. The front half was mounted on to the lateral guide rails by attaching roller bearing blocks to the bottom of the box and therefore it was movable. The rear half of the box was fixed and was positioned to the same vertical height as the front half supported by the rail and block assembly. The motor and load cell assembly were mounted on the base plate and a load cell was also attached to the front box. Experimental results were expressed as the

average tensile stress at plane of failure versus the displacement of the front box with respect to the fixed half.

Mikulitsch and Gudehus (1995) designed and constructed a direct tension device similar to that developed by Perkins as shown in **Figure 2.35**. Two pairs of sloped walls (wedge-like) kept the sample in place and reduced slippage. Similar to the apparatus describe by Perkins (1991), this specimen box was split in to two movable and fixed halves The tensile force was introduced by slowly filling water into a bucket hanging by a thread. The horizontal surface and two lateral slits were covered by plates in order to prevent evaporation. At failure, the sample broke into two halves just like the operation of Perkins's apparatus. The main improvement of this apparatus over the one developed by Perkins was the sloped inside-wall of the specimen container, which facilitated contact between the soil specimen and container as tension developed across the plane of failure.

Kim (2001) developed the direct tension apparatus shown as in **Figure 2.36**. The sample container consists of a 17.8 cm x 17.8 cm x 17.8 cm box that can split in two equal halves. The movable half was mounted on roller bearings attached to the bottom of the device. The fixed half was rested on two aluminium blocks to position it at the same height as the front part. Four wedges were attached inside the box to facilitate contact between the specimen and the box as tension is developed across the plane of separation. The device was rested on a loading table with two pulleys installed to connect loading wires to the movable half of the box. The rear loading container was attached to the movable half and was initially used to balance the system against the front loading bucket. Tensile load was applied by introducing water into the front loading container. The point of tensile failure was determined when the movable half of the specimen box moved away from the fixed half.

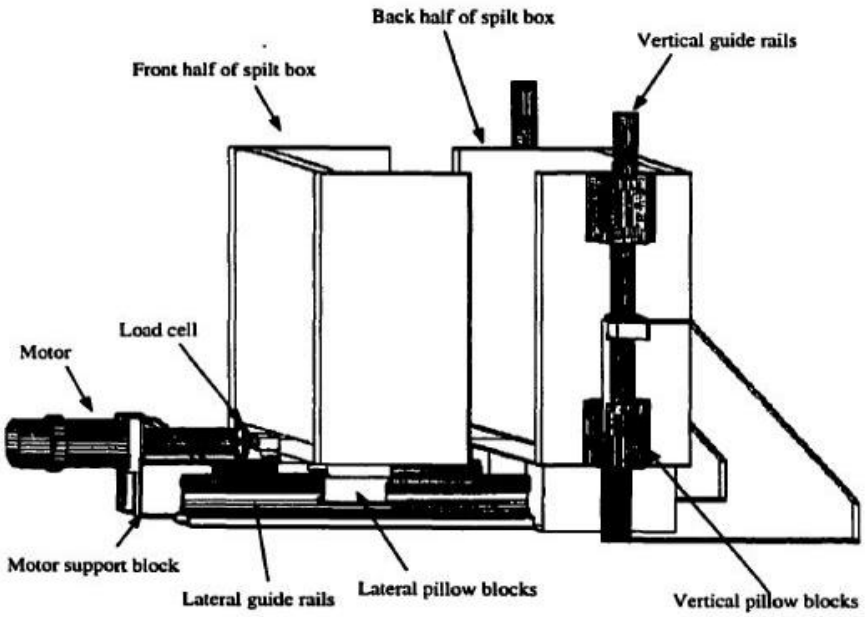

Figure 2.34 Direct tension apparatus (Perkins 1991)

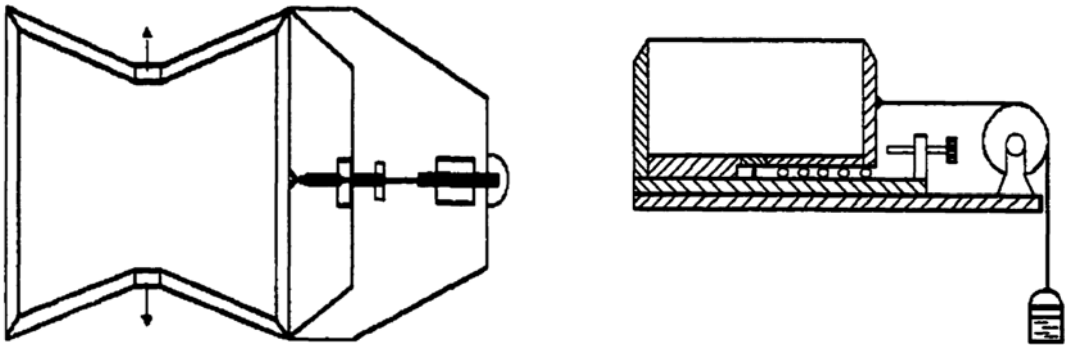

(a) **(b)**

Figure 2.35 Device for direct tension test (a) Top view, (b) Side view. (Mikulitsch and Gudehus 1995)

Lu et al. (2005, 2007) developed a tensile strength apparatus for coarse-grained soils as shown in **Figure 2.37**. The apparatus consisted of a specimen confining tube (split in the middle), mounting plate, adjustable table for inclining the specimen tube, and a digital probe for measuring the inclination angle. The specimen tube had two sections that are clamped together during sample preparation and released prior to testing. One section was fixed on the table, and the other part was free to slide on roller bearings. The table was inclined progressively to increase the gravitational force along the longitudinal direction of the sample, thus applying a tensile force. The inclination angle was recorded when the sample fails and used to back-calculate tensile strength from the mass of the movable section.

Tamrakar et al. (2005, 2007) developed a tensile test apparatus that consisted of a horizontal platform upon which a tensile mold is placed (**Figure 2.38**). This tensile mold consisted of two separate "C" shaped forms which were almost circular in shape except at the middle portion where these two halves were joined. Inner surface area of the tensile mold was 38.506 cm^2 with a depth of 5 cm. The tensile mould had a minimum width of 3 cm where two halves of the mould were joined. The two halves of the mold were attached to the horizontal platform. The attachment was done in a way such that one half of the box was fixed while another half was able to move freely on the platform in the horizontal direction. The friction in the apparatus was reduced by using linear sliding rollers in between the movable body and the platform. Movable box was subjected to tensile forces by the motor attached with the horizontal platform. The specimen was pulled at a constant speed of 0.0083 mm/s. A load cell placed between the motor shaft and the movable box, which measured the tensile force at failure. Tests were performed on compacted soil specimens containing mixtures of kaolin and Toyoura sand and silt (CFP) and Toyoura sand prepared at various volumetric water contents and dry density values. Unlike the stress controlled direct tension tests described by Perkins (1991) and Kim (2001), this direct tension test was strain-controlled. However, the efficacy of this setup to conduct stain-controlled direct tension tests on unsaturated sands is not known yet.

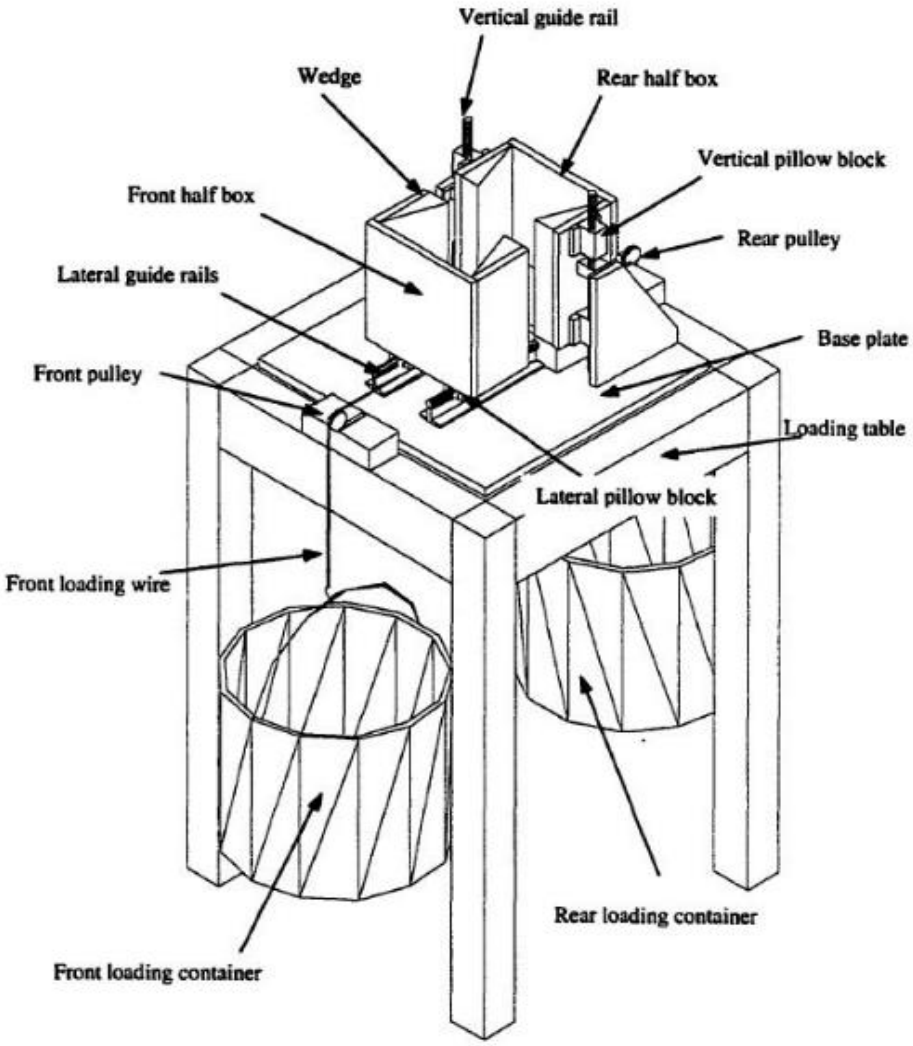

Figure 2.36 Direct tension apparatus. (Kim 2001)

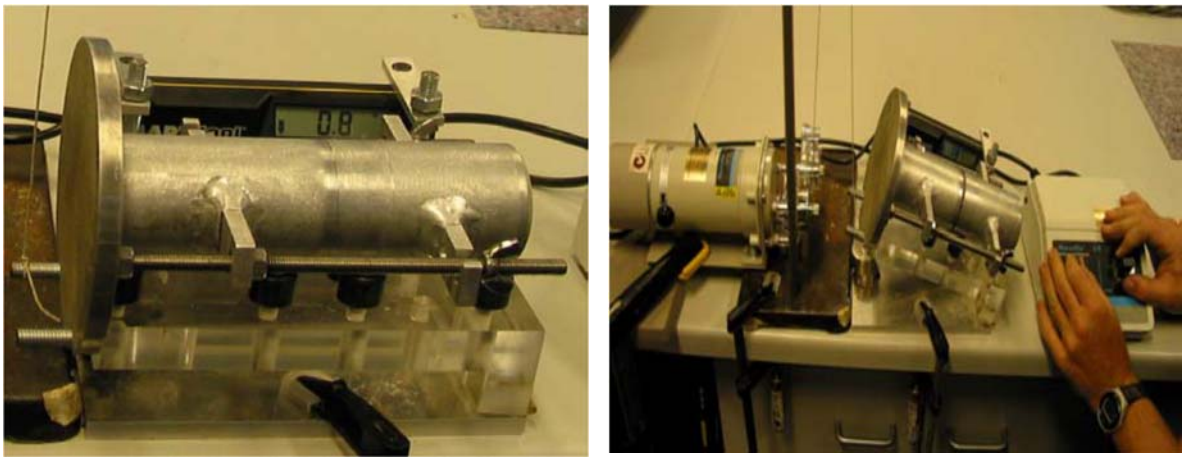

Figure 2.37 Tensile testing device developed by Lu et al. (2007)

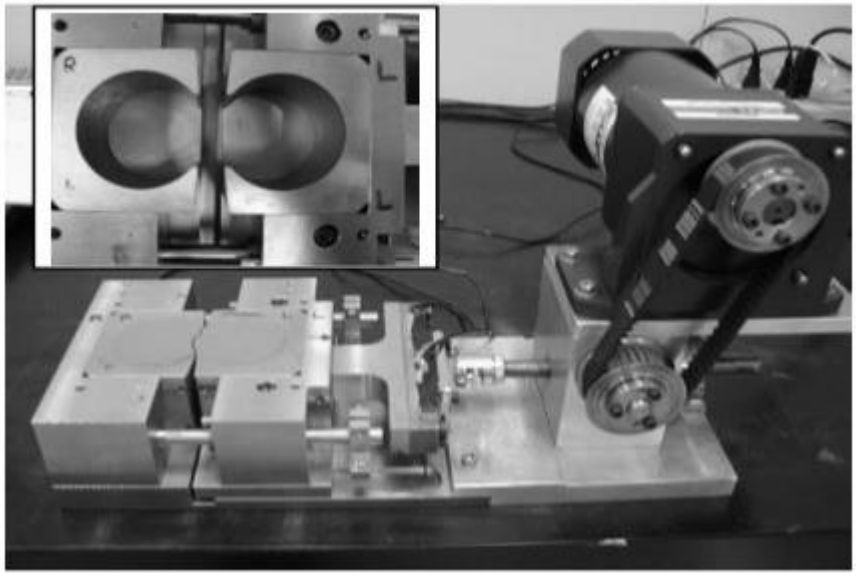

Figure 2.38 Tensile strength testing device. (Tamrakar et al. 2007)

3 MATERIALS AND METHODOLOGY

This chapter describes materials used in this research, including geotechnical engineering properties of silica sand and the properties of the surfactant used to vary the surface tension of distilled water. The custom-built direct tension apparatus used to measure the tensile strength of unsaturated sands is described in details. The chapter also outlines the experimental program and the experimental procedure used to perform direct tension tests.

3.1 MATERIAL CHARACTERIZATION

All the specimens were prepared using silica sand, produced by Sil Industrial Minerals, AB, Canada. According to the American Society of Testing and Materials (ASTM) Standard D2487, silica sand is a uniform, poorly graded sand (SP) with a specific gravity of 2.65 (ASTM Standard D854), a coefficient of uniformity of 1.69 and a coefficient of curvature of 0.97. From the particle size distribution curve, average particle size (d_{50}) and effective particle size (d_{10}) of the silica sand was found to be 0.40 mm and 0.28 mm, respectively. **Figure 3.1** shows the particle size distribution curves of four samples of silica sand, taken at random from different sand bags.

Laboratory experiments were performed on silica sand specimens prepared at different gravimetric moisture contents. Distilled water was used for specimen preparation, having a density of 1000 kg/m^3 and boiling and melting points of 99.98˚C and 0˚C, respectively. It has a surface tension values of 72 mN/m at 25˚C. For manipulating the surface tension of distilled water, 1-butanol was selected as the surface-active solute (or surfactant). 1-butanol was obtained from EMD Millipore with a reported purity of 99.4% and was used without further purification. 1-butanol has a boiling point and melting point of 118˚C and -89˚C respectively. The solubility of 1-butanol in water ranges from 7.7% w/w at 20˚C to 7.1% w/w at 30˚C (BASF 2008)

1-butanol was selected as the surfactant in this research for many reasons. The surface tension of distilled water reduces significantly with addition of 1-butanol, even at low concentrations. **Figure 3.2** shows the variation of surface tension of distilled water as a

function of concentration of 1-butanol (Bikerman 1970). From **Figure 3.2**, it can be inferred that the surface tension of 7% w/w 1-butanol solution is 24.8 mN/m, which is approximately one-third to that of distilled water. At 7% w/w concentration, the density of 1-butanol solution is 99.0% that of distilled water (Smith 1995). Henry et al. (1999) compared two sand samples premixed with distilled water and 7% w/w 1-butanol solution and confirmed that there was no observable variation in gravimetric water content as a result of solution density differences. 1-butanol has a low vapor pressure (< 0.5 kPa at 20˚C) and small Henry's law partition-coefficient (log $P_{butanol/water}$ = 0.003) limiting concerns about vapor transport or loss due to evaporation. More importantly, it has been documented in previous studies (Smith 1995; Dury et al. 1998; Smith and Gillham 1999; Henry et al. 1999, 2001; Bashir et al. 2007) that SMCCs for soils wetted with 7% w/w 1-butanol solution can be predicted by scaling the matric suction of the SMCCs for a water-wetted system by the ratio of the surface tension of 7% 1-butanol solution to distilled water. This observation implies that reduction in matric suction expected by changing the concentration of 1-butanol is directly proportional to the ratio of surface tension of 1-butanol solution to distilled water. This also suggests that the effect of contact angle on matric suction due addition of 7% 1-butanol in water is insignificant.

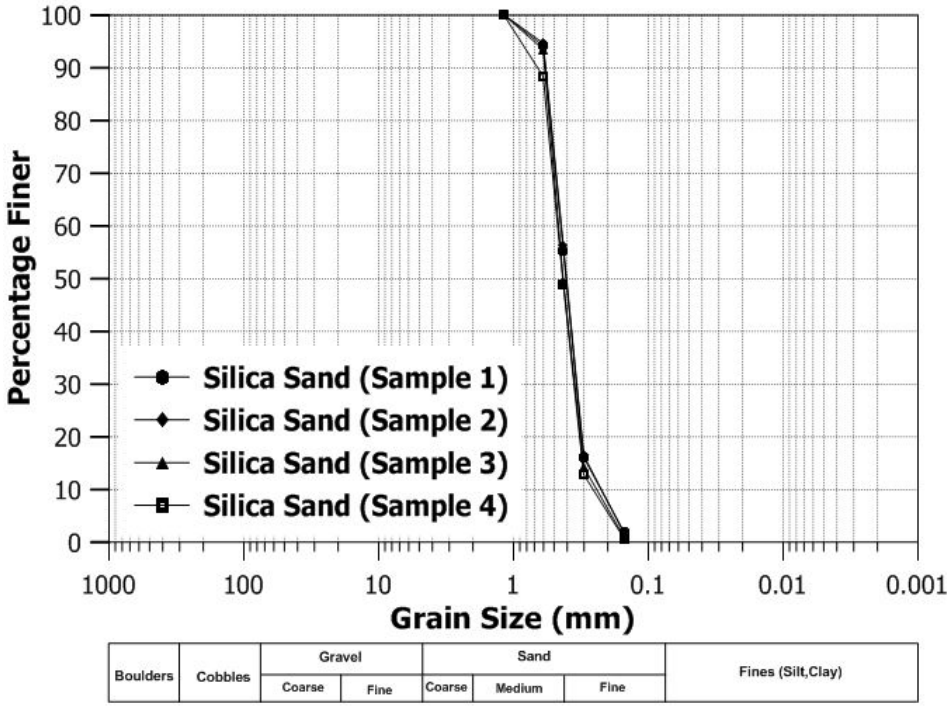

Figure 3.1 Particle size distribution curve of silica sand

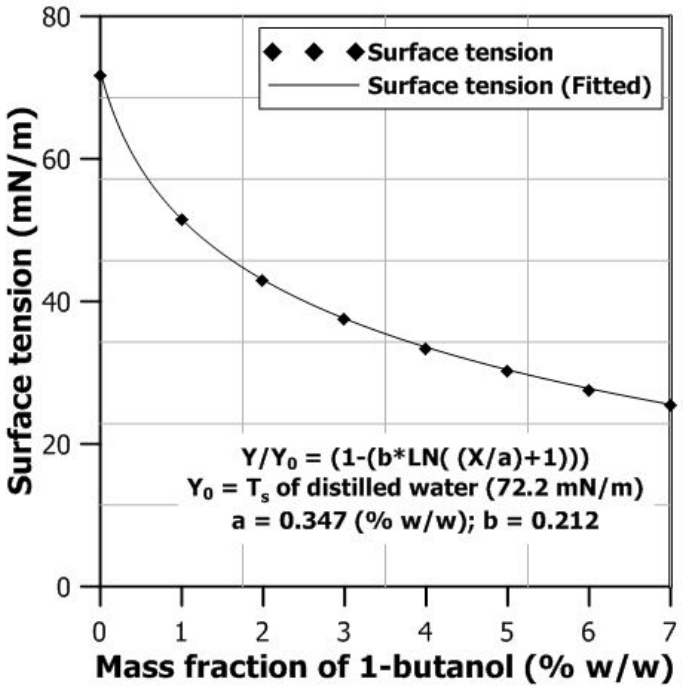

Figure 3.2 Variation of surface tension of distilled water as function of concentration of 1-butanol. (data from Bikerman 1970)

3.2 EXPERIMENTAL APPARATUS

The tensile strength testing device used for this research was based on the direct tension equipment originally developed by Perkins (1991). Mikulitsch and Gudehus (1995), Kim (2001) and Goulding (2006) have also used modified versions of direct tension apparatus as described by Perkins. The specimen container consisted of a 152 mm by 152 mm by 152 mm box split in two equal halves (**Figure 3.3**). The movable half was mounted on a set of roller bearings sliding on single guide rail attached to the bottom of the specimen container. The fixed half of the specimen container rested on two solid spacers to position it at the same height as the movable half. This assembly of the guide rail, bearings and spacers prevented any lateral or vertical movements of specimen container during direct tension test (**Figure 3.4**). A stopper was placed at one end of the guide rail to prevent derailing of the movable half after specimen reached tensile failure. Four 20º wedges were attached inside the box to facilitate contact between the specimen and the internal walls of the specimen container and to ensure uniform distribution of tensile forces across the plane of separation.

Both halves of the specimen container and the guide rail rested on a base plate with two frictionless pulleys installed at two ends of the base plate. A thin, strong and inextensible wire was attached to the bottom of the movable half and connected to the front loading container through the front pulley (**Figure 3.5(a)**). To prevent any movement of the movable half before the start of the direct tension test, a rear loading container was also attached to the movable half, connected through the rear pulley (**Figure 3.5(b)**). This ensured that the direct tension apparatus was in equilibrium against the weight of the front loading container and load cell at the start of the test (See **Appendix A** for details). The role of this balance system is important as unsaturated sands have low tensile strength and any imbalance in the system can affect the measurements significantly. The tensile load was applied by filling the front loading container with water at a pre-determined flow rate. The flow rate, or the loading rate, was maintained by using a constant head apparatus.

A tamping device having angular edges was designed and constructed to evenly compact soil inside the specimen container (**Figure 3.6**). The tamping device was made of a base plate connected to a rod of height 55 cm and a sliding mass of 985 g. The sliding mass had an inside hole of with diameter of 14.5 mm and could freely move along the rod without any appreciable friction. The area of the base plate was 190 cm^2 and thickness of 12.7 mm. The drop height of the sliding mass was 52 cm.

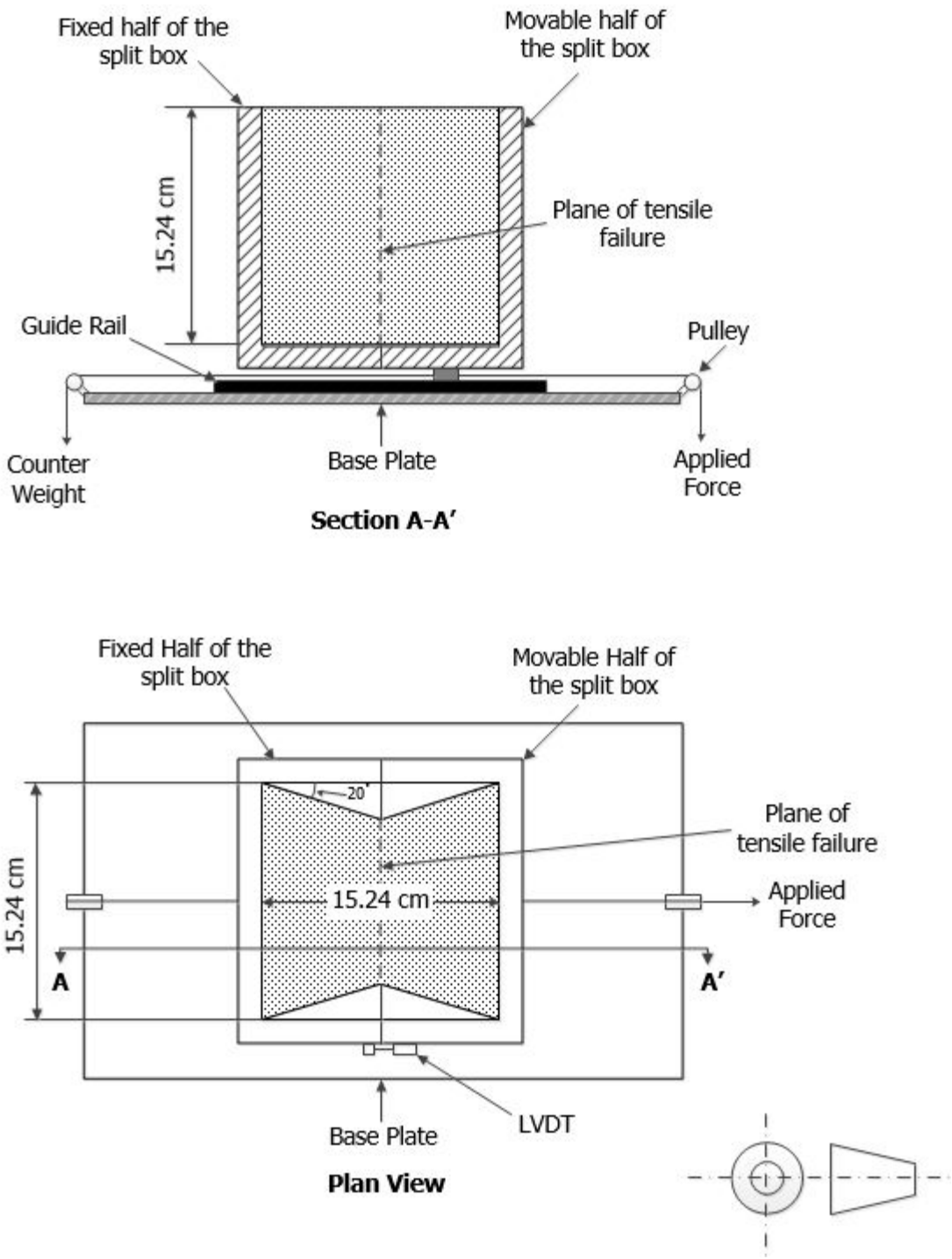

Figure 3.3 Schematic representation of direct tension apparatus

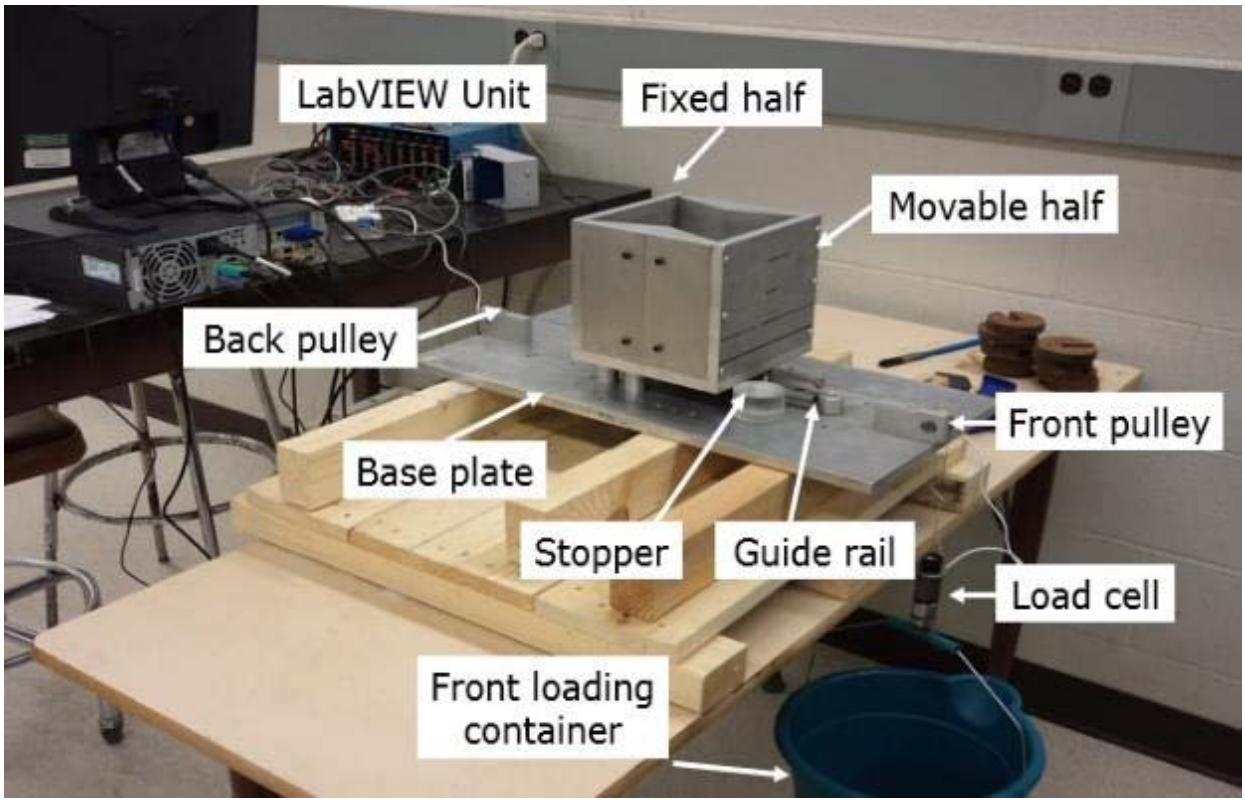

Figure 3.4 Labelled photograph of the direct tension apparatus

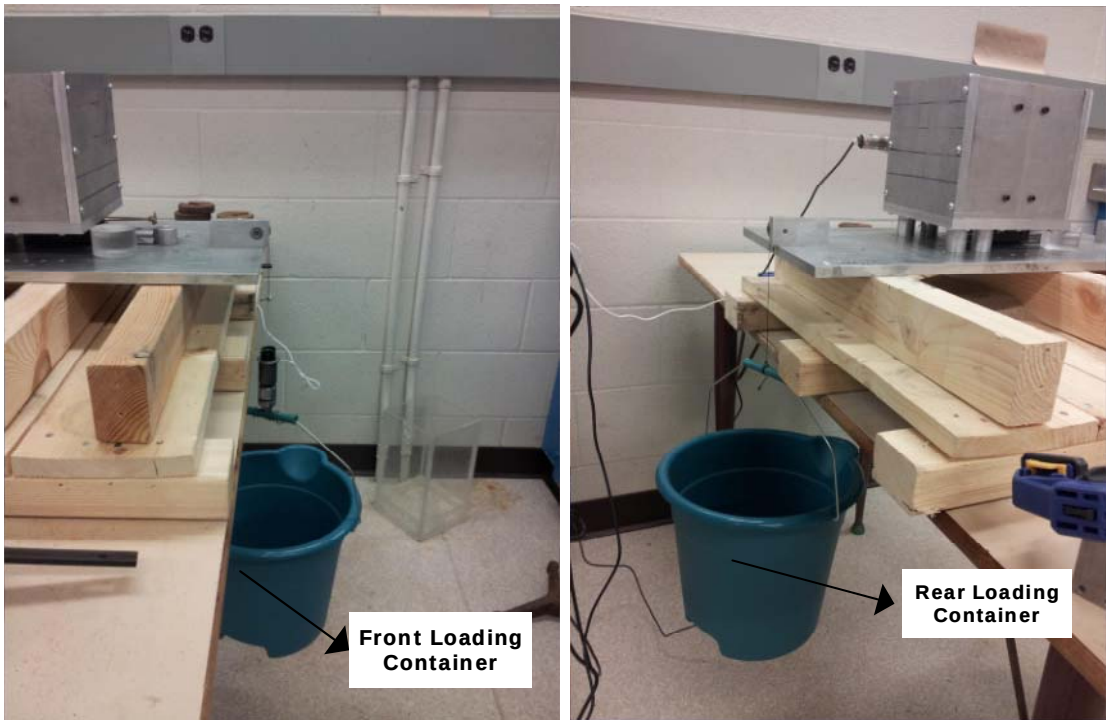

(a) **(b)**

Figure 3.5 (a) Front loading container with load cell and pulley, (b) back loading container with pulley

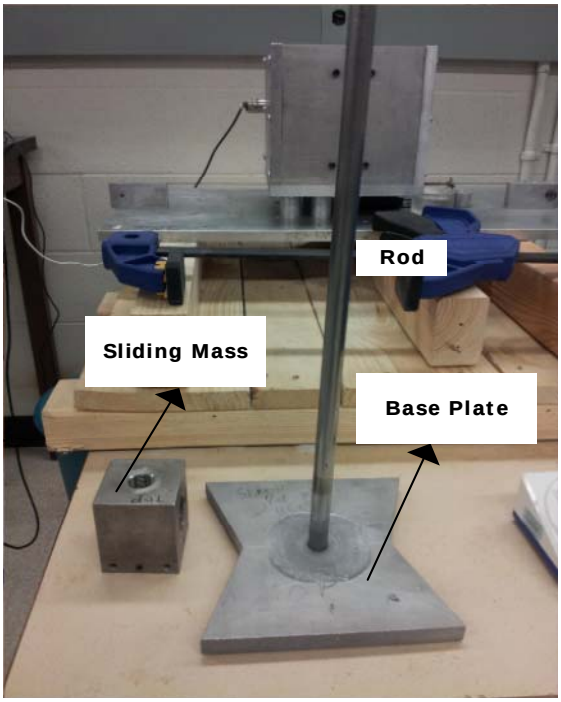

Figure 3.6 Tamping Device

Accurate measurements of the failure tensile load and time of failure are important factors during direct tension tests. Perkins (1991) and Kim (2001) relied on the visual observations of moment of failure and no attempt was made to measure deformations which could be indicative of the tensile failure. Goulding (2006) used a dial gage to measure deformations parallel to the plane of separation with deformation readings taken from the dial gage every 10 seconds, which is a significantly large time interval. Therefore, in order to capture the point of tensile failure with good accuracy, load cell and linearly-variable differential transformer (LVDT) were installed in the direct tension apparatus. The load cell was attached to the front loading container for independent measurement of the tensile load in the front loading container. The deformations parallel to the plane of separation during the direct tension tests were measured using LVDT. It was attached to one of the lateral side of the specimen container as shown in the **Figure 3.7**. Both the load cell and the LVDT were connected to the amplifier and the USB chassis (National Instrument cDAQ-9174). The amplifier was used to step-up the signal from the load cell and the LVDT while the USB chassis converted the analog signal from load cell and LVDT to digital signal and transmitted it to a data acquisition software. All the data from load cell and LVDT were recorded using LabVIEW©.

Figure 3.8 shows the load and deformation measurement curves from a typical direct tension test. The linearity of the load cell data curve confirms that the loading rate remained constant during the entire duration of the direct tension test. The exact time of failure was determined using the combination of load cell and deformation curves. As the tension test begins, LVDT shows a constant reading as the two halves of the specimen container are joined together. The movable half slowly drifts apart from the fixed half as the tensile load increases, and at failure the two halves are completely separated. On failure, the deformation reading from LVDT quickly jumps to a very high value. Load cell reading corresponding to this spike in LVDT reading is then used to determine the exact point of tensile failure.

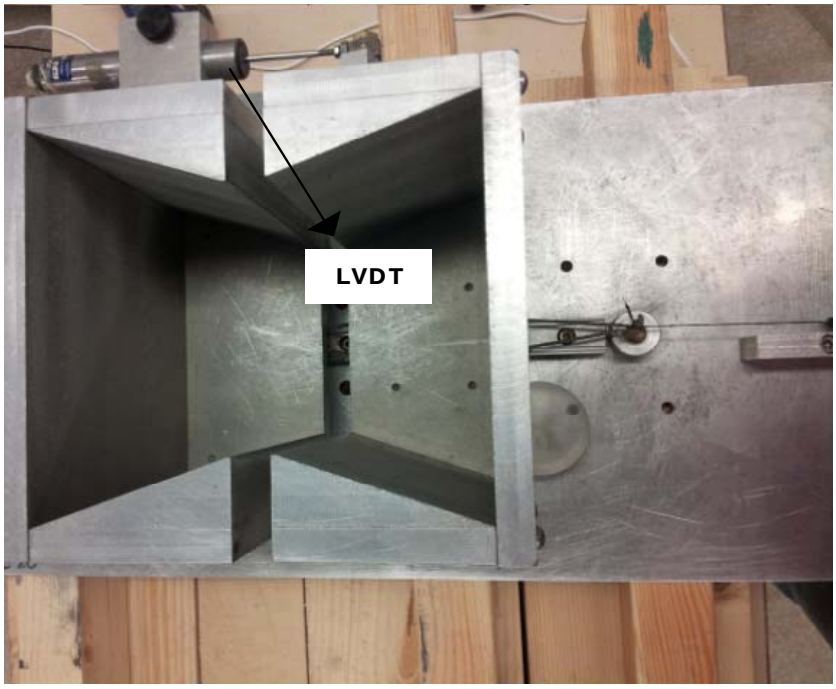

Figure 3.7 LVDT attached to the direct tension apparatus

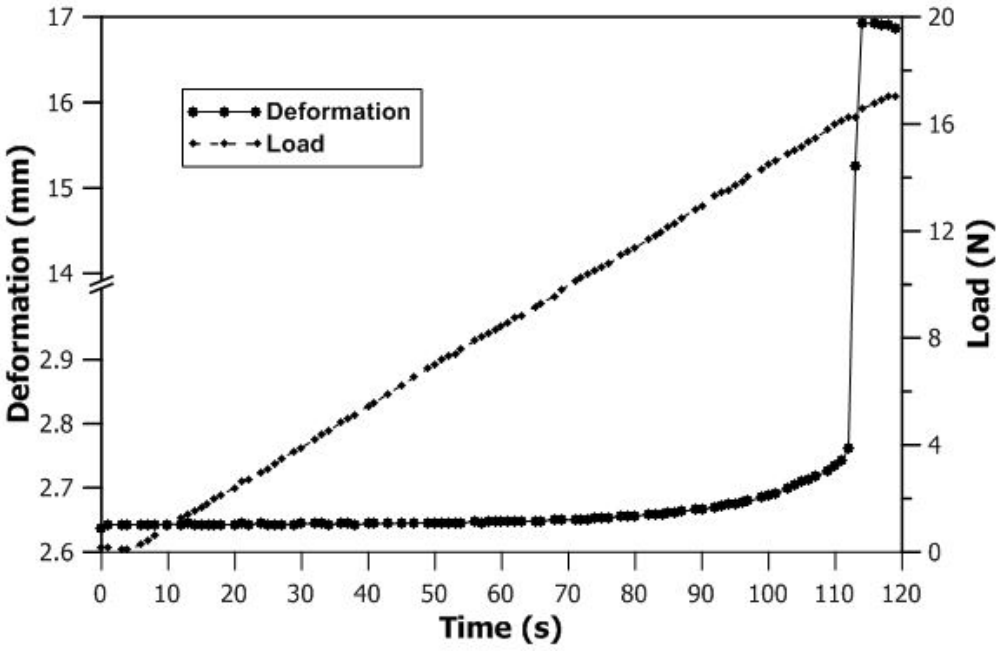

Figure 3.8 Load-deformation curve from load cell and LVDT data

3.3 SPECIMEN PREPARATION

To prepare the specimen, silica sand was mixed with distilled water or 1-butanol solutions at various concentrations at a desired moisture content. The two halves of the specimen container were secured together using bar clamps. The specimen was then added to the container in three lifts and compacted using the tamping device to a desired dry density. Before compacting each layer, the top surface of the previous compacted layer was scarified using spatula to avoid any layering effect. **Figure 3.9** shows the compacted specimen of silica sand inside the clamped specimen container.

Figure 3.9 Compacted specimen of silica sand

Two major challenges were faced in the preparation of specimen for tensile strength measurements. Firstly, it was very difficult to prepare specimens with uniform and low moisture contents. Conventional method of manual mixing of water and sand was slow and would lead to non-uniform mix. Significant portion of the water can also be lost due to evaporation while mixing. To prepare the specimen, oven-dried sand was mixed with distilled water or 1-butanol solutions in a sealed, air-tight plastic bags. The sample bag was wrapped

with an additional sealed plastic bag to prevent any loss of moisture due to evaporation. This method provided a convenient and efficient way to produce homogenous samples. Secondly, compaction of specimen at a predictable, measurable and repeatable dry density was another challenge. As the weight of the sliding mass and sliding height during compaction was constant and known, the number of blows per lift controlled the density of the specimen. The amount of compaction energy, or number of blows per lift, required to achieve similar dry densities had to be determined for specimens wetted with different media, i.e., distilled water or 1-butanol solutions, at different moisture contents.

An attempt was made to develop a relationship between compactive effort and dry density of the specimen. Compaction tests were performed using the direct tension apparatus. The numbers of blows per lift were varied from 10 to 40 in the increments of 5 blows. Silica sand was compacted into the specimen container in three equal lifts. For any given number of blows, the corresponding density was calculated by subtracting the amount of sand left in the plastic bag from the initial quantity and dividing it by the volume of the specimen container. Results are shown in **Figure 3.10(a)** for distilled water and **Figure 3.10(b)** for 3.5% w/w 1-butanol solution. Using regression analysis, it was observed that the trend between the achieved dry density and number of blows is approximately linear. Using these regression equations, number of blows required for a desired dry density can be calculated. The density values obtained, using this procedure, were found to be predictable and repeatable.

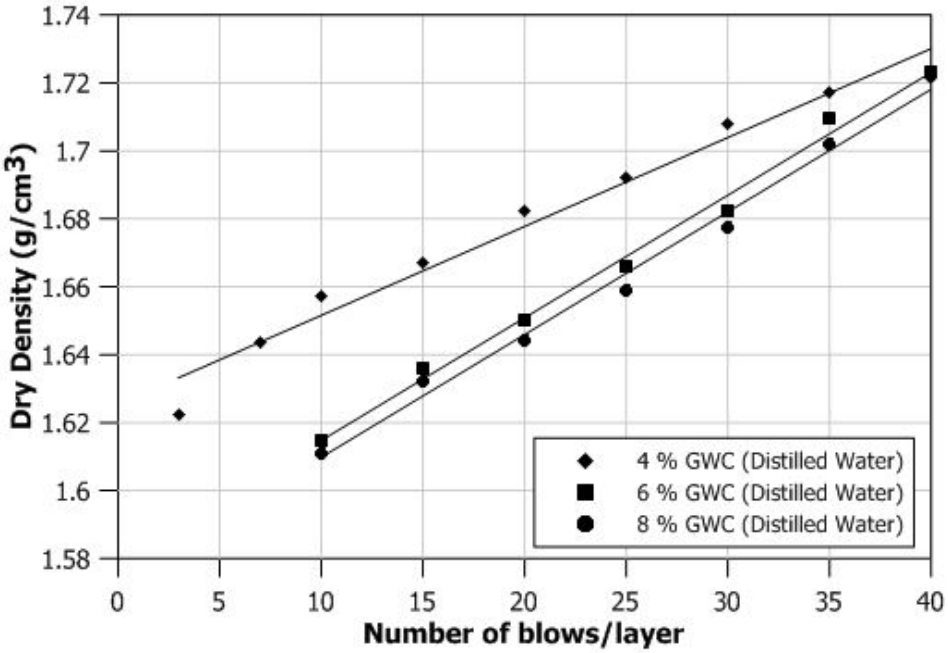

(a)

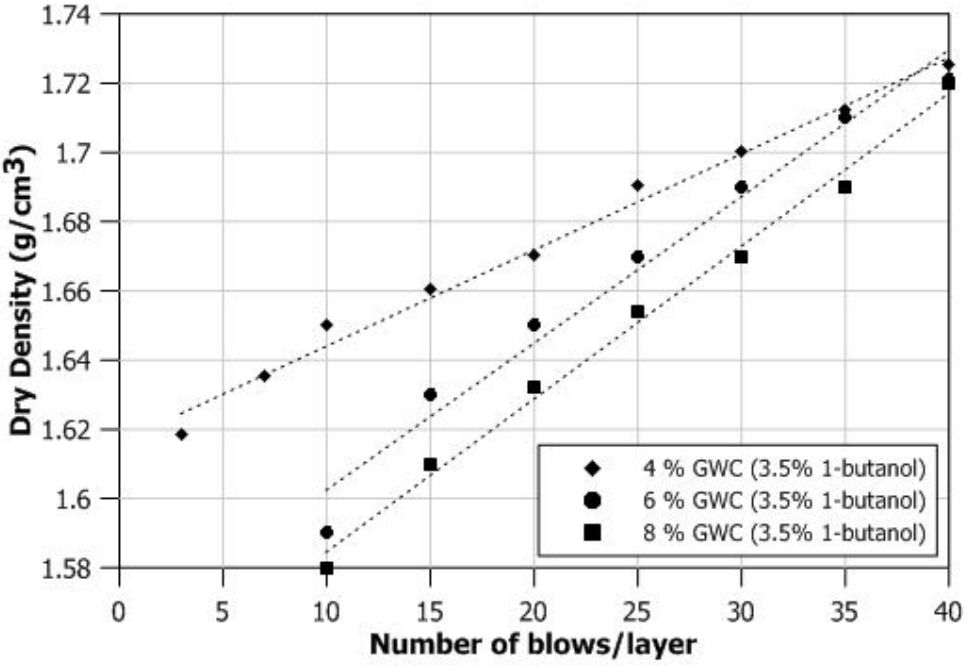

(b)

Figure 3.10 Dry density vs number of blows at different moisture contents (a) distilled water, (b) 3.5% w/w 1-butanol

3.4 EXPERIMENTAL PROCEDURE

The experimental apparatus was first cleaned using brush and air pressure gun. Lubricant (WD-40) was applied to the roller bearing blocks and rails in the bottom of the front box to reduce the friction. The magnitude of initial friction was measured by conducting several tests on the empty specimen container box. The average value of internal friction was determined to be F_{in} = 3.8 N. This value was subtracted from the final tensile load to calculate the corrected tensile load at failure. The method to calculate the internal friction in the direct tension apparatus is discussed in **Appendix B**. The two halves of loading container were secured together using a bar clamp and the specimen was prepared by the procedures described previously.

Prior to the tensile loading, the bar clamps were removed. The tensile load was applied by introducing water into the front loading container at a controlled loading rate. The load was applied until failure was achieved. Failure of the specimen was marked by the sudden separation of the movable half from the fixed half of the specimen container (**Figure 3.11**). The total tensile load at failure, i.e. weight of water on the front loading container was subtracted by the average friction value to obtain the corrected failure load. The tensile strength was then calculated by dividing the corrected tensile load at failure with the area of the failure surface. This was immediately followed by measuring the weight of the moist sample to check for the moisture content achieved. Three samples of moist soil were taken from top, middle and bottom part of the specimen container and were weighed both before and after oven drying for 24 hours (ASTM Standard D2216). Because 1-butanol's boiling point is 117.4°C, moisture content samples for specimens prepared using 1-butanol solution were dried in an oven set at 130°C to ensure complete evaporation of the pore-liquid. Since 1-butanol, upon evaporation, does not leave any solid residue, the rest of procedure for determination of moisture content for specimens containing 1-butanol solution was the same as that for samples containing distilled water. This entire procedure was followed to determine the tensile strength and moisture content of the specimen for each direct tension test.

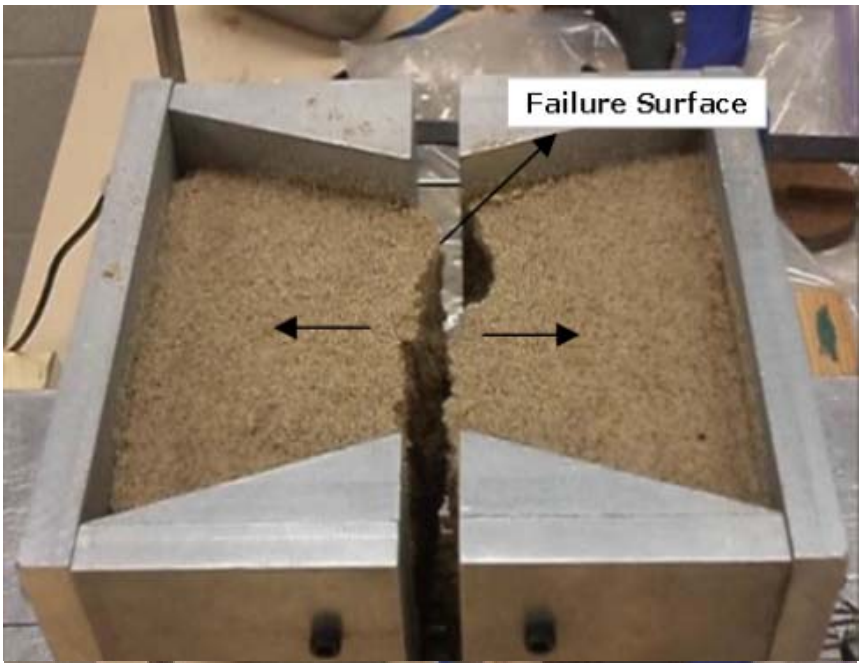

Figure 3.11 Direct tension apparatus at point of tensile failure

3.5 EXPERIMENTAL PROGRAM

The main objective of this research is to quantify the effect of pore-water surface tension on tensile strength of unsaturated sands. The effect of density of the specimen and loading rate on tensile strength is also studied. **Table 3.1** lists the main experimental program of the direct tension tests. The tests were carried out at two different dry densities, 1.65 g/cm^3 and 1.61 g/cm^3, and at two different loading rates, 4.2 g/s and 13 g/s. The experimental program was divided into three sub-categories – Case-1, Case-2 and Case-3. Direct tension tests on specimen with dry densities of 1.65 g/cm^3 and 1.61 g/cm^3 at a loading rate of 4.2 g/s were referred to as Case-1 and Case-2, respectively, whereas direct tension tests on specimen with dry density of 1.65 g/cm^3 at a loading rate of 13 g/s was referred to as Case-3. Thus, comparison of between Case-1 and Case-2 experimental results will provide information related to effect of density on tensile strength, as loading rate is kept constant. On the other hand, comparison of Case-1 and Case-3 results will establish a qualitative relationship between tensile strength and loading rate, since the dry density of specimen is kept constant. In order to study the effect on pore-water surface tension on tensile strength of unsaturated sands, unsaturated specimens were prepared using distilled water (S1) and three different concentrations of 1-butanol

solutions – 1.75% (S2), 3.50% (S3) and 7.00% (S4) - corresponding to the surface tension values of approximately 72 mN/m, 48 mN/m, 36 mN/m and 24 mN/m, respectively. Since no direct measurements were performed, the surface tension values of 1-butanol solutions were estimated using the regression curves shown **Figure 3.2**. To study the effect of moisture on tensile strength, seven different moisture contents were considered - 1%, 2%, 3%, 4%, 6%, 8% and 10%. In total, 84 directs tension tests were performed under the current experimental program.

Direct tension tests were also performed at higher moisture content (w = 15%) on silica sand containing S1 and S2 solutions as an extension of Case-2 program. But it was observed that direct tension tests at higher moisture contents were difficult to perform. As the moisture content of the specimen increases, the capillary forces which hold the pore-liquid within the soil matrix was dominated by the gravitational force. This leads to leakage of the pore-liquid from the specimen through the gap in between the two halves of the specimen container. The condition aggravated for specimens containing higher concentrations of 1-butanol solutions since the water holding capacity of unsaturated sands decrease with increase in concentration of surfactant in pore-liquid due to decrease in the magnitude of surface tension. As a result, a vertical moisture profile was established, wherein, the moisture content of the specimen increased from top to bottom portion of the specimen. This resulted non-uniform distribution of moisture across the specimen.

Another series of tests (Case-4) were performed to study the effect of loading rate on tensile strength of unsaturated sand, exclusively. In this series of tests, S1 and S3 solutions were used to prepare specimens with three different moisture contents values of 4%, 6% and 8%. Three different loading rates were adopted - 4.2 g/s, 8 g/s and 13 g/s. It was ensured that all the direct tension tests were performed at a dry density of 1.65 g/cm^3.

Table 3.1 Experimental program

Experimental Program	Packing Density	Rate of Loading	Solution used to prepare sample	Gravimetric Moisture Content
Case-1	1.65 g/cm^3	4.2 g/s	S1 - Distilled water S2- 1.75% 1-butanol S3- 3.5% 1-butanol S4- 7% 1-butanol	1%, 2%, 3%, 4%, 6%, 8%, 10%
Case-2	1.61 g/cm^3	4.2 g/s		
Case-3	1.65 g/cm^3	13 g/s		
Case-4	1.65 g/cm^3	4.2, 8, 13 g/s	S1 – Distilled water S3 – 3.5% 1-butanol	4%, 6%, 8%

4 OVERVIEW OF THE DIRECT TENSION TESTS

This chapter summarizes the results of the direct tension tests. The effect of saturation, density, loading rate and concentration of 1-butanol on tensile strength of unsaturated sands were studied as a part of the experimental program described in **Table 3.1**. Measurements were recorded for moisture content, dry density of the specimen, tensile loading rate, and tensile strength of the unsaturated samples at failure.

Results from the experimental program has been summarized in **Table 4.1 to Table 4.3**. For all the three cases, tensile strength is plotted as a function of degree of saturation and as a function of mass fraction of butanol in **Figure 4.1** to **Figure 4.3** and **Figure 4.4 to Figure 4.6,** respectively.

Table 4.1 Tensile strength measurements for Case-1 experiments

Saturation %	Gravimetric Moisture Content %	Tensile Strength (Pa)			
		Water only	1.75 % 1-butanol w/w	3.5 % 1-butanol w/w	7% 1-butanol w/w
4	1	566.4	474.8	368.8	308.7
9	2	732.7	540.7	463.4	389.0
14	3	898.6	686.8	557.5	457.7
18	4	988.9	795.7	686.8	526.4
28	6	1067.8	959.0	778.4	597.5
37	8	1171.1	1008.4	827.7	712.6
48	10	1259.4	1051.5	870.2	761.3

Table 4.2 Tensile strength measurements for Case-2 experiments

Saturation %	Gravimetric Moisture Content %	Tensile Strength (Pa)			
		Water only	1.75 % 1-butanol w/w	3.5 % 1-butanol w/w	7% 1-butanol w/w
4	1	492.7	333.5	290.2	233.4
9	2	570.6	451.0	398.0	347.4
14	3	664.6	566.6	486.8	423.6
18	4	779.2	640.4	568.5	481.8
28	6	855.7	720.5	621.4	551.4
37	8	920.1	797.7	679.8	612.5
48	10	978.0	850.9	746.5	698.7

Table 4.3 Tensile strength measurements for Case-3 experiments

Saturation %	Gravimetric Moisture Content %	Tensile Strength (Pa)			
		Water only	1.75 % 1-butanol w/w	3.5 % 1-butanol w/w	7% 1-butanol w/w
4	1	492.7	333.5	290.2	233.4
9	2	570.6	451.0	398.0	347.4
14	3	664.6	566.6	486.8	423.6
18	4	779.2	640.5	568.5	481.8
28	6	855.6	720.6	621.4	551.4
37	8	920.1	797.8	679.8	612.5
48	10	978.0	851.0	746.5	698.7

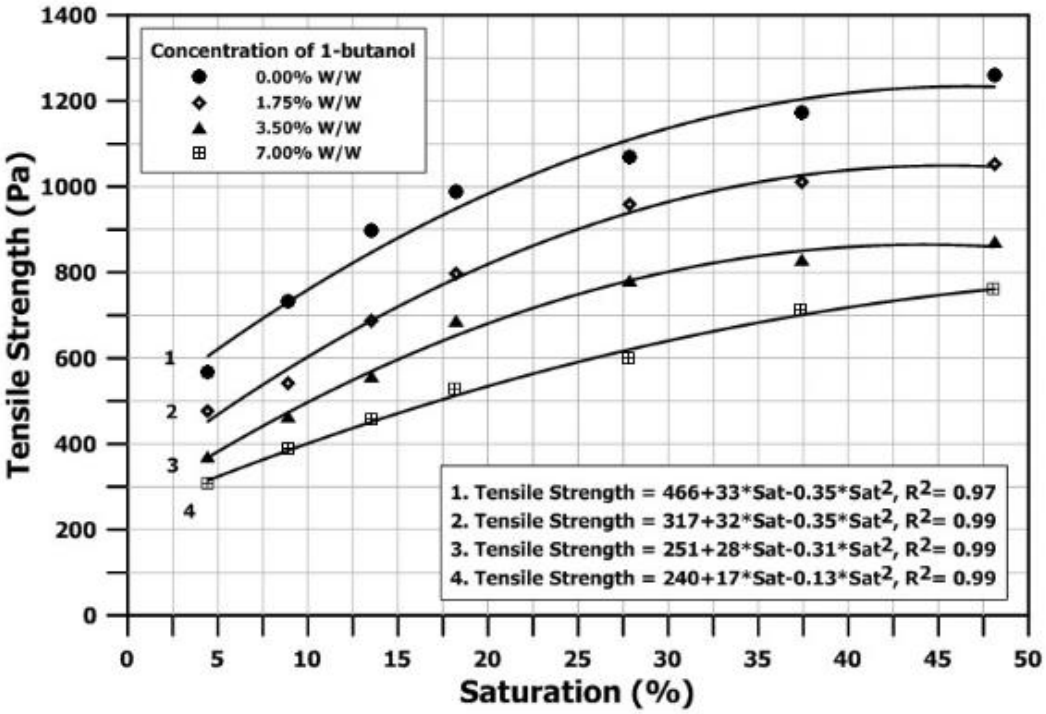

Figure 4.1 Tensile strength as function of saturation for Case-1 tests

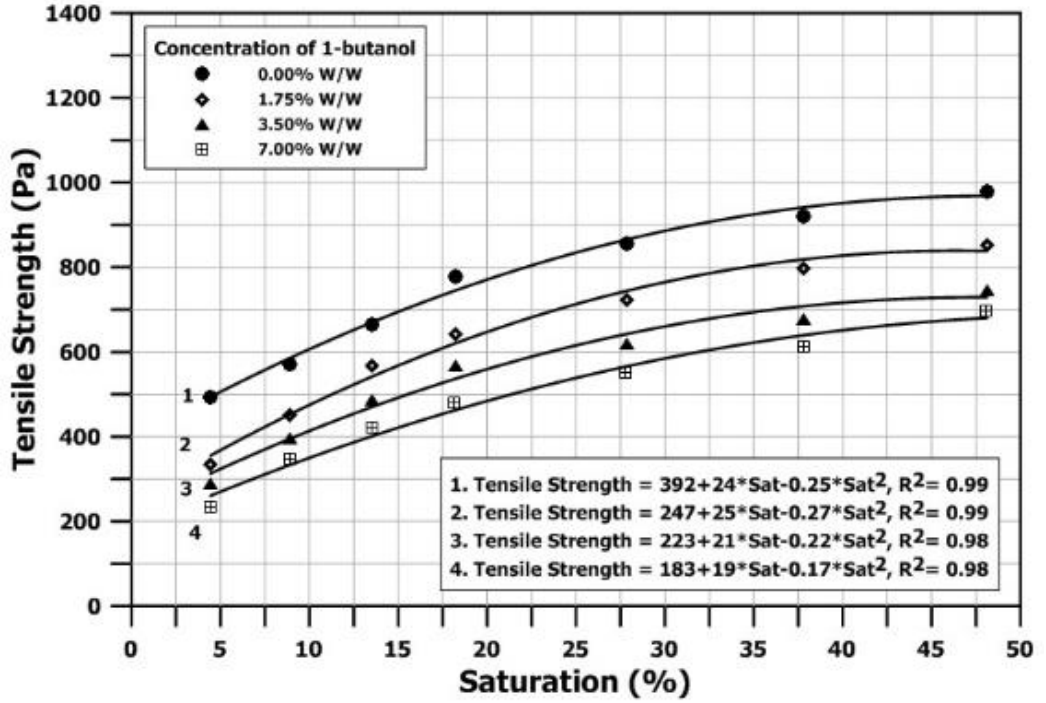

Figure 4.2 Tensile strength as function of saturation Case-2 tests

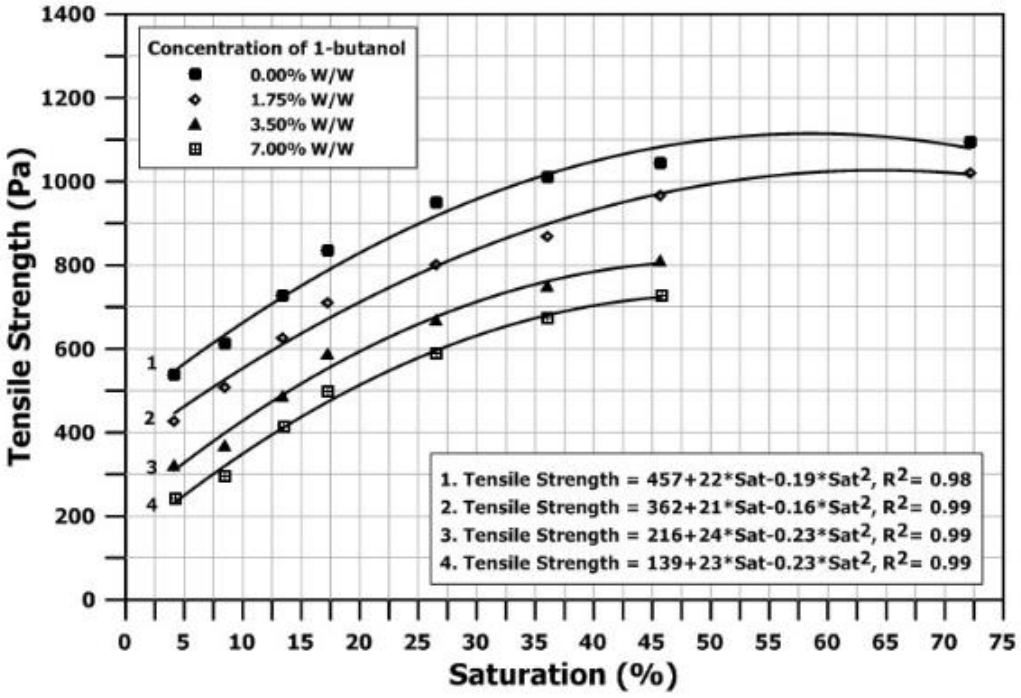

Figure 4.3 Tensile strength as function of saturation for Case-3 tests

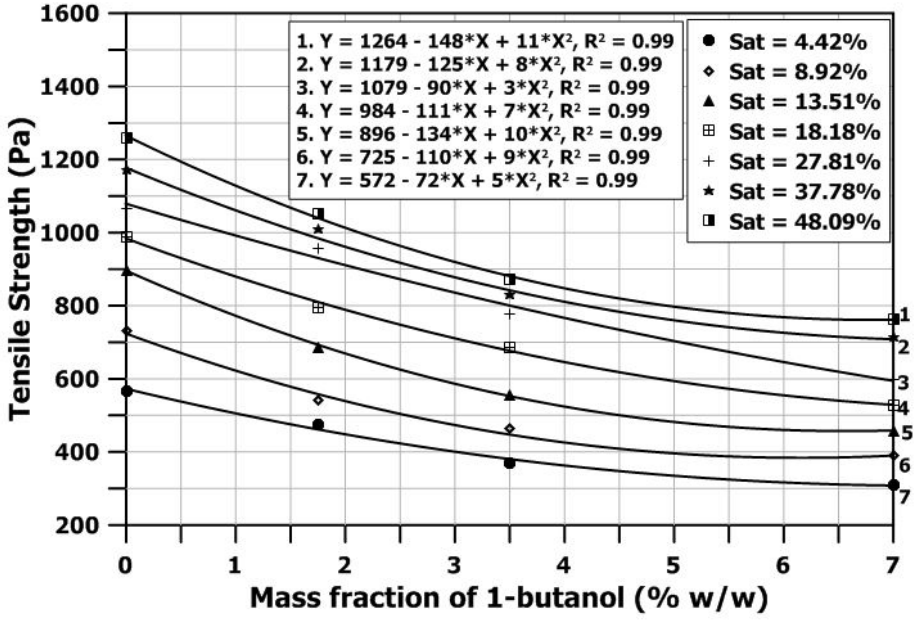

Figure 4.4 Variation of tensile strength with mass fraction of butanol for Case-1 tests

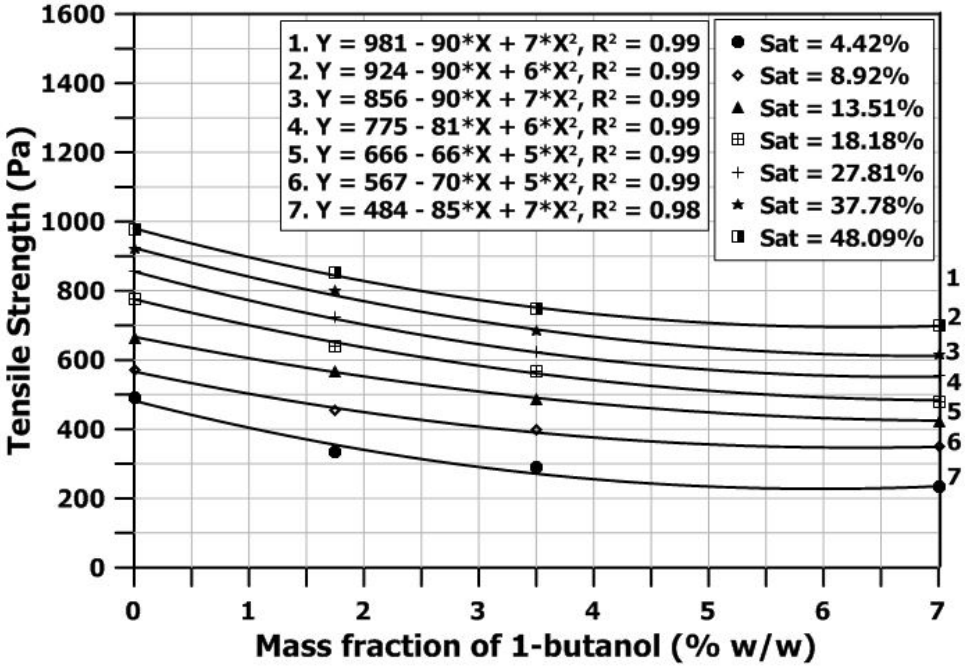

Figure 4.5 Variation of tensile strength with mass fraction of butanol for Case-2 tests

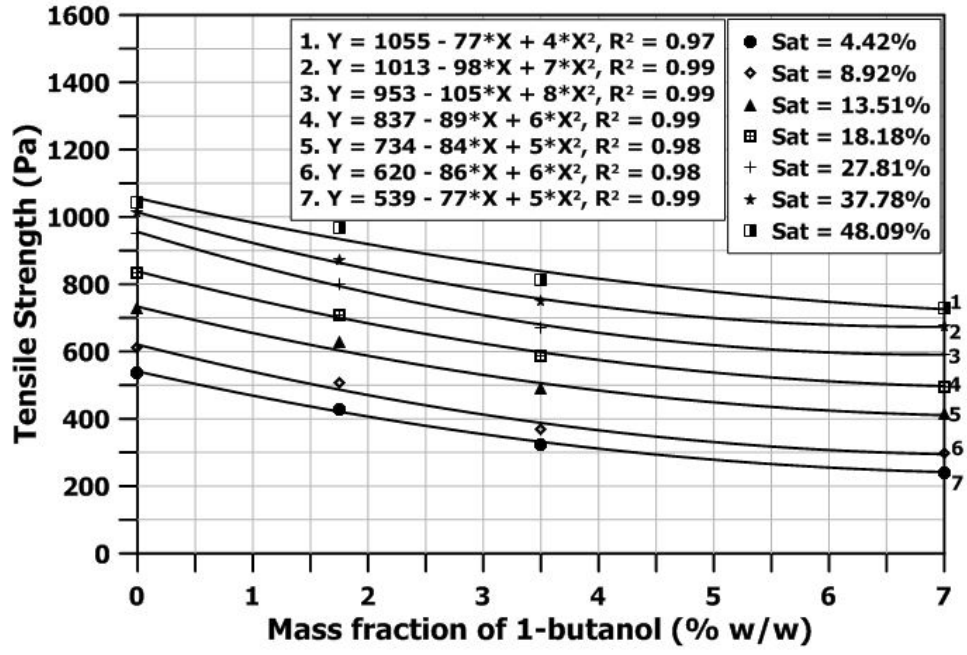

Figure 4.6 Variation of tensile strength with mass fraction of butanol for Case-3 tests

Figure 4.1 to **Figure 4.3** shows that the tensile strength initially increases with the increase saturation and then reaches a plateau value. For saturation in the range of 5% to 25%, the tensile strength increases rapidly. Beyond saturation level of 25%, the tensile strength keeps increasing but with a gradual slope and eventually starts to level off at a saturation of 50%. Kim (2001) and Lu et al. (2007) also reported similar observation in tensile strength as a function of saturation. As explained earlier, direct tension tests beyond saturation levels of 50% were not possible due to dominance of gravitational force over the water holding capacity of the unsaturated specimens. However, for Case-3, two direct tension tests were performed using specimens prepared with S1 and S2. It was observed that the tensile strength remains almost unchanged in between saturation levels of 50% and 70%.

Comparing **Figure 4.1** and **Figure 4.3**, it can be observed that the tensile strength tends to increase as the packing density of the specimen increases, irrespective of the solution used to prepare the specimen. At saturation level of 45%, the tensile strength of specimens packed at density of 1.61 g/cm^3 and 1.65 g/cm^3 is approximately 1000 Pa and 1200 Pa, respectively, for specimens containing distilled water. Similar trend in tensile strength behaviour was also reported by previous researchers (Mikulitsch and Gudehus 1995; Kim and Sture 2004; Lu et al. 2007; 2009). This observation indicates that the tensile strength is very sensitive to the density of the specimen. As the packing density of specimen increases, the soil particles pack closer together and the pore-size decreases. Smaller pores contribute more towards the tensile strength as a result of increased matric suction.

The tensile strength measurements are also presented as a function of mass fraction of butanol in **Figure 4.4 to Figure 4.6**. These figures clearly show that there is reduction in tensile strength as the concentration of butanol increases, even for specimens with same packing density and saturation levels. This trend was expected since the surface tension of the pore-liquid decreases with increase in 1-butanol concentration and ultimately weakens the capillary mechanisms contributing to the tensile strength. It was also observed that the decrease in tensile strength is not proportional to the decrease in surface tension of the pore-liquid. For example, compared to distilled water, surface tension reduction for 7% 1-butanol solution is approximately 67% with respect to distilled water; however, the reduction in the tensile strength is only 40% for specimens containing 7% 1-butanol solution with respect to specimens

containing distilled water. Therefore, contrary to the theoretical tensile strength model, decrease in tensile strength is not a simple multiple of ratio of surface tension of the pore-liquid.

A cursory review of the historical work shows that the effect of loading rate on the tensile strength of unsaturated sands has not been documented previously. Most of the researchers have only mentioned the loading rate adopted for the direct tension tests. But no information was provided to describe the mechanism used to control the loading rate and the effect of loading rate on tensile strength of unsaturated sand was not studied. In order to study the effect of tensile loading rate on tensile strength, a series of direct tension tests were performed as described in Case-4 (**Table 3.1)**.

Table 4.4 summarizes the tensile strength values for different loading rates. **Figure 4.7** shows the variation of tensile strength as a function of rate of loading, when water and 3.5% w/w 1-butanol solution were used to prepare unsaturated specimens, respectively. It was observed that the tensile strength of unsaturated sand decreases as the rate of tensile loading increases. This trend was consistent with specimens prepared with both water and 3.5% w/w 1-butanol solution. Using regression curves to fit the experimental data, it was concluded that the tensile strength varies quite linearly with loading rate. For specimens containing distilled water (S1), tensile strength decreases by an average value of 15 Pa for every unit decrease in the loading rate. Similarly for specimens containing 3.5% w/w 1-butanol solution, the tensile strength decreases by an average value of 13.5 Pa for every unit decrease in the loading rate. Therefore, the effect of loading rate on tensile strength is quite similar irrespective of the solution used to prepare the specimens for the direct tension tests. In order to determine the maximum tensile strength, y-intercept values of the regression curves can be used. These values corresponds to loading rate of 0 g/s, which qualitatively means that the loading rate is very slow. However, during a direct tension test, if the time taken to reach tensile failure is very long, a considerable amount of the pore-liquid may escape due to evaporation. This will change the moisture content of the specimen as well as the surfactant concentration, which will affect the tensile strength significantly. Hence, direct tension tests at very small loading rates were avoided.

Table 4.4 Summary of direct tension test results at different loading rates

Rate of loading (g/s)	Gravimetric Moisture Content %	Tensile Strength (Pa)		Dry Density (g/cm^3)
		Water	3.5% butanol w/w	
4.2	4.0	695.4	606.9	1.65
	6.0	997.3	860.4	1.65
	8.0	1154.6	985.3	1.65
8.0	4.0	628.0	568.4	1.65
	6.0	909.0	803.0	1.65
	8.0	1105.2	917.7	1.65
13.0	4.0	555.5	529.7	1.65
	6.0	845.7	742.5	1.65
	8.0	1042.5	861.4	1.65

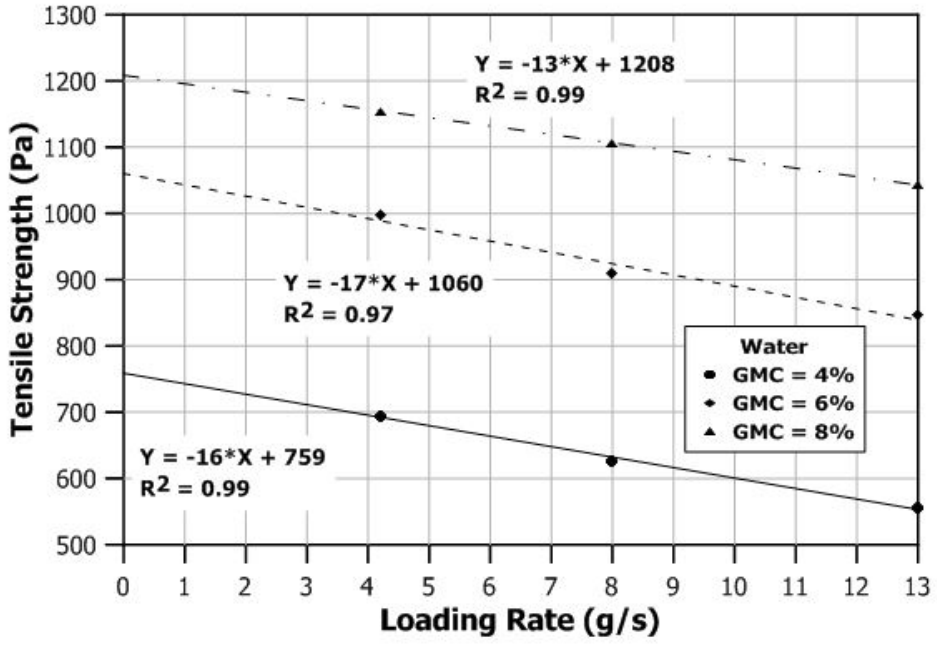

(a)

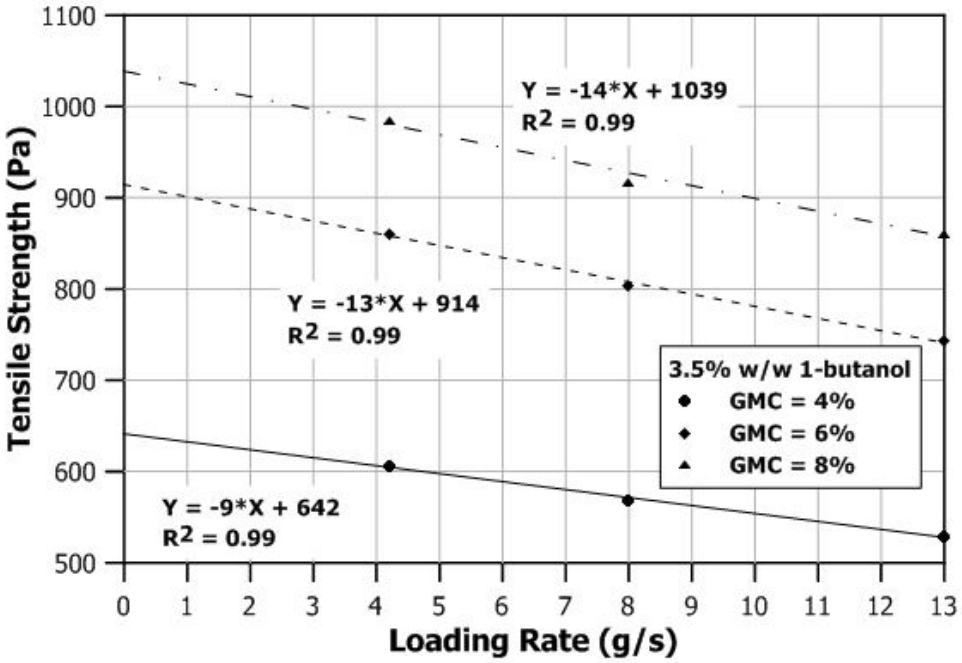

(b)

Figure 4.7 Tensile strength as function of loading rate for specimens wetted with (a) distilled water and (b) 3.5% w/w 1-butanol solution

5 ANALYSES USING THEORETICAL TENSILE STRENGTH MODELS

In this chapter, comparisons between experimental results from the direct tension tests performed on unsaturated silica sand specimens are compared with the predicted values using micro-mechanical and macro-mechanical models of tensile strength, as described in **Chapter 2**. The predicted model curves using both the models have been simulated using MATLAB©. The efficacies and drawbacks of both models have been discussed. Based on experimental results, few modifications to the existing models are also proposed.

5.1 ANALYSIS USING MICRO-MECHANICAL MODEL

Micro-mechanical model has been already described in details in **Section 2.2.1**. The experimental results were compared with the micro-mechanical model curves. The model curves were simulated for all first two cases, Case-1 and Case-2, wherein the loading rates and packing dry densities were 4.2 g/s and 1.65 g/cm^3 and 4.2 g/s and 1.61 g/cm^3, respectively. In each case, unsaturated silica sand specimens were prepared using S1, S2, S3 and S4 solutions and direct tension tests were performed at different moisture contents. The experimental program has been discussed in **Section 3.5**.

Table 5.1 lists the model parameters which were used to simulate the model curves. For each case, model parameters for S1 results were used as reference for S2, S3 and S4. The simulations were performed using effective particle size, $d = d_{10}$. Contact angle was assumed to be zero, irrespective of the concentration of 1-butanol. Simulations were performed using three different packing arrangements – simple cubic (k = 6, e = 0.92), body-centered cubic (k = 8, e = 0.68) and hexagonal closest packed or face-centered cubic (k = 12, e = 0.35). Since the a/d ratio is not known initially, a/d values ranging from 0.005 to 0.05 is used for the simulation. The best fit model curve was then determined using least root mean square error value, which corresponds to a given packing arrangement and a/d ratio. It should be noted here that direct tension tests were performed beyond the funicular state due to experimental limitations; hence, no comparisons could made with the predicted model curves.

Table 5.1 Model parameters for analysis using micro-mechanical model

MODEL PARAMETERS	
Surface tension, T_s (mN/m)	72 (S1), 48 (S2), 36 (S3), 24 (S4)
Diameter, d_{10} (mm)	0.28
Contact angle (degrees)	0.0
Specific gravity, G_s	2.65
Co-ordination number, k	{6, 8, 12}
Void ratio, e	{0.92,0.68,0.35}
Residual Saturation, S_r	0.15
Capillary Saturation, S_c	0.90
a/d ratio	0.005-0.05

For Case-1 with S1 solution, the model curve fitted the experimental results for *a/d* ratio = 0.037 and HCP packing arrangement (k = 12 and e = 0.35). Since the packing dry density was kept constant, this set of *a/d* ratio and packing arrangement was used for simulating model curves for Case-1 with S2, S3 and S4 solutions. The results have been summarized in **Figure 5.1**. From **Figure 5.1**, it can be seen that the predicted curve accords well with the experimental results for specimens containing S1 within the pendular state and at the beginning of the funicular state. In the latter part of the funicular state, the model slightly over-predicts the tensile strength. Comparisons beyond funicular state were not possible. For specimens containing S2, S3 and S4 solutions, the model curves under-predict the tensile strength significantly, both in pendular and funicular states. Moreover, the difference between the model curves and experimental results became larger with increasing concentration of 1-butanol in the pore-liquid.

Out of all the parameters used in the micro-mechanical model, surface tension, contact angle are the only two parameters which can vary depending on the type of pore-liquid used to prepare the specimens. Since contact angle is assumed to be zero for the current analysis, there is one possibility which can arise – the relationship between the tensile strength and surface tension could be non-linear. Therefore, new set of simulations were performed to improve the goodness of fit of the model curves by using surface tension as a fitting parameter and using other parameters from Case-1-S1 simulations. It was found that the model curves

fitted the experimental results for surface tension values which are higher than the actual surface tension of the corresponding solution. The model curves fitted the experimental results for surface tension values of 60 mN/m, 50.4 mN/n and 40.8 mN/m for S2, S3 and S4 solutions, respectively. These results are shown in **Figure 5.2**.

Similar to Case-1, model curves using micro-mechanical model were simulated and compared with Case-2 experimental results. Difference between the experiments from Case-1 and Case-2 is that the packing density of the soil specimen was decreased to 1.61 g/cm^3 from 1.65 g/cm^3. Therefore, it is expected that the model curves will fit the experimental results for higher *a/d* ratio. Using model parameters as described for Case-1 simulations, the model curves fitted the Case-2-S1 experimental results. The model curves fitted the experimental results for *a/d* = 0.044. Comparing to Case-1, the model curve fitted Case-2 experimental results for higher *a/d* ratio. This is because the packing density of Case-2 specimen is lower and, hence, the distances between the soil particles are comparatively larger. This set of parameters was used for simulating other results for Case-2 for specimens prepared using S2, S3 and S4. The results have been summarized in **Figure 5.3**. Similar to Case-1 comparisons, it was found that the model curves did not match the experimental results for reduced surface tension of pore-liquid. The discrepancy between the model predictions and experimental values increased with increasing concentration of 1-butanol in the solution. The model curves were also simulated using surface tension as fitting parameter and they fitted the Case-2 experimental results for 62.4 mN/m, 50.4 mN/n and 43.2 mN/m for S2, S3 and S4 solutions respectively **(Figure 5.4)**. Similar to Case-1 simulations, model curves fitted the experimental results for surface tension values which are higher than the actual surface tension of the corresponding solution. Moreover, the surface tension 'mobilized' during direct tension tests using S2, S3 and S4 solutions is approximately same for both Case-1 and Case-2. Therefore, comparison of model curves with experimental results might indicate a non-linear relationship between the surface tension and tensile strength of unsaturated sands. However, further validation of this hypothesis is required.

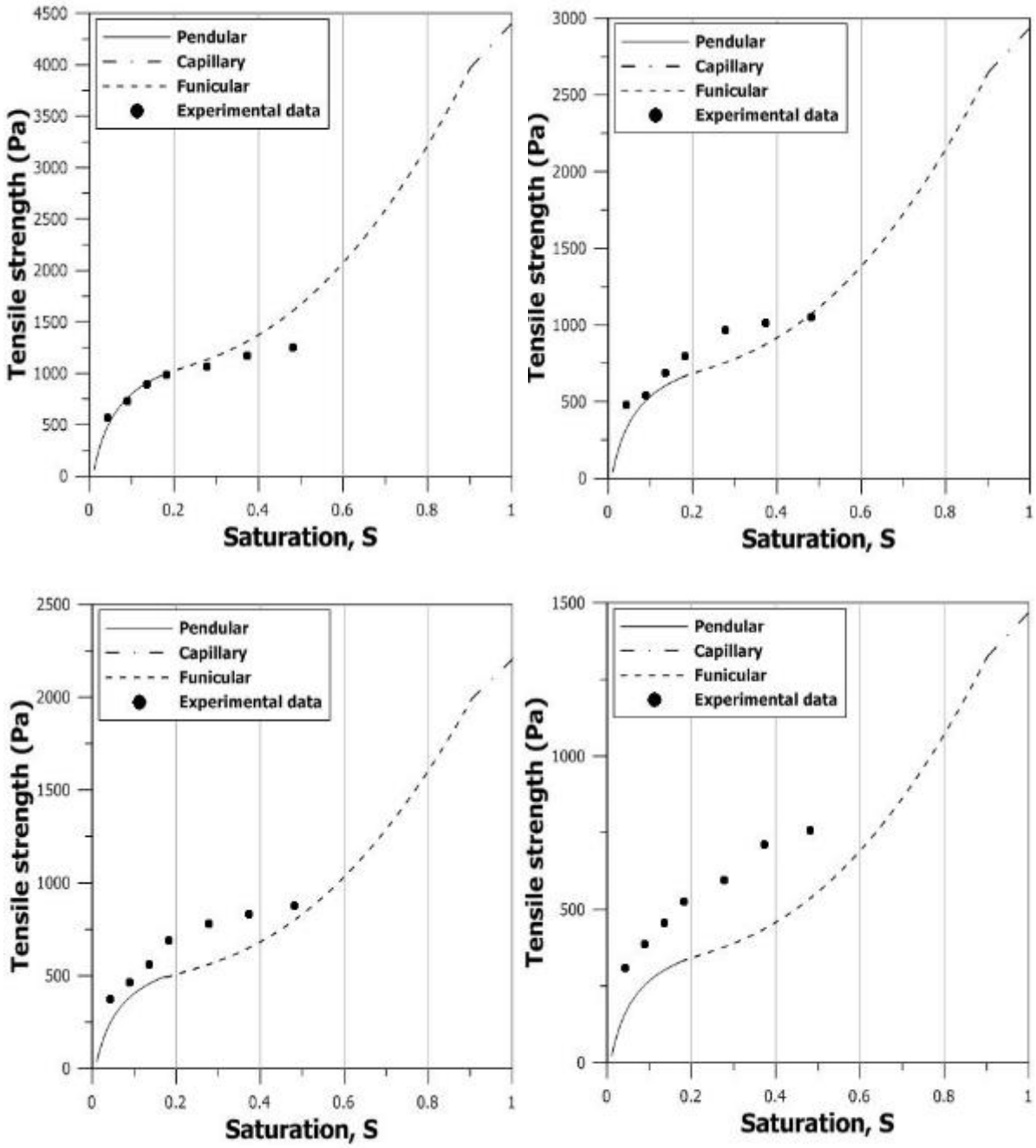

Figure 5.1 Comparison of the measured and predicted tensile strength for Case-1 experiments using micro-mechanical model (a/d = 0.037; k = 12; e = 0.35) (a) water; (b) 1.75% w/w 1-butanol; (c) 3.5% w/w 1-butanol; (d) 7% w/w 1-butanol

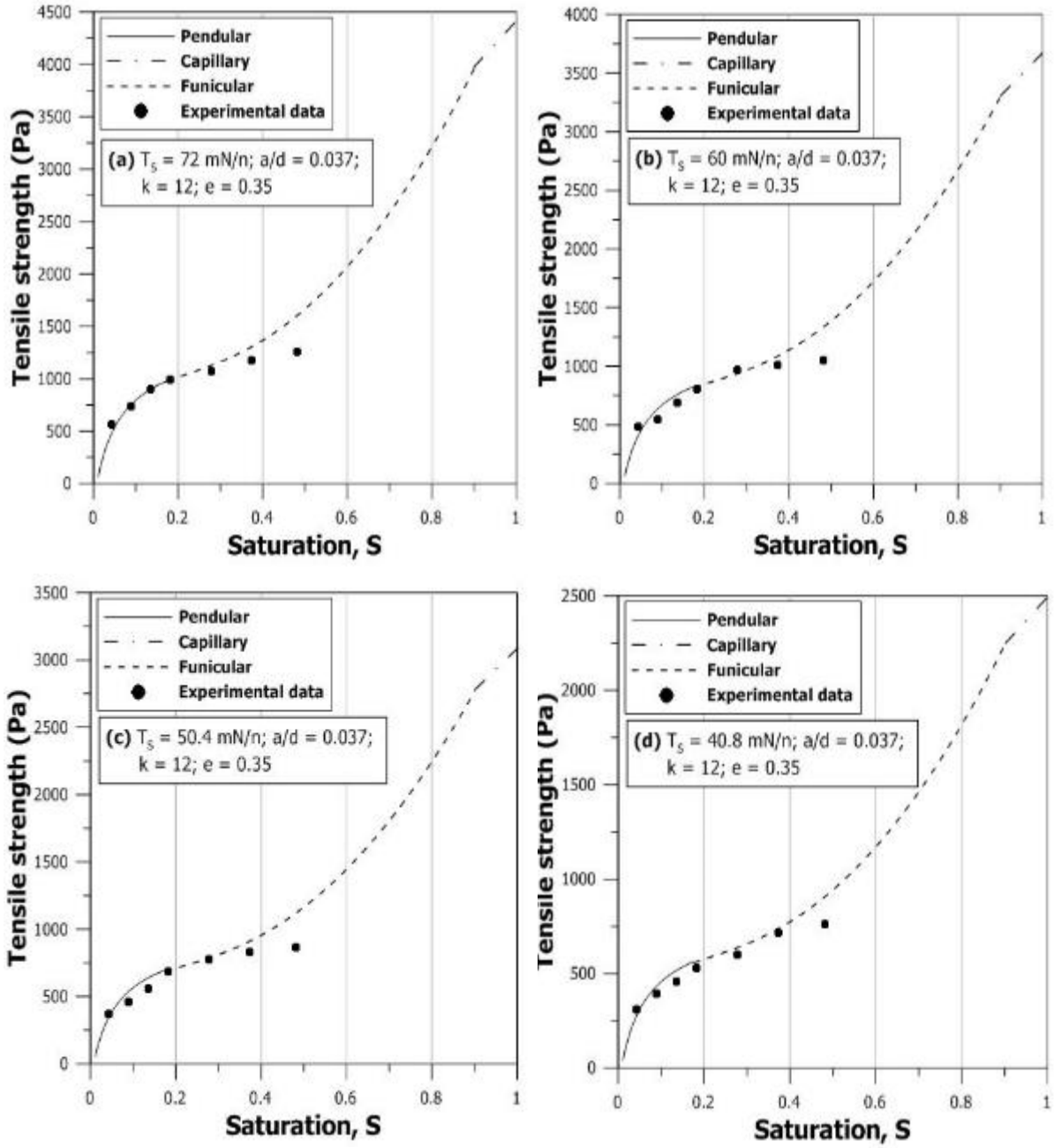

Figure 5.2 Comparison of the measured and predicted tensile strength for Case-1 experiments using surface tension as fitting parameter (a/d = 0.037; k = 12; e = 0.35) (a) water; (b) 1.75% w/w 1-butanol; (c) 3.5% w/w 1-butanol; (d) 7% w/w 1-butanol

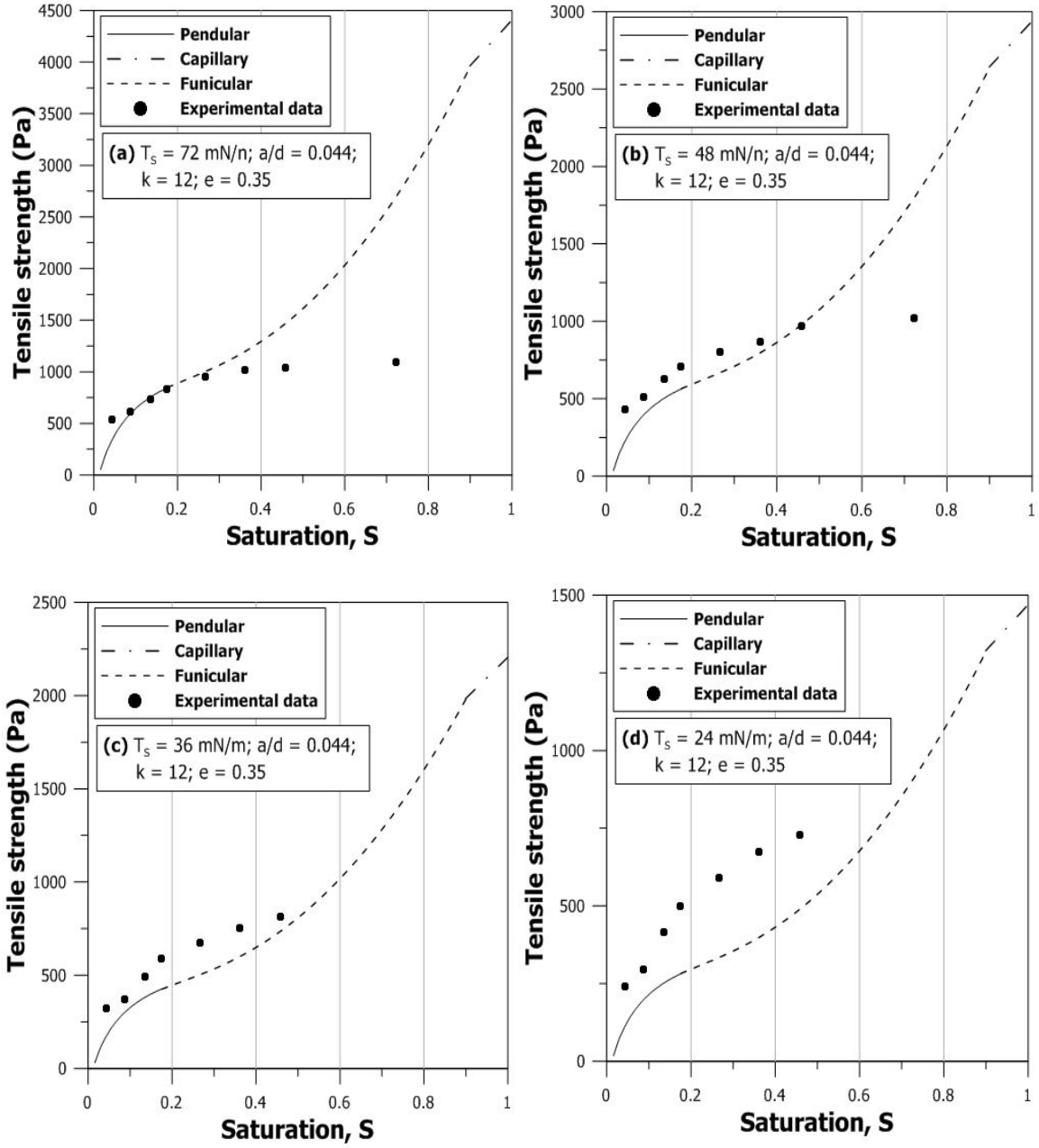

Figure 5.3 Comparison of the measured and predicted tensile strength for Case-1 experiments using micro-mechanical model (a/d = 0.037; k = 12; e = 0.35) (a) water; (b) 1.75% w/w 1-butanol; (c) 3.5% w/w 1-butanol; (d) 7% w/w 1-butanol

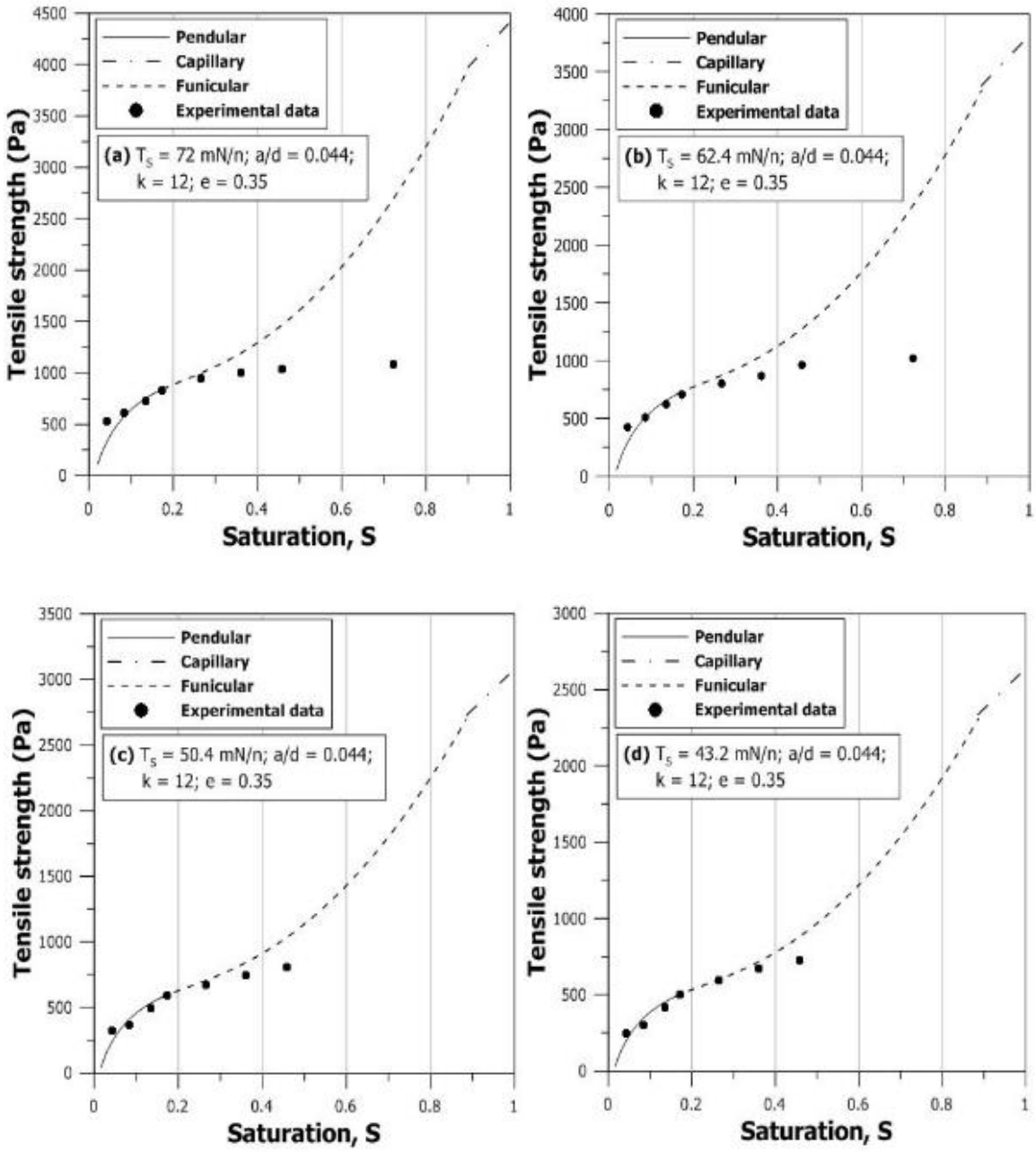

Figure 5.4 Comparison of the measured and predicted tensile strength for Case-2 experiments using surface tension as fitting parameter (a/d = 0.044; k = 12; e = 0.35) (a) water; (b) 1.75% w/w 1-butanol; (c) 3.5% w/w 1-butanol; (d) 7% w/w 1-butanol

5.2 ANALYSIS USING MACRO-MECHANICAL MODEL

Macro-mechanical model has been described in details in **Section 2.2.2**. The experimental results were compared with the model curves simulated using macro-mechanical model. The results were simulated for Case-1 and Case-2 experiments, wherein the loading rates and packing densities were 4.2 g/s and 1.65 g/cm^3, 4.2 g/s and 1.61 g/cm^3, respectively. In each case, unsaturated silica sand specimens were prepared using S1, S2, S3 and S4 solutions and direct tension tests were performed at different moisture contents. The experimental program has been discussed in **Section 3.5**.

Eight simulations were performed to obtain model curves which were compared with experimental results from Case-1 and Case-2. Lu et al. (2009) compared experimental results and model curves simulated using the macro-mechanical model and found that the model predicts the tensile strength of unsaturated sand specimens, when wetted with water, with reasonable accuracy over the entire range of saturation. Therefore, simulations for each case with S1 was considered as the reference analysis to calculate model parameters. Model parameters from the reference analysis was used to simulate results for cases with S2, S3 and S4 solutions. The main objective of simulating and comparing model curves and experimental results was to check the effectiveness of the macro-mechanical model to predict the tensile strength at reduced surface tension of the pore-liquid.

Macro-mechanical model uses four parameters – residual saturation (S_r), internal friction angle (ϕ), inverse of AEV (α') and pore size distribution parameter (n). The last two parameters are van Genuchten SMCC curve-fitting parameters. Since SMCC and direct shear test measurements for silica sand were not performed experimentally, a representative value of friction angle was used and van Genuchten parameters were calibrated using the experimental tensile strength results. The value of residual saturation was taken to be 0.15, which was obtained from the SMCC of F-75 Ottawa sand (Kim and Sture 2008). It has been reported that granular materials at small normal stress levels show very high friction angle values in the range of 47˚ to 70˚ (Sture et al. 1998). Friction angle for medium to fine sands generally ranges from 50˚ to 55˚ at small normal stress level (Kim 2001, Lu et al. 2007). On

this basis, friction angle of 56˚ was adopted and different sets of α' and n values for silica sand were used to fit the model curve against the experimental results.

Using ϕ = 56˚, model curves were simulated and it was found that at n = 2.8 and α' = 0.44 kPa^{-1}, the model curves predictions were found to match Case-1 experimental results reasonably well, where S1 solution was used. The value of α' was scaled for S2, S3, S4 solutions by the ratio equal to the ratio of surface tension of corresponding solution to distilled water. **Table 5.2** lists the values of α' used for simulations following the macro-mechanical model. Therefore, the simulations for Case-1 experiments using S2, S3 and S4 solutions were performed using ϕ = 56˚, n = 2.8 and α' as described in **Table 5.2**. The results have been summarized in **Figure 5.5**. Using the given model parameters, it was observed that the model curves did not match the experimental results for Case-1 experiments using S2, S3 and S4 solutions. Moreover, as the surface tension of the pore-liquid became smaller, the difference between the experimental and predicted values became larger. Similar to micro-mechanical model, the discrepancy between experimental values and model curves suggests that the relationship between tensile strength and surface tension of the pore-liquid might not be linear. As a result, similar to micro-mechanical analyses, values of α' for S2, S3 and S4 solutions were calculated by back analyzing the results from predicted model curves and comparing them with experimental results.

Therefore, using ϕ = 56˚, n = 2.8 and α' as a fitting parameter, simulations were performed for Case-1 experiments for S2, S3 and S4 solutions. The results have been summarized in **Figure 5.6**. It was observed that the predicted model curves fitted the experimental results when α' = 0.53 kPa^{-1}, 0.64 kPa^{-1} and 0.77 kPa^{-1} for S2, S3 and S4 solutions, respectively. Compared to **Table 5.2**, these α' values are much smaller; smaller α' suggests higher AEV and higher surface tension.

Table 5.2 Values of α' used for macro-mechanical simulations

Solution used	Surface tension (mN/m)	Reduction factor	α' (kPa^{-1})
Distilled water (S1)	72	72/72 = 1.00	0.44
1.75% w/w 1-butanol (S2)	48	48/72 = 0.67	0.66
3.50% w/w 1-butanol (S3)	36	36/72 = 0.50	0.88
7.00% w/w 1-butanol (S4)	24	24/72 = 0.33	1.32

Similar to Case-1 simulations, Case-2 experimental results were compared with the predicted model curves based on macro-mechanical model. Difference between the experiments from Case-1 and Case-2 is that the packing density of the soil specimen was reduced to 1.61 g/cm^3 from 1.65 g/cm^3. It is known that any reduction in the packing density of the soil specimen will result in higher void ratio and lower AEV (i.e., higher α' value) (Aitchison 1960; Gallage and Uchimura 2010). On this basis, it was expected that the model curves would predict the Case-3 experimental results at lower AEVs as compared to Case-1 results. Based on the literature review, a unique correlation is between packing density and SMCC is not available. The correlation is highly dependent on the soil type, grain-size distribution, porosity and dry density, and, hence, has to be formulated for any given soil experimentally. Further, the magnitude of ϕ and n will also depend on the packing dry density of the soil specimen.

However, for the current analysis, it was assumed that ϕ and n values do not change considerably for a small change in the dry density; hence, ϕ and n values from Case-1 can be used for simulating results for Case-3 experiments. Therefore, using ϕ = 56˚, n = 2.8 and α' as the fitting parameter, simulations were performed for Case-3 experiments using S1, S2, S3 and S4 solutions. The results have been summarized in **Figure 5.7**. It was observed that the predicted model curves fitted the experimental results when α' = 0.51 kPa^{-1}, 0.58 kPa^{-1}, 0.71 kPa^{-1} and 0.83 kPa^{-1} for S1, S2, S3 and S4 solutions, respectively. As expected, α' values for Case-3 simulations were considerably higher than Case-1 simulations, which meant that the model curves fitted the experimental results for lower AEVs. Therefore, for the given assumptions and model parameters, it can be inferred that the macro-mechanical model is able to predict the expected trend in tensile behaviour of unsaturated sand at different dry densities reasonably well.

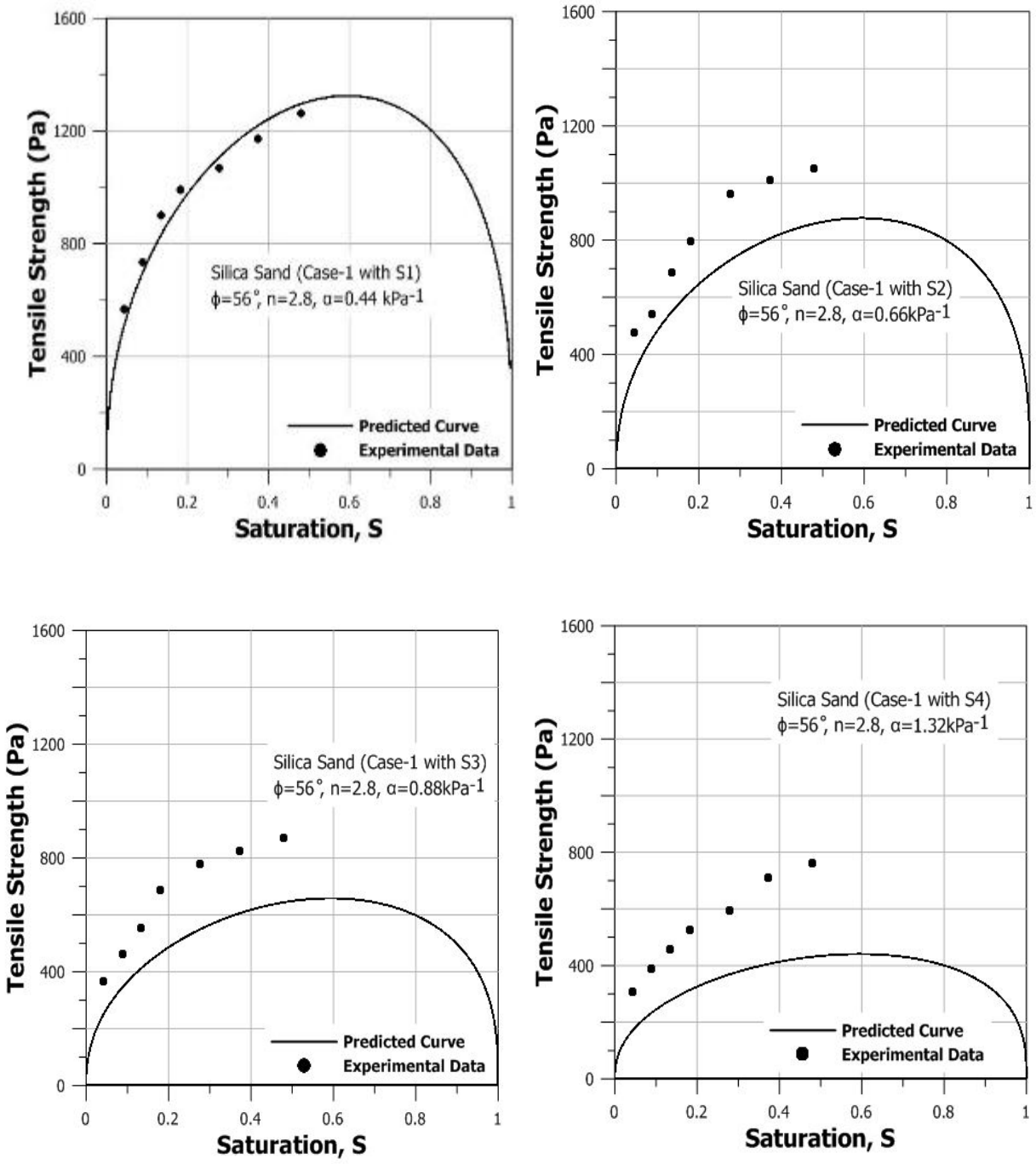

Figure 5.5 Comparison of the measured and predicted tensile strength for Case-1 experiments using macro-mechanical model

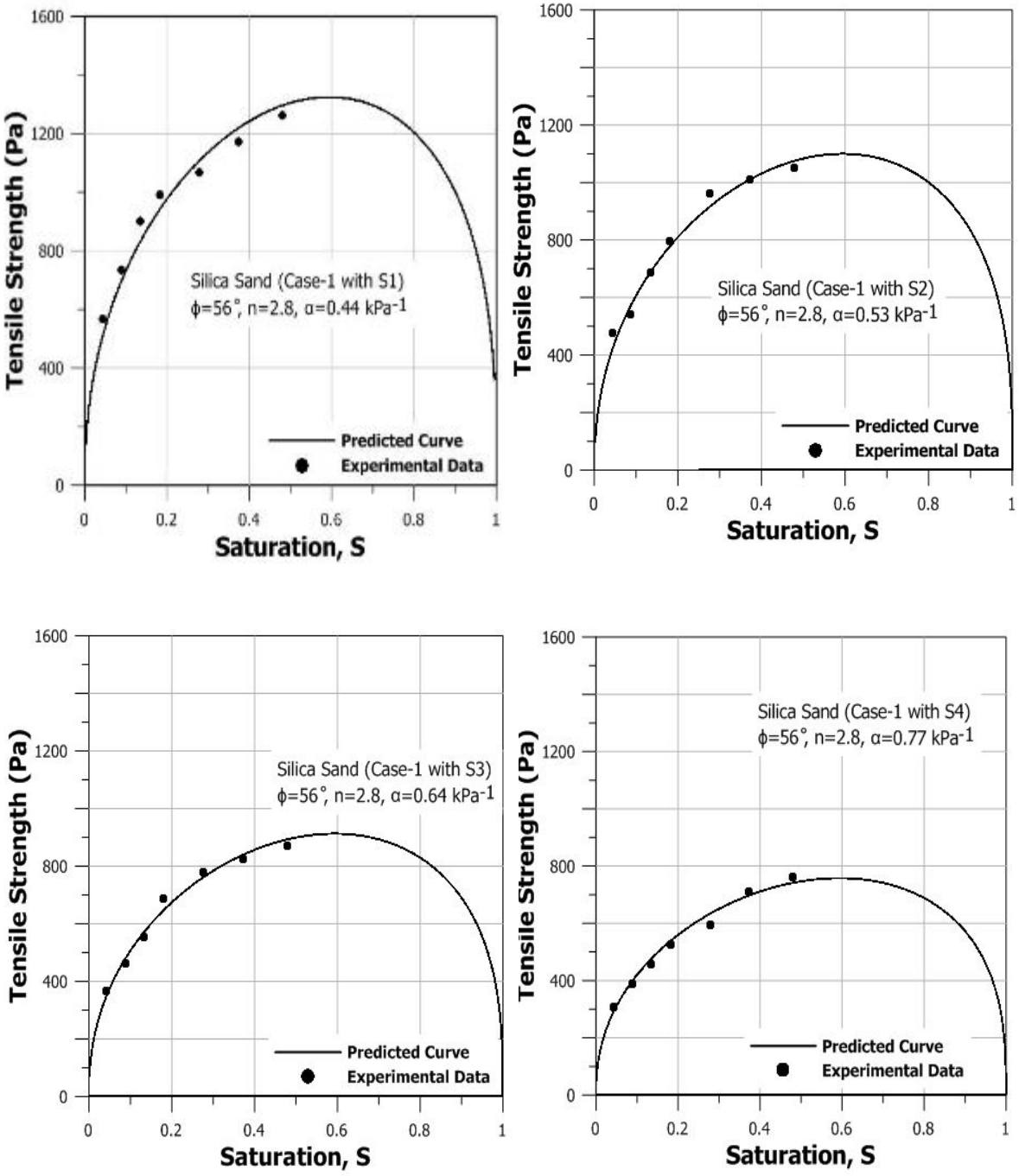

Figure 5.6 Comparison of the measured and predicted tensile strength for Case-1 experiments using α' as the fitting parameter (macro-mechanical model)

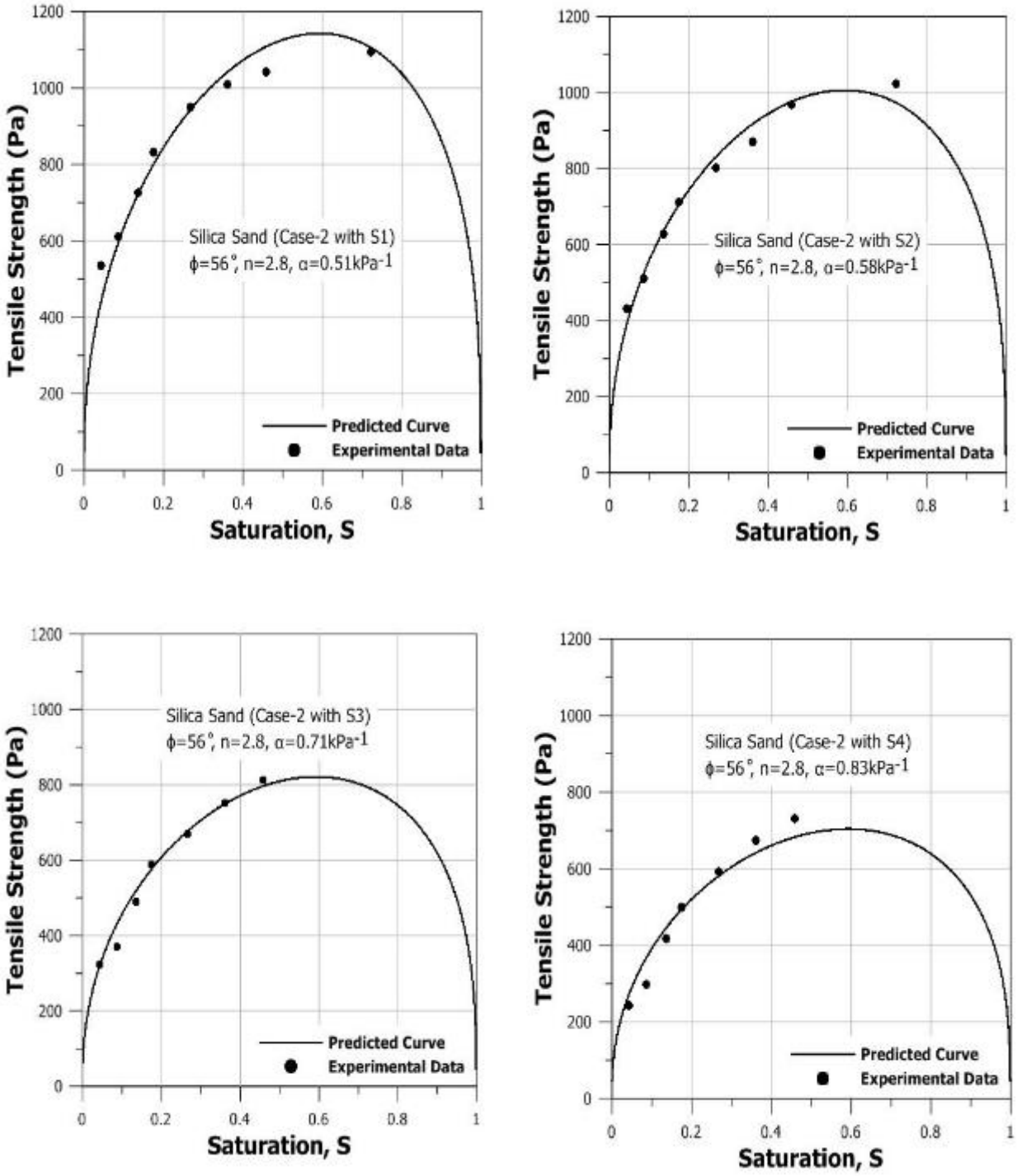

Figure 5.7 Comparison of the measured and predicted tensile strength for Case-2 experiments using α' as fitting parameter (macro-mechanical model)

6 CONCLUSIONS AND RECOMMENDATIONS

6.1 SUMMARY OF EXPERIMENTAL RESULTS AND THEORETICAL MODELING

As the focus on unsaturated soil mechanics is on the rise, qualitative and quantitative knowledge of tensile strength of unsaturated sands is the next major step and it can prove to be very significant in the design and analysis of many geotechnical structures and systems. A detailed experimental and theoretical investigation was performed to study the effect the pore-water surface tension on the tensile strength of unsaturated sands. It is already known that surface tension affects the matric suction and that the tensile strength of unsaturated sands is a function of surface tension and matric suction. Hence, an elaborate tensile testing procedure was developed to study the effect of concentration-dependent surface tension on the tensile strength. A custom-built direct tension apparatus was used to measure the tensile strength. Load cell and LVDT along with LabVIEW data acquisition system were used to measure the load vs time and deformation vs time measurements. Using this set-up, it was possible to determine the tensile load at failure and the exact time of tensile failure accurately. This can be considered as a major improvement in the direct tension apparatus as previous researchers relied on manual measurements only. Tensile strength measurements were further improved by eliminating the error due to friction in the apparatus.

Based on the experimental results, it was found that the tensile strength of unsaturated sands decrease significantly when the surface tension of the pore-liquid is reduced. Lower the surface tension of the pore-liquid, lower is the tensile strength. Contrary to the theoretical tensile strength models, it was found that the decrease in the tensile strength is not linearly proportional to the decrease in the surface tension. In other words, decrease in tensile strength is not a simple multiple of the decrease in the ratio of surface tension of the pore-liquid. Tensile strength was also dependent on the rate at which tensile load was applied to the specimen. As the loading rate increased, the tensile strength decreased. Using regression analysis, it was found that the tensile strength decreased linearly with increase in the loading rate. Also, the rate of decrease in tensile strength with loading rate was independent of the solution used for

specimen preparation. Experimental results were also analyzed and investigated using the micro-mechanical and macro-mechanical tensile strength theoretical models.

Micro-mechanical model consists of two parts: Rumpf's model to predict the tensile strength in the pendular state and Schubert's model to predict the tensile strength in the funicular and capillary states. Based on the simulation results, it was found that Rumpf's model was able to predict the tensile strength in the pendular state reasonably well. However, at reduced surface tension, Rumpf's model under-predicted the tensile strength. The goodness of fit of model curves was improved by using higher surface tension values instead of surface tension values of the corresponding solutions. This implies that, unlike matric suction, the tensile strength of unsaturated sands does not scale linearly with reduction in surface tension of pore-liquid. On the other hand, Schubert's model over-predicts the tensile strength significantly. The discrepancies in the model can be due to following reasons: (1) Rumpf's and Schubert's models were proposed for perfect spherical granular materials with a definite packing arrangement. Hence, these models can prove to be very simplistic to represent real soil behaviour; (2) while simulating the model curves, the contact angle is assumed to be zero and contact angle hysteresis is not considered. These assumptions might result in significant deviations of model curves when compared to experimental results; (3) the surface tension values of the 1-butanol solutions were estimated using the data published in existing literature and it was assumed that the 1-butanol solutions prepared in the laboratory were homogeneous. It is recommended that direct measurements of surface tension of 1-butanol solutions should be performed to improve the reliability of the experimental results. Therefore, further investigations are required to understand the tensile mechanisms, especially at higher saturation levels. Comparing Case-1 and Case-2 experimental and predicted results, it was found that when the density of the specimen is changed, only a/d ratio is affected and it becomes an important fitting parameter.

Macro-mechanical model is also able to predict the tensile strength of the unsaturated sand with reasonable accuracy across pendular and funicular saturation states for specimens containing distilled water. The macro-mechanical model curve under-predicted the experimental results at reduce surface tension of the pore-liquid. Based on the simulation results, it was found that the model curves fitted the experimental results for 1-butanol

containing specimens at suction values higher than the suction values of the 1-butanol solutions scaled using the ratio of surface tension of distilled water to 1-butanol solution. Hence, similar to micro-mechanical model, macro-mechanical model comparisons also show that the relationship between tensile strength and surface tension of the pore-liquid may not be linear. Comparison of Case-2 with Case-1 experimental and predicted results shows that the macro-mechanical model is able to predict the decrease in uniaxial tensile strength with decrease in packing density of the specimen. When packing density is changed keeping loading rate constant, knowledge of all three parameters (α', n, φ) becomes important. Therefore, the effectiveness of the macro-mechanical model is highly dependent on the accurate measurements of SMCCs and internal friction angles at different dry densities and calibration of van Genuchten SMCC parameters.

6.2 FUTURE SCOPE OF WORK

Many experimental and theoretical limitations were encountered during the course of the study which warrants further studies. Following are few recommendations which can prove to be useful for future studies on tensile strength of unsaturated sands:

1. An avenue for future research is to have tensiometers or similar suction-measuring device installed along with the direct tension apparatus. The use of tensiometer should be considered to measure in-situ matric suction independently. This will be extremely useful to correlate matric suction and tensile strength, and understand the role of reduced surface tension of pore-water on tensile strength of unsaturated sands.
2. The accuracy and reliability of the results can be further improved by measuring the surface tension of 1-butanol solutions directly prior to direct tension tests. In this context, it also recommended to measure the SMCC curves for silica sands using standard laboratory techniques. This will help in determining the model parameters for micro-mechanical and macro-mechanical model more accurately.
3. Direct tension tests performed at saturation levels of 70% and above were subjected to leaking of the pore-liquid from the soil specimen during compaction and testing. Thus, direct tension apparatus must be modified and improved to perform tests at higher saturation levels. To prevent gravity drainage of pore-water from the specimens, the depth of the specimen container can be decreased while keeping the area of the failure

surface constant. The resulting specimen container will therefore be cuboidal in shape with wider base and shorter depth.

4. Since micro-mechanical model was developed for granular materials idealized as perfect spheres with smooth outer surfaces (such as glass beads, powders), some significant changes needs to be incorporated to take in account the irregular shapes and rough outer surfaces of the sand particles. For example in the pendular regime, certain amount of pore-liquid gets adsorbed on the surface of the sand particle but this component is not included in micro-mechanical model of tensile strength.
5. While simulating results using micro-mechanical model, contact angle was assumed to be zero and contact angle hysteresis was completely ignored. However, in case of real soils, this assumption might significantly affect the tensile strength, since, contact angle plays an important role in controlling the shape the liquid meniscus (r^* and h^*). Hence, it is recommended to study how concentration-dependent surface tension of the pore-liquid might effect of the contact angle and significance of contact angle hysteresis in tensile strength predictions.
6. An extensive study is recommended to validate the predictions using macro-mechanical model. SMCCs of silica sand should be experimentally measured at different densities. Measurements of internal friction angle should also be made using direct shear tests at different strain rates and packing densities. These measurements along with tensile strength measurements using direct tension apparatus can then be used to validate the macro-mechanical model more accurately.

6.3 FINAL NOTE

Considering the difficulty and uncertainty in measuring and monitoring unsaturated soil property functions, both in-situ and experimentally, the application of unsaturated soil mechanics in the field of geotechnical engineering has been limited. Another argument is that the design procedure using classical saturated soil mechanics is considered to be on the conservative side, hence using unsaturated soil mechanics is redundant (Sheng et al. 2013). These perceptions have proved to be a major hindrance towards implementation in actual field practice. Nevertheless, numerous forensic analyses of geotechnical problems related to slope stability (Griffiths and Lu 2005; Gens 2010; Sorbino and Nicotera 2013), foundations on

expansive soils (Attwooll et al. 2006), settlement of railway embankments (Cardoso et al. 2012) and problems related to geo-environmental engineering and mining engineering have provided some insight on engineering applications of unsaturated soil mechanics. For example, Alonso and Olivella (2006) reported that embankments and dams can experience significant deformations under the influence of seasonal wetting and drying cycles.

Fredlund (2000) rightly said that the implementation of unsaturated soil mechanics into practice will require years of collaboration between researchers and geotechnical engineers. Recent use of SMCCs, unsaturated hydraulic conductivity functions and suction-dependent shear strength in geotechnical practices have been a major step. Similarly, unsaturated soil mechanics have been used to develop methodologies for determining ground surface flux boundary condition. This is relevant for problems dealing with unsaturated-saturated seepage analysis of earthen dams and design of soil covers. But the application of tensile strength of unsaturated sands in geotechnical practice would need further research and validation of available testing techniques and theoretical models.

A cursory review into tensile strength of unsaturated sand shows that researchers started to show some interest in the fundamental concepts and experimental techniques only in the 1990s. Prior to 1990s, most of the works on tensile strength was limited to fine-grained soils and cemented soils. Most of the experimental techniques and theories have been derived from the work and research in the field of powder technology, soil science and tensile strength of clay and cemented soils (Rumpf 1961; Pietsch and Rumpf 1963; Conlon 1966; Bofinger 1970; Schubert 1975a, 1975b, 1979, 1984; Pierrat and Caram 1997; Tang and Graham 2002). More recently, Lu et al. (2009) have developed a macro-mechanical model to determine tensile strength in unsaturated sands using the concept of suction stress (Lu and Likos 2006). In the current research work, effect of pore-water surface tension on tensile strength have been studied. It was found that the tensile strength of unsaturated sands decreases on lowering the surface tension of the pore-liquid. Tensile strength of unsaturated sands is also dependent on the packing density of the specimen and the rate at which tensile load is applied. This result can be significant for various geotechnical (e.g. slope stability and landslides) and geo-environmental engineering problems (e.g. sub-surface remediation).

REFERENCES

Aitchison, G.D., and Donald, I.B. 1956. Effective stresses in unsaturated soils. In Proceedings of 2nd Aust. N.Z. Conference on Soil Mechanics, 192-199.

Aitchison, G.D. 1960. Relationships of the moisture stress and effective stress functions in unsaturated soils. In Proceedings of Pore Pressure and Suction in Soils, Butterworths, London, 47-52.

Ajaz, A., and Parry, R.H. 1976. Bending test for compacted clays. Journal of the Geotechnical Engineering Division (ASCE), 102(9): 929-943

Al-Hussaini, M.M., and Townsend, F.C. 1973. Tensile testing of soils: A literature review. Soils and Pavement Laboratory, U.S Army Engineer Waterways Experiment Station, Vicksburg, Miss.

Alonso, E., and Olivella, S. 2006. Unsaturated soil mechanics applied to geotechnical problems. In Proceedings of Unsaturated Soils 2006 (ASCE), 1-35.

Ashton, M., Cheng, D.-H., Farley, R., and Valentin, F. 1965. Some investigations into the strength and flow properties of powders. Rheologica Acta, 4(3): 206-218.

ASTM D698 Standard Test Methods for Laboratory Compaction Characteristics of Soil Using Standard Effort

ASTM D854 Standard Test Methods for Specific Gravity of Soil Solids by Water Pycnometer.

ASTM D2216 Standard Test Methods for Laboratory Determination of Water (Moisture) Content of Soil and Rock by Mass

ASTM D2487 Standard Practice for Classification of Soils for Engineering Purposes (Unified Soil Classification System)

Attwooll, B., Reins, J., and Lykosh, P. 2006. Heave at manufacturing facility: Observations and response. In Unsaturated Soils 2006. ASCE. pp. 323-334.

BASF The Chemical Company. March 2008. n-Butanol Technical Leaflet. M 2084 e.

Bashir, R. 2007. Quantification of surfactant induced unsaturated flow in the vadose zone. Ph.D. thesis, Department of Civil Engineering, McMaster University, Hamilton, ON

Bashir, R., Stolle, D.F., and Smith, J.E. 2007. Flux-based alternative formulation for variably saturated subsurface flow. Journal of Hydrologic Engineering (ASCE), 12(5): 501-512.

Bear, J. 1972. Dynamics of fluids in porous media. American Elsevier Publishing Company, Inc., New York.

Bikerman, J.J. 1970. Physical surfaces. Academic Press, New York and London.

Bishop, A.W. 1959. The principles of effective stress. Teknisk Ukeblad, 39: 859-863.

Bishop, A.W., and Blight, G. 1963. Some aspects of effective stress in saturated and partly saturated soils. Géotechnique, 13(3): 177-197.

Bishop, A.W., and Garga, V.K. 1969. Drained tests on London clay. Géotechnique, 19(2): 309-312.

Bofinger, H.E. 1970. The measurement of the tensile properties of soil cement. RRL Report LR 365, Road Research Laboratory, Ministry of Transport, Crowthome, Berkshire.

Braunack, M.V., Hewitt, J.S., and Dexter, A.R. 1979. Brittle fracture of soil aggregates and the compaction of aggregate beds. European Journal of Soil Science, 30(4): 653-667.

Burland, J. 1965. Some aspects of the mechanical behaviour of partly saturated soils. In Moisture Equilibria and Moisture Changes in Soils beneath Covered Areas, a Symposium, Butterworth, Sydney, Australia, 270-278.

Cardoso, R., Fernandes, V., Ferreira, T.M., and Teixeira, P.F. 2012. Settlement Prediction of High Speed Railway Embankments Considering the Accumulation of Wetting and Drying Cycles. In Unsaturated Soils: Research and Applications. Springer. pp. 291-298.

Cheng, D.C.-H. 1968. The tensile strength of powders. Chemical Engineering Science, 23: 1405-1420.

Cho, G.C., and Santamarina, J.C. 2001. Unsaturated particulate materials - Particle-level studies. Journal of Geotechnical and Geoenvironmental Engineering (ASCE), 127(1): 84-96.

Conlon, R.J. 1966. Landslide on the Toulnustouc River, Quebec. Canadian Geotechnical Journal, 3: 113-144.

DallaValle, J.M. 1948. Micromeritics: the technology of fine particles. Pitman Publishing Corporation, New York and Chicago.

Demond, A.H., and Roberts, P.V. 1991. Effect of interfacial forces on two-phase capillary pressure-saturation relationships. Water Resources Research, 27(3): 423-437.

Demond, A., Desai, F., and Hayes, K. 1994. Effect of cationic surfactants on organic liquid-water capillary pressure-saturation relationships. Water Resources Research, 30(2): 333-342.

Desai, F., Demond, A., and Hayes, K. 1991. Influence of surfactant sorption on capillary pressure-saturation relationships. Transport and Remediation of Subsurface Contaminants, ACS Symposium Series, 491(11): 133-148.

Dobbs, H., and Yeomans, J. 1992. Capillary condensation and pre-wetting between spheres. Journal of Physics: Condensed Matter, 4(50): 10-23.

Dury, O., Fischer, U., and Schulin, R. 1998. Dependence of hydraulic and pneumatic characteristics of soils on a dissolved organic compound. Journal of Contaminant Hydrology, 33(1): 39-57.

Farrell, D.A., Greacen, E.L., Larson, W.E. 1967. The effect of water content on axial strain in a loam soil under tension and compression. Soil Science Society of America Journal, 31 (4): 445-450.

Fredlund, D.G., and Morgenstern, N.R. 1977. Stress state variables for unsaturated soils. Journal of Geotechnical and Geoenvironmental Engineering (ASCE), 103(GT5): 447-466.

Fredlund, D.G., Morgenstern, N.R., and Widger, R.A. 1978. The shear strength of unsaturated soils. Canadian Geotechnical Journal, 15(3): 313-321.

Fredlund, D., Rahardjo, H., and Gan, J. 1987. Non-linearity of strength envelope for unsaturated soils. In Proceedings of 6th International Conference on Expansive Soils, New Delhi, India, 49-54.

Fredlund, D.G. 1998. Bringing unsaturated soil mechanics into engineering practice. In Keynote address, 2nd International Conference on Unsaturated Soil, Beijing, China.

Fredlund, D.G., and Rahardjo, H. 1993. Soil mechanics for unsaturated soils. John Wiley & Sons, Inc., New York.

Fredlund, D.G. 2000. The 1999 RM Hardy Lecture: The implementation of unsaturated soil mechanics into geotechnical engineering. Canadian Geotechnical Journal, 37(5): 963-986.

Fredlund, D.G., Rahardjo, H., and Fredlund, M.D. 2012. Unsaturated soil mechanics in engineering practice. John Wiley & Sons, Inc., New York.

Fredlund, M.D., Fredlund, D.G., and Wilson, G.W. 2000. An equation to represent grain-size distribution. Canadian Geotechnical Journal, 37(4): 817-827.

Gallage, C.P.K., and Uchimura, T. 2010. Effects of dry density and grain size distribution on soil-water characteristic curves of sandy soils. Soils and Foundations, 50(1): 161-172.

Gan, J., Fredlund, D., and Rahardjo, H. 1988. Determination of the shear strength parameters of an unsaturated soil using the direct shear test. Canadian Geotechnical Journal, 25(3): 500-510.

Gens, A. 2010. Soil–environment interactions in geotechnical engineering. Géotechnique, 60(1): 3-74.

Goulding, R.B. 2006. Tensile strength, shear strength and effective stress for unsaturated sand. Ph.D. thesis, Department of Civil Engineering, University of Missouri, Missouri Columbia.

Griffith, A.A. 1921. The phenomena of rupture and flow in solids. Philosophical Transactions of the Royal Society of London, Series A, 221: 163-198.

Griffiths, D., Lu, N. 2005. Unsaturated slope stability analysis with steady infiltration or evaporation using elasto-plastic finite elements. International Journal for Numerical and Analytical Methods in Geomechanics, 29(3): 249-267.

Haefeli, R. 1951. Investigation and measurements of the shear strengths of saturated cohesive soils. Géotechnique, 2(3): 186-208

Hartley, P., and Parfitt, G. 1984. An improved split-cell apparatus for the measurement of tensile strength of powders. Journal of Physics E: Scientific Instruments 17(5): 347-349.

Hasegawa, H., and Ikeuti, M. 1964. On the tensile strength of disturbed soils. In Proceedings of the Symposium on Rheology and Soil Mechanics. Berlin, Germany, 405-412.

Heibrock, G., Zeh, R., and Witt, K. 2005. Tensile strength of compacted clays. Unsaturated soils: Experimental studies, Springer Proceedings in Physics, 93: 395-412

Henry, E., Smith, J., and Warrick, A. 1999. Solubility effects on surfactant-induced unsaturated flow through porous media. Journal of Hydrology, Elsevier, 223(3): 164-174.

Henry, E., Smith, J., and Warrick, A. 2001. Surfactant effects on unsaturated flow in porous media with hysteresis: horizontal column experiments and numerical modeling. Journal of Hydrology, Elsevier, 245(1): 73-88.

Jennings, J. 1961. A revised effective stress law for use in the prediction of the behaviour of unsaturated soils. In Proceedings of Pore Pressure and Suction in Soils, London. Butterworths, 26-30.

Jennings, J.E., and Burland, J.B. 1962. Limitations to the use of effective stresses in partly saturated soils. Géotechnique, 12(2): 125-144.

Karagunduz, A., Pennell, K.D., and Young, M.H. 2001. Influence of a non-ionic surfactant on the water retention properties of unsaturated soils. Soil Science Society of America Journal, 65(5): 1392-1399.

Karube, D., and Kawai, K. 2001. The role of pore water in the mechanical behavior of unsaturated soils. Geotechnical & Geological Engineering, 19(3-4): 211-241.

Khalili, N., and Khabbaz, M. 1998. A unique relationship of chi for the determination of the shear strength of unsaturated soils. Géotechnique 48(5): 681-687.

Khalili, N., Geiser, F., and Blight, G. 2004. Effective stress in unsaturated soils: review with new evidence. International Journal of Geomechanics, 4(2): 115-126.

Kim, T.-H. 2001. Moisture-induced tensile strength and cohesion in sand. Ph.D. thesis, Department of Civil Engineering, University of Colorado, Boulder, Columbia.

Kim, T.-H., and Hwang, C. 2003. Modeling of tensile strength on moist granular earth material at low water content. Engineering Geology, 69(3-4): 233-244.

Kim, T.-H., and Sture, S. 2004. Effect of moisture on attraction force in beach sand. Marine Georesources and Geotechnology, 22(1-2): 33-47.

Kim, T.-H., and Sture, S. 2008. Capillary-induced tensile strength in unsaturated sands. Canadian Geotechnical Journal, 45(5): 726-737.

Kohgo, Y., Nakano, M., and Miyazaki, T. 1993*a*. Theoretical aspects of constitutive modelling for unsaturated soils. Soil and Foundations, 33(4): 49-63.

Kohgo, Y., Nakano, M., and Miyazaki, T. 1993*b*. Verification of the generalized elasto-plastic model for unsaturated soils. Soil and Foundations, 33(4): 64-73.

Krishnayya, A.V.G., Eisenstein, Z., and Morgenstern, N.R. 1974. Behavior of compacted soil in tension. Journal of the Geotechnical Engineering Division (ASCE), 100(9): 1051-1061

Kumar, S., and Malik, R. 1990. Verification of quick capillary rise approach for determining pore geometrical characteristics in soils of varying texture. Soil Science, 150(6): 883-888.

Lambe, T., and Whitman, R. 1969. Soil Mechanics. John Wiley & Sons, Inc., New York.

Leavell, D.A., and Peters, J.F. 1987. Uniaxial tensile test for soil. Technical report GL-87-10. Department of the Army, Waterways Experiment Station, U.S Army Corps of Engineers, Vicksburg, Miss.

Letey, J., Osborn, J., and Pelishek, R. 1962. Measurement of liquid-solid contact angles in soil and sand. Soil Science, 93(3): 149-153.

Lu, N., and Likos, W.J. 2004. Unsaturated soil mechanics. John Wiley and Sons, Inc., New York.

Lu, N., and Likos, W.J. 2006. Suction stress characteristic curve for unsaturated soil. Journal of Geotechnical and Geoenvironmental Engineering (ASCE), 132(2): 131-141.

Lu, N., Wu, B., and Tan, C. 2005. A tensile strength apparatus for cohesionless soils. In Proceedings of Experus 2005, Trento, Italy, 105-110.

Lu, N., Wu, B., and Tan, C.P. 2007. Tensile strength characteristics of unsaturated sands. Journal of Geotechnical and Geoenvironmental Engineering (ASCE), 133(2): 144-154.

Lu, N., Kim, T.-H., Sture, S., and Likos, W.J. 2009. Tensile strength of unsaturated sands. Journal of Geotechnical and Geoenvironmental Engineering, (ASCE) 135(12): 1410-1419.

Lu, N., Godt, J.W., and Wu, D.T. 2010. A closed-form equation for effective stress in unsaturated soil. Water Resources Research, 46(5): W05515.

Malik, R., Laroussi, C., and De Backer, L. 1979. Experimental investigation of the penetration coefficient in capillary tubes. Soil Science, 127(4): 211-218.

Mikulitsch, A.W., and Gudehus, G. 1995. Uniaxial tension, biaxial loading and wetting tests on Loess. In Proceeding of the 1st International Conference on Unsaturated Soils, Paris, France, 45-150.

Mitchell, J.K. 1976. Fundamentals of soil behaviour. Wiley Publications, New York.

Molenkamp, F., and Nazemi, A.H. 2003. Interactions between two rough spheres, water-bridge and water vapour. Géotechnique, 53(2): 255-264.

Or, D., and Tuller, M. 2005. Capillarity. In Encyclopedia of Soils in the Environment, Elsevier Science, 155-164.

Orr. F.M., Scriven, L.E., Rivas, A.P. 1975. Pendular rings between solids: Meniscus properties and capillary force. Journal of Fluid Mechanics, 67: 723-742

Peirrat, P., and Caram, H.S. 1997. Tensile strength of wet granular materials. Powder Technology, 91(2): 81-93.

Perkins, S.W. 1991. Modeling of regolith structure interaction in extraterrestrial constructed facilities. Ph.D. thesis, Department of Civil Engineering. University of Colorado, Boulder, Columbia.

Pietsch, W. 1968. Tensile strength of granular materials. Nature, 217: 736-737.

Pietsch, W., and Rumpf, H. 1967. Haftkraft, kapillardruck, flüssigkeitsvolumen und grenzwinkel einer flüssigkeitsbrücke zwischen zwei kugeln. Chemie Ingenieur Technik, 39(15): 885-893.

Rogowski, A.S., Moldenhauer, W.C., and Kirkham, D. 1968. Rupture parameters of soil aggregates. Soil Science Society of America Journal, 32(5): 720-724.

Rogowski, A.S., and Kirkham, D. 1976. Strength of soil aggregates: influence of size, density and clay organic matter content. Mededelingen van de Faculteit Landbouwwetenschappen Rijksuniversiteit, Gent, Belgium, 41(1): 85-100.

Rumpf, H. 1961. The strength of granules and agglomerates. In Agglomeration. Edited by W.A. Knepper. Interscience, New York, 379-418.

Schubert, H. 1975*a*. Tensile strength of agglomerates. Powder Technology, 11(2): 107-119.

Schubert, H., Herrmann, W., and Rumpf, H. 1975*b*. Deformation behaviour of agglomerates under tensile stress. Powder technology, 11(2): 121-131.

Schubert, H. 1979. Grundlagen des agglomerierens. Chemie Ingenieur Technik, 51(4): 266-277.

Schubert, H. 1984. Capillary forces-modeling and application in particulate technology. Powder Technology, 37(1): 105-116.

Sheng, D., Zhang, S., and Yu, Z. 2013. Unanswered questions in unsaturated soil mechanics. Science China Technological Sciences, 56(5): 1257-1272.

Smith, J.E. 1995. The effect of concentration dependent surface tension on vadose zone flow and transport. Ph.D. thesis, Department of Civil Engineering, University of Waterloo, Waterloo, ON.

Smith, J.E. 1999. Comment on 'Dependence of hydraulic and pneumatic characteristics of soils on a dissolved organic compound' by Dury et al. 1998 Journal of Contaminant. Hydrology 33: 39–57. Journal of Contaminant Hydrology, 39: 3-5.

Smith, J.E., and Gillham, R.W. 1999. Effects of solute concentration–dependent surface tension on unsaturated flow: Laboratory sand column experiments. Water Resources Research, 35(4): 973-982.

Snyder, V.A., and Miller, R.D. 1985. Tensile strength of unsaturated soils. Soil Science Society of America Journal, 49(1): 58-65.

Sorbino, G., and Nicotera, M.V. 2013. Unsaturated soil mechanics in rainfall-induced flow landslides. Engineering Geology, 165: 105-132.

Sture, S., Costes, N.C., Batiste, S.N., Lankton, M.R., AlShibli, K.A., Jeremic, B., Swanson, R.A., and Frank, M. 1998. Mechanics of granular materials at low effective stresses. Journal of Aerospace Engineering, 11(3): 67-72.

Tamrakar, S.B., Mitachi, T., Toyosawa, Y., and Itoh, K. 2005. Tensile strength of compacted and saturated soils using newly developed tensile strength apparatus. Soils and Foundations, 45(6): 103-111.

Tamrakar, S.B., Mitachi, T., and Toyosawa, Y. 2007. Measurement of soil tensile strength and factors affecting its measurement. Soils and Foundations, 47(5): 911-918.

Tang, G.X., and Graham, J. 2000. A Method for Testing Tensile Strength in Unsaturated Soils. Geotechnical Testing Journal, 23(3): 377-382.

Terzaghi, K. 1943. Theoretical Soil Mechanics. John Wiley & Sons, New York.

Tschebotarioff, G.P., Ward, E.R., and DePhillippe, A.A. 1953. The tensile strength of disturbed and compacted soils. In. Proceedings of the 3rd International Conference on Soil Mechanics and Foundation Engineering, Switzerland, 207-210.

Uchida, I., and Matsumoto, R. 1961. On the test of the modulus of rupture of soil sample. Soil and Foundations, 2(1): 51-55

Van Genuchten, M.T. 1980. A closed-form equation for predicting the hydraulic conductivity of unsaturated soils. Soil Science Society of America Journal, 44(5): 892-898.

Vomocil, J.A., and Chancellor, W.J. 1967. Compressive and tensile failure strengths of three agricultural soils. Transactions of American Society of Agricultural Engineers, 10(6): 771-774.

Young, T. 1805. An essay on the cohesion of fluids. Philosophical Transactions of the Royal Society of London, 95: 65-87.

Appendix A CALIBRATION OF LOAD CELL and LVDT

A.1 Load Cell Calibration

A load cell is a transducer that is used to convert a force into electrical signal. This conversion is indirect and happens in two stages. Through a mechanical arrangement, the force being sensed deforms a strain gauge. The strain gauge measures the deformation (strain) as an electrical signal, because the strain changes the effective electrical resistance of the wire. A load cell usually consists of four strain gauges in Wheatstone bridge configuration. Load cells with one strain gauge (quarter-bridge) or two strain gauges (half bridge) are also available. The electrical signal output is typically in the order of a few millivolts and requires amplification by an amplifier, before the signal can be processed. The output of the transducer can be scaled to calculate the force applied to the transducer.

Load cell was calibrated using the data acquisition unit as described in **Section 3.2**. The load cell was calibrated up to 50 N because the maximum tensile load was expected to be around 20-30 N.

1. The load cell was connected to the front loading container and movable half of the specimen box via pulley and string system. This arrangement has already been shown in **Figure 3.4**.
2. Initial voltage reading from the load cell was taken from the graphical user interface (GUI) unit of LabVIEW, when there was no additional weight added to the load cell.
3. Weights of 453.6 g each were used for calibration. A set of 11 weights was used to calibrate the load cell up to almost 50 N.
4. The first weight was added to the load cell and it was ensured that the weight along with the load cell is stationary. Once the system was perfectly still, the voltage reading was taken.
5. Similarly, more weights were attached to the load cell, and the voltage reading was taken after adding each weight.
6. The above steps 5 and 6 were repeated until the weight limit was reached; in this case it was 50 N.

7. The whole procedure (steps 1 to 6) was repeated thrice in order to check the repeatability.
8. Finally, the voltage values obtained were plotted against the calibrated weights, where voltage obtained was the independent variable and weights added were the dependent variable. (**Table A.1** and **Figure A.1**). The experimental data points were analyzed via regression analysis and the equation of the regression curve was calculated. Using the regression equation, the tensile load applied to the soil specimen during the direct tension test was determined by using the corresponding voltage reading of the load cell as the input value.

Table A.1 Load cell calibration

Load (g)	Load (N)	Voltage Values (mV)		
		Trial 1	Trial 2	Trial 3
287	2.81	0.272	0.273	0.272
741	7.26	0.266	0.266	0.265
1195	11.72	0.259	0.260	0.260
1649	16.18	0.252	0.252	0.253
2103	20.63	0.246	0.245	0.246
2557	25.08	0.240	0.239	0.240
3011	29.54	0.233	0.233	0.234
3465	33.99	0.226	0.227	0.226
3919	38.45	0.217	0.217	0.218
4373	42.90	0.213	0.212	0.212
4827	47.35	0.206	0.206	0.205

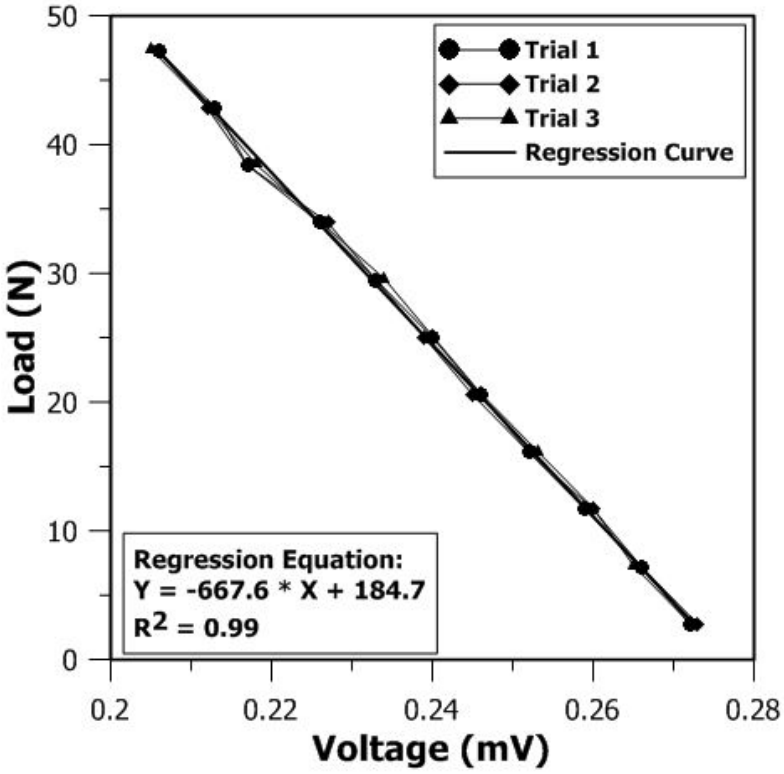

Figure A.1 Calibration curve for load cell

A.2 LVDT Calibration

The linear variable differential transformer (LVDT) is a type of electrical transformer used for measuring linear displacement. The transformer has three solenoid coils placed end-to-end around a tube. The center coil is the primary, and the two outer coils are the secondary. A cylindrical ferromagnetic core, attached to the object whose position is to be measured, slides along the axis of the tube. An alternating current is driven through the primary, causing a voltage to be induced in each secondary proportional to its mutual inductance with the primary. The frequency is usually in the range 1 to 10 kHz.

As the core moves, the mutual inductance changes, causing the voltage induced in the secondary to change. The coils are connected in reverse series, so that the output voltage is the difference between the two secondary voltages. When the core is in its central position, equidistant between the two secondary, equal but opposite voltages are induced in these two coils, so the output voltage is zero.

When the core is displaced in one direction, the voltage in one coil increases as the other decreases, causing the output voltage to increase from zero to a maximum. This voltage is in phase with the primary voltage. When the core moves in the other direction, the output voltage also increases from zero to a maximum, but its phase is opposite to that of the primary. The magnitude of the output voltage is proportional to the distance moved by the core (up to its limit of travel), which is why the device is described as "linear". The phase of the voltage indicates the direction of the displacement.

The following steps were used to calibrate the LVDT:

1. With the data acquisition system connected properly, the LabVIEW program was started. A graph of voltage response would appear on the computer screen as well as a digital read-out of the LVDT's voltage.
2. The pin on the LVDT was pressed in and out to observe the change in voltage, when the core was outside, inside and then outside again. This was to verify whether the whole system is connected and working properly.
3. The LVDT was prepared for calibration by mounting it in the screw gauge fixture, such that the central core of the LVDT was completely inside and just touched the micrometer at zero position.
4. The micrometer was checked for any zero error. The dial was rotated by 0.5 mm, from 0 mm to 25 mm. For each increment, the corresponding value of voltage was noted down.
5. The whole process was repeated thrice in order to check the repeatability.
6. Finally, the voltage values from LVDT were plotted against the known displacements (**Table A.2** and **Figure A.2**). The experimental data points were analyzed via regression analysis and the equation of the regression curve was calculated. Using the regression equation, the deformations (or displacements) during the direct tension test was determined by using the corresponding voltage reading of the LVDT as the input value.

Table A.2 LVDT Calibration

Displacement (mm)	Voltage Values (mV)		
	Trial 1	Trial 2	Trial 3
0	-4.35	-4.36	-4.35
0.5	-4.3	-4.29	-4.3
1	-4.27	-4.26	-4.26
1.5	-4.18	-4.20	-4.19
2	-4.11	-4.10	-4.11
2.5	-4.06	-4.05	-4.04
4	-3.79	-3.79	-3.79
5	-3.65	-3.6	-3.7
8	-3.05	-3.06	-3.08
10	-2.64	-2.60	-2.66
15	-1.58	-1.59	-1.59
20	-0.55	-0.55	-0.55
21	-0.32	-0.33	-0.31
22	-0.11	-0.118	-0.12
23	0.093	0.095	0.096
24	0.32	0.29	0.31
25	0.50	0.51	0.52

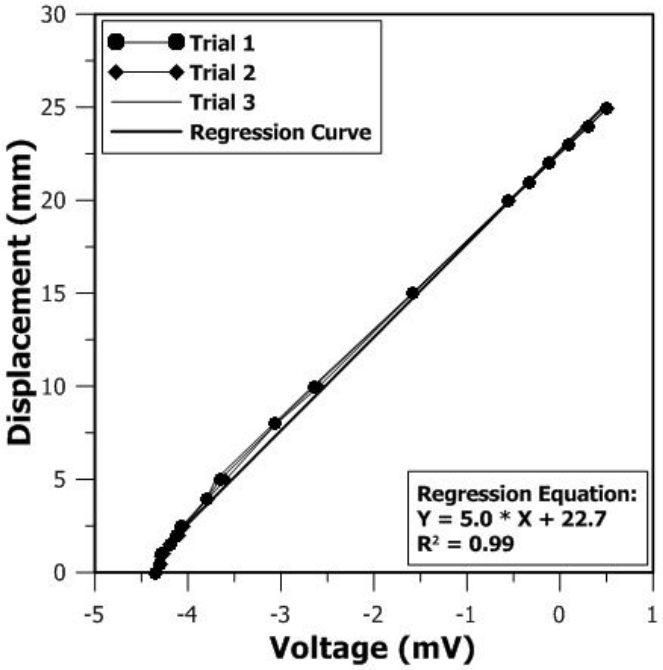

Figure A.2 Calibration curve for LVDT

Appendix B FRICTION CALCULATION IN DIRECT TENSION APPARATUS

The calculation of friction in the direct tension apparatus was very important. As the tensile strength values for unsaturated sands are on the lower side, in the range of few hundreds to few thousands of Pascal, friction value equivalent to 100 Pa becomes quite significant. The friction in the system was determined using the method of statics. The free body diagram of the direct tension apparatus is shown in **Figure B.1**.

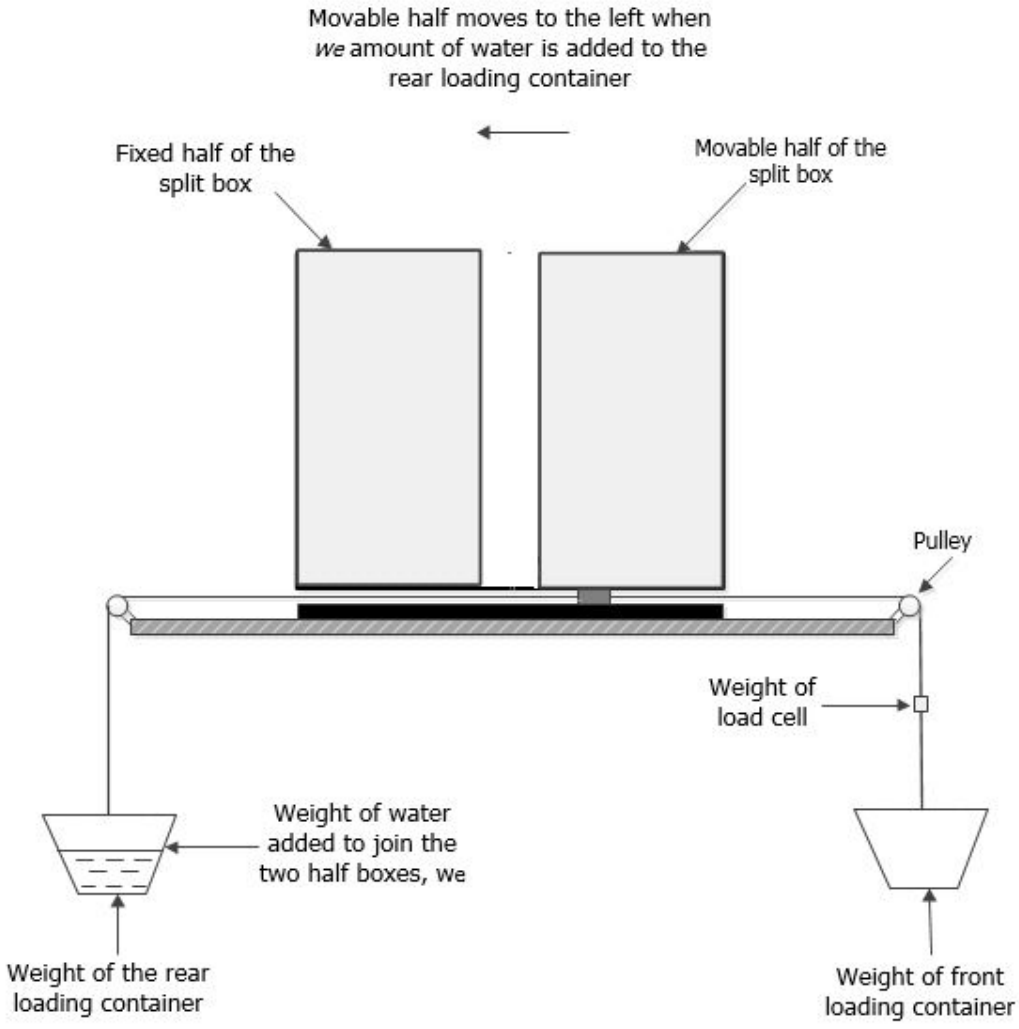

Figure B.1 Free body diagram of direct tensile apparatus

As shown in **Figure B.1**, the two halves of the specimen box are not touching each other. Although the front (w_f = 243.2 g) and back (w_b = 236.9 g) loading containers on the either side of the apparatus almost weigh the same, the additional weight of the load cell pulls the front, movable half towards the right. The back loading container was loaded with water equivalent to the weight of the load cell (w_l = 275.2 g) and the difference in the weight of the front and back loading containers was also taken into account. It was observed that the two halves were still not touching each other. This is attributed to the friction in the system in the right-hand side direction. To overcome this friction, more water was added to the back loading container until the two halves just touched each other. This amount of water was measured to be w_e. During the actual direct tension test, the movable box moves toward the right-hand side direction at failure. In this case, the friction acts on the opposite direction (i.e., left-hand side direction). The value of this friction is determined by loading the front loading container with water, when the two halves are just touching each other and are empty. The water is added to the front loading container until the boxes just move apart (**Figure B.2**). The total amount of water (w_t) was calculated by multiplying the time taken for the two halves to move apart and rate of loading of water into the front loading container. Finally, the total friction in the system (w_{fr}) is the vector summation of the two different frictions, i.e., the weight of the water in the front loading container at failure (w_t) minus the extra water added in the back loading container (w_e).

This procedure was repeated 15 times to check the repeatability and average value of friction was calculated (**Table B.1** and **Figure B.3**). The average friction (w_{fr}) in the system was equal to 3.91 N which is equivalent to tensile strength of 270 Pa for failure surface of 144 cm^2. The corrected readings for all direct tension tests were calculated by subtracting the calculated frictional load from final tensile load obtained after failure.

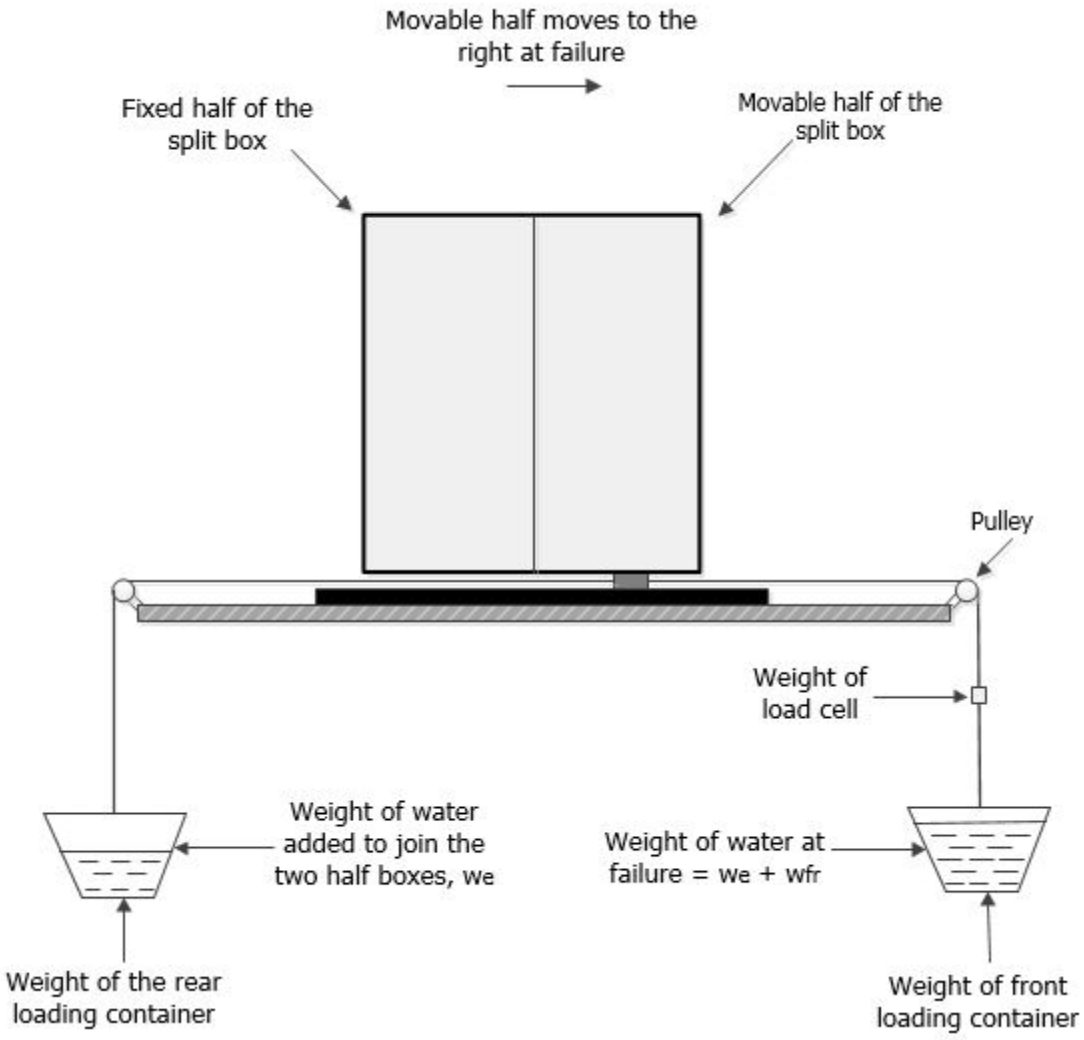

Figure B.2 Free body diagram of the direct tensile apparatus at failure

Table B.1 Friction calculation

Sr. No	Time(s)	w_t (g)	$w_t - w_e$ (g)	Friction, w_{fr} (N)
1	48	685.7	385.7	3.8
2	47	671.4	371.4	3.6
3	48	685.7	385.7	3.8
4	47	671.4	371.4	3.6
5	48	685.7	385.7	3.8
6	50	714.2	414.2	4.1
7	50	714.2	414.2	4.1
8	49	700.0	400.0	3.9
9	50	714.2	414.2	4.1
10	50	714.2	414.2	4.1
11	49	700.0	400.0	3.9
12	50	714.2	414.2	4.1
13	50	714.2	414.2	4.1
14	49	700.0	400.0	3.9
15	49	700.0	400.0	3.9

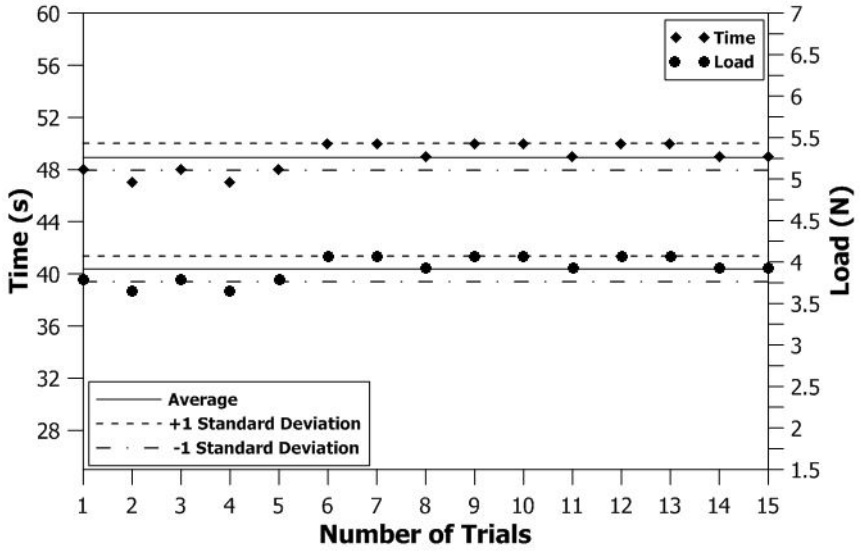

Figure B.3 Friction in the direct tension apparatus